University of Padua

Department of Industrial Engineering

Electrical Energy Engineering

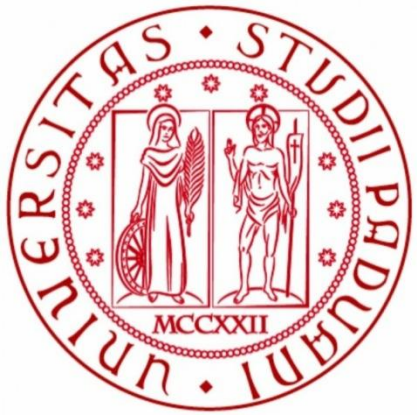

Master Thesis

PERFORMANCE OF TEXTURED INSULATORS FOR OVERHEAD LINES AND SUBSTATIONS UNDER POLLUTED CONDITIONS

Supervisor: Prof. Roberto Turri
Department of Industrial Engineering

Co-supervisor: Prof. Manu Haddad
School of Engineering, Cardiff University

Student: Thomas Zago
Number: 1128740

Academic Year 2016-2017

Acknowledgements

I want to express my gratitude to Prof. Roberto Turri, to have given me the possibility to make this international experience, working on a topic which will be a key for the future. Furthermore, his pleasantness and the trust who gave me were very enjoyed.

My gratitude goes also to Prof. Manu Haddad, Dr. Maurizio Albano and the “Advanced High Voltage Engineering Centre” at Cardiff University, in particular to Michail Michelarakis and Jonathan James for their friendship.

My greatest thank you goes to my family and my friends to have given me all the support I needed, endless.

Never give up researching the innovation

Abstract

In the present work, starting from the state of art, a research on the insulators performances, especially for outdoor applications has been executed.
A literature review was made to acquire the previous work and to understand which could be the most interesting step to develop.
A big quantity of tests have been done in the past, since was known that the silicone rubber (SiR) insulators could replace the nowadays cap and pin made up of ceramic and glass.
Materials assigned for the manufacturing of high voltage outdoor insulation should be assessed for their ability to prevent tracking and erosion. The gradual degradation of the insulation surface to form conductive paths called tracks or the loss of insulation material due to leakage current or surface discharging is most unwanted for outdoor insulators. Extensive tracking and erosion severely undermines the insulating effectiveness and the mechanical robustness when eroded rubber exposes the fibreglass core to partial discharge attack.
Silicone rubber for composite insulators includes special flame retardant fillers to increase the resistance against erosion and tracking by absorbing heat from surface discharges and releasing water vapour. Several ways to test the SiR samples have been studied and a particular attention was put on the Inclined Plane Test. It is a well-established material test for the assessment of the resistance of insulating materials against tracking and erosion and is described in the IEC 60587 international standard [1]. Rectangular standard size samples are mounted at a 45^{o} angle and subjected to high voltage stress. A salt contaminant solution is fed from the top of the sample and traverses the test surface. The test is designed to encourage the formation of dry-bands and surface discharges in order to monitor surface erosion and tracking.
For the purpose of this project, rectangular silicone rubber samples were prepared with dimensions as per the standard (120[mm] x 50[mm] x 6[mm]). Samples with a plain surface and samples employing fine texturing were tested to compare the performance against surface tracking and erosion.
Infrared recordings and high-speed photography provided useful information for the interpretation of the test results.
Textured samples showed significantly different discharge behaviour, which is accounted for the substantial improvement introduced by these textures in terms of resistance against tracking and erosion, compared with conventional samples.
A dedicated data acquisition program was used based on the National Instruments LabVIEW platform. This high-resolution program monitored and stored in files the waveforms of voltage and currents.
Some cylinder insulators both conventional and textured and a shedded conventional prototype of 11 [kV] were manufactured.
All the silicone rubber insulators were developed in-house, using vacuum injection

casting techniques. These composite insulators consist of a silicone rubber housing made of commercially available silicones and moulded over a reinforced glass fibre core.

Research objectives

The research programme was diverse with tasks ranging from insulation design and vacuum injection casting to high voltage testing and software programming.
The main aims of this research work are as follows:
(a) To prove the effectiveness of textured surfaces in reducing the thermal damage on silicone rubber insulation due to surface heating induced by surface discharges.
(b) To identify the optimum textured designs (among the tested) that show the maximum reduction of surface erosion and that could be employed for the development of a full shedded insulator.
(c) To establish a comprehensive test procedure for the testing of the samples in the IPT ageing unit, adding the infrared and the high speed photography where necessary. Include the investigation of the dry-bands formation during artificial pollution testing, deeply researching how the streamer is developing on the surface and carrying out the differences with the conventional samples.
(d) To manufacture the full textured silicone rubber insulator that would employ the textured patterns explored in step (b).
(e) To develop a high-resolution data acquisition system that would monitor the test voltage and leakage current and also store these data into files for post-processing analysis.

Several fields of study have been touched: the preponderant part was the electric and power system knowledge, the chemistry has been used to work with the silicone rubber components and the pollution contaminant, the samples fabrication in various mould materials involved the mechanics, electronics was referred to the I/O board on the IPT machine and the connector block pins, while informatics involved the acquisition software and the post processing program knowledge to analyse the acquired data.

Contents

Acknowledgements……3
Abstract ……5
Research objectives……7
1. Introduction……11
1.1 UK electricity network……11
1.2 Insulators description and comparison……13
1.2.1 Textured insulators ……15
1.3 Summary……16
1.4 Measurement of hydrophobicity……17
1.5 Dry-band formation……19
1.6 Overview of possible tests ……24
1.6.1 Inclined plane test ……24
1.6.2 Rotating wheel dip test……25
1.6.2.1 Rotating wheel dip test set-up and facilities……25
1.6.3 Fog chamber test……26
1.6.3.1The fog chamber……27
2. Fabrication of new samples……28
2.1 Vacuum casting machine……30
2.2 First sample fabrication……34
2.3 Procedure……36
3. Inclined Plane Test……41
3.1 Standard IEC 60587:2007……41
3.2 Inclined Plane Test facilities……45
3.2.1 The accelerated ageing unit……45
3.2.2 The Data Acquisition System……51
3.2.3 Camera recordings……55
3.3 Inclined Plane Test setup……60
4. The experimental tests……67
4.1 Test Day 10th April……67
4.2 Test Day 10th May……69
4.2.1 Test A……70
4.2.2 Test B……74
4.3 Test Day 6th June……79
4.3.1 Test 1……80
4.3.2 Test 2……84
4.3.3 Test 3……86
5. Post-processing analysis and comments to the results……93
6. Full insulator manufacture……101

6.1 Casting of full insulators using metal moulds……..102
6.2 Casting of textured insulators using silicone moulds ……..104
7. Conclusions……..107
7.1 Future work…….108
Bibliography……..111

CHAPTER 1
Introduction

1.1 UK electricity network

The first electricity networks have been developed around 120 years ago as localised street systems and have evolved to become today's interconnected national transmission and distribution network. Transmission is the bulk, often over long distance, movement of electricity at high voltages (400[kV] and 275[kV]) from generating stations to distribution networks and to a small number of large industrial customers as big companies. Distribution is electricity provision to the majority of customers through lower voltage, more localised networks (from 132[kV] to 230[V]). The levels of MV are 11 and 22 [kV].

The UK Electricity Supply Industry (ESI) has a structure (figure ##) characterised by:
• large-scale generation plants;
•high voltage networks;
•integrated generation, transmission, distribution and supply functions.

There are four transmission systems in the UK: one in England and Wales, two in Scotland, and one in Northern Ireland. Each one is separately operated and owned. The largest, in terms of line length and share of total transmission is the National Grid Company (NGC) system, covering England and Wales.

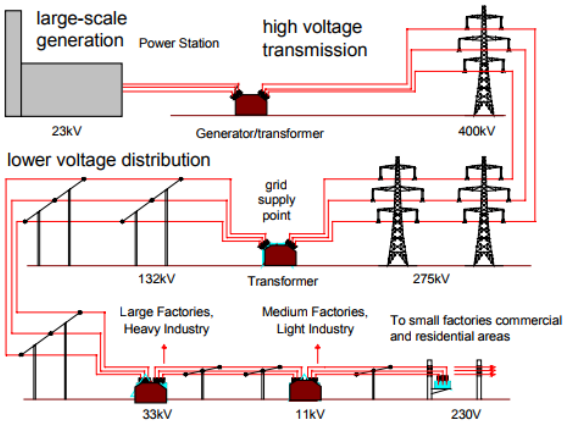

Figure 1.1: an interconnected electricity system

There are 12 licensed Distribution Network Operators (DNOs) in England and Wales, two in Scotland and one in Northern Ireland. They include GPU Power UK, Norweb and SEEBOARD Power Networks, and their size and number of customers varies.

From the previous decades the electricity network around the world is changing and the UK system is following (and drawing) the trend. The old system was thought to bring

electricity from few big power plants to the customers, instead today there is a bidirectional power flow. In fact the energy often goes from the customers to the grid: this because the distributed generation (DG) is taking place. The main driver which is bringing to DG is the insertion of RES (Renewable Energy Sources) in the way to generate power. This is a consequence of years of increased environmental concerns among the humans, induced by the visible impact of global warming, the worsening of air we are breathing causing by an increase of the carbon dioxide (CO2). Another driver which is bringing to the "Smart Grid" is the location of generating plants nearer to the demand, thus reducing transmission charges along the line.

A new model for electricity networks? All these factors may lead to a considerable increase in 'embedded' electricity generation, where small-scale generating units (which may include renewable sources) are directly connected to the lower voltage distribution networks. Including existing embedded generation, the targets imply that, at most, 20-25 gigawatts [GW] (around one third of total capacity) would be embedded in the distribution networks. However, this level of "embedded capacity cannot be accommodated on the currently configured networks without significant change". Such changes will require the reconfiguration of existing electricity networks into a 'distributed electricity system' that accommodates changed electricity flows.

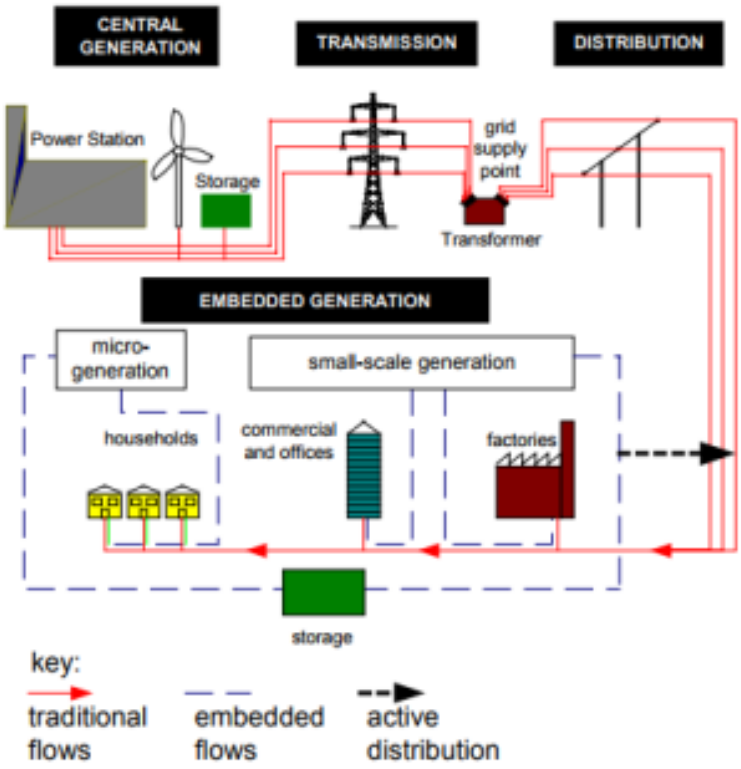

Figure 1.2: distributed electricity system

Distributed electricity system

A distributed electricity system combines electricity from large and small generation units. Large power stations and any large-scale renewables, e.g. offshore wind, remain connected to the high voltage transmission network providing national back up and ensuring quality of supply. Small generators are connected directly to factories, offices, households (e.g. with domestic CHP or PV roofs) and to lower voltage distribution networks (figure 1.2). Electricity not used by customers directly connected to small-scale units is fed back into active distribution networks to meet demand elsewhere. Electricity storage systems are being developed that may be able to store any excess generation. These may also accommodate variable output of some forms of generation. [2]

1.2 Insulators description and comparison

To ensure a proper operation and allow a future power system development, which probably will require an increment of the voltage levels nowadays reached, insulation is a fundamental field of interest.
Increasing the voltages means improve the insulation properties of the insulators, change their designs or assess new materials for this purpose.
Due to the critical importance of a reliable and efficient power transmission, outdoor insulation has inevitably been at the epicentre of research interest in an endeavour to eliminate or alleviate the problems associated with insulation failure.
The main functions of insulators are to withstand the mechanical stress of supporting electrical conductors and to electrically isolate equipment of different potential and inhibit flashover events from occurring.
Flashover performance of insulators is mostly dictated by their ability to deal with the complications introduced by the accretion of contaminants on the insulating surface.
An insulator in service is susceptible to pollution by air-borne contaminants that are deposited on the insulation surface. When this pollution layer is wet, it conducts a leakage current with a non-uniform density. Local heating at regions of high current density is accompanied by the formation of dry zones, called dry-bands.
When the voltage gradient across these dry-bands reaches a critical value, they are spanned by surface discharges. The latter have a decisive impact on the insulator performance as it makes it vulnerable to degradation and to the electrical bridging of the energised conductors in the form of a hot flashover arc.
Two main categories of insulators have been employed for overhead lines (OHL) and substations depending on the material used: ceramic and polymeric insulators.
Ceramic insulators have been in service since the early 20th century with an excellent service record. The mechanisms leading to a pollution flashover event are fairly understood.
However, over the last 30 years, polymeric materials have gained extensive acceptance,

mainly due to their superior performance at severe ambient conditions compared with their ceramic counterparts.
The key advantage of polymeric insulators is the hydrophobicity of the insulating surface. This water repellent property forces water to be deposited in a form of discrete beads unlike the hydrophilic case for ceramics, which form a thin spread layer on their surface. The reduction of surface wetting consequently leads to a reduction of discharge activity on polymeric surfaces and to an enhanced antipollution performance.
Silicone rubber is a polymer widely adopted for outdoor insulation [35]. Unlike other polymers, like EPDM (ethylene propylene diene monomer), it retains its hydrophobic status throughout service life and, in addition, has the ability to transfer this hydrophobicity to the adhering pollutants. However, like all polymers, it is vulnerable to long-term degradation due to aging and weathering.
Pollution flashover constitutes the predominant parameter for the design, specification and dimensioning of high voltage insulators.
The international standard [3] , overturned the traditional approach where the shortest distance between the insulation terminals, called creepage distance, determined the selection process for polluted environments. It is now accepted that other factors strongly influence the pollution performance as well. These are related to the electrical system requirements, the type of environment and pollution, and the insulator design.
There are two types of pollution [3]:
Type A: this solid layer pollution consists of a soluble and non-soluble component that is deposited on the insulator surface. Under conditions of slow humidification (dew, drizzle, mist, fog etc.), this layer becomes conductive. This type of pollution is mostly associated with inland, industrial and desert areas. The non-soluble component acts as a binder between the soluble component and the insulator surface, and for polymeric insulators, it masks the hydrophobic layer. The soluble component consists of low and high solubility salts.
Type B: this type has no or little non-soluble component and comes in the form of salt spray of conductive fog. It simulates the pollution found at coastal areas. Within this category, crop sprays at agricultural areas, acid rain and chemical mists are included.
The IEC-60507 [4] recommends tests to simulate the conditions of pollution that insulators are subjected to in the field.
These tests are:
a. The Salt-Fog method: the insulator is subjected to fog produced by a salt (NaCl) solution. This test best simulates contamination by pollution type B.
b. The Solid-Layer method: also referred as Clean-Fog method, this procedure suggests the direct application of solid pollution on the insulator surface and represents best pollution type A.
The IEC 60507 standard is specifically concerned for ceramic insulators. Its applicability to polymeric insulators is limited. Due to the dynamic nature of the polymeric material and its wetting properties, it has been difficult to establish a commonly accepted

method. One of the approaches followed is the use of existing methods employed for the testing of ceramic insulators [4] or modified versions of these conventional methods.

1.2.1 Textured Insulators

The hydrophobic surface of polymeric insulators offers a significant advantage compared with glass or ceramic units used in overhead transmission and distribution systems in coastal or industrial environments. However, under severe ambient conditions, dry band formation is not totally eliminated, especially before hydrophobic recovery can occur in the overlaying pollution layer.
A critical region is the recessed area below the shed of the insulator, where washing is least effective and deposits may accumulate. The geometry of the insulator shows that the density of surface discharge currents flowing from one end of the insulator to the other is highest at the shank of the insulator. As a consequence, the surface electric field strength is also at a maximum in this region, and there is a heightened risk of surface heating, which may cause dry bands, partial arcs on the surface and consequential thermal damage. This action is limited in the case of glass and ceramic cap and pin insulators by 'anti-fog' designs having additional rims on the underside of the sheds which lengthen the creepage distance and reduce the magnitude of the leakage current [5].
However, because of the nature of the moulding process, this is not possible in multi-shed polymeric insulators. A patented design programme aims to deal with these challenges and improve the pollution properties of a silicone rubber surface by employing a textured finish [6].
Textured patterns consist of intersecting or contiguous hemispherical protuberances [7]. This raised geometry does not impede the removal of the insulator from the mould during casting. The main aim of surface texturing is to lower power dissipation on the insulator surface by reducing both leakage current density and the electric field gradient. An increase of surface area can reduce the leakage current density in the vulnerable shank region, and a substantial increase in the longitudinal creepage distance could reduce the electric field stress. Moreover, the texture pattern can have paths of preferential contamination and conduction, which can lead to several parallel current paths.

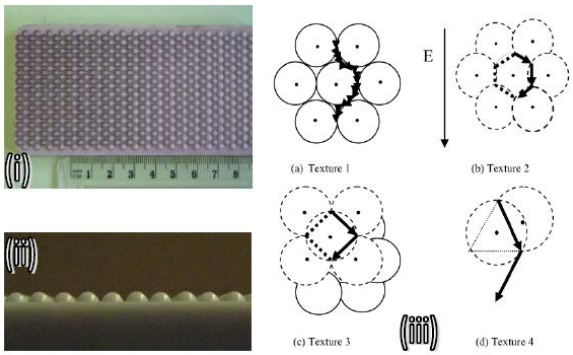

Figure 1.3: example of texturing, i) top view ii) side view iii) texture designs [6]

As soon as a path is conducting, the resulting heat and drying will increase the resistance of that path. Nevertheless, an adjacent current path of higher conductance will be available, thus switching the conduction path from the original path before the insulation surface sustains thermal damage.
This design concept aspires to reduce tracking and erosion on the insulator surface and to improve the flashover strength under conditions of heavy pollution. This research programme set out to complete a series of laboratory investigations to assess the performance of such textures and to investigate the predicted advantages introduced compared with conventional silicone rubber insulation.

1.3 Summary

To summarise the differences between the textured prototypes and the conventional flat ones, advantages and disadvantages have to be analysed.
Silicone rubber installations lead to several advantages in comparison to the ceramic and glass classic insulators.
The most important is the hydrophobicity property, which they can transfer to the adhering pollutant. This provide an intrinsic resistance against leakage current, while the hydrophilic glass and ceramic can be easily wetted causing a formation of a path for the current flow.
They can represent an anti-pollution system, since the applications of the insulators are basically everywhere (with a huge range of different environmental conditions).
They have a lighter weight in comparison to the ceramic and glass rods, which are very heavy. For the overhead lines they require a strong connection with the charged pylon that has to hold up them.
Furthermore, considering the huge number of rods installed for each kilometer of line, the substitution with the polymeric insulator would mean unloading the pylons from this onerous task.
The high mechanical strength reached today with the polymeric insulators makes them very competitive also regarding the mechanical properties for which they are stressed on the field.
Another advantage is the small volume with whom they are designed: it means a reduced impact view and the environment would benefit from this, especially where the overhead lines cross important or historic environments.
Other advantages are the convenient installation and less maintenance performance during service and the interesting fact that they are easier to handle and to transport in site.
Another characteristic is that they are anti-vandalism designed, which could be a great feature.
Polymeric insulators have a good electrical strength, but the main disadvantage is the limited time range in the form of aging. In fact they have been tested in this research project to study how the performances are limited when the time is accelerated.
The tracking and erosion of the material are the main issues of these installations,

especially in outdoor applications where they are more stressed. This has to be addressed to the fact that the polymeric materials have weaker bonds than porcelain. A considerable improvement on this aspect will bring to a massive installation of these insulators worldwide.
The last consideration can be referred to the costs. Polymeric insulators, when they would be adopted on a big scale, will have an installation cost significantly lower than the ceramic and glass classic rods. This will bring to a benefit for the TSO (Transmission System Operator)[1] and for the customers, who will benefit from less bill costs. Considering that the maintenance cost is almost zero, this means that the general cost should be convenient if compared with the classic ceramic rods.
At present the most realistic condition assessment techniques are visual inspections, hydrophobicity evaluations, and leakage current measurements.

1.4 Measurement of hydrophobicity

Hydrophobicity is the ability of a surface to repel water, so that water on the surface forms individual droplets rather than a film. Hydrophobicity is the most important property of silicone rubber insulators and its measurement has been investigated and widely used as an indication to the insulator performance [8].

Contact angle

The contact angle is a function of the surface tension of the liquid and the interfacial free energy of the solid surface [9]. Contact angle measurements can be greatly affected by surface roughness [10] and wettability, which is primarily related to the surface energy. The surface free energy and contact angle (θ) are inter-related via Yaung-Dupre equation.

$$\gamma GS=\gamma SL+\gamma LG.\cos\theta \quad \ldots\ldots\ldots\ldots\ldots\ldots\ldots\ldots\ldots\ldots \quad (2\text{-}1)$$

Materials with high surface energy can be easily wetted, and a water film forms continuously on their surfaces and thus they are classified as hydrophilic. On the other hand, materials with low surface energy such as silicone rubber, have inherent water-repellency, and are termed hydrophobic. Water droplets on the surface tend to bead up and run down from the surface (the contact angle is greater than 90^{O}).
The contact angle was used in is this work as a measure of the SiR surface hydrophobicity. It has been shown to be an effective way to provide reliable information on the hydrophobicity condition. Figure 1.4 shows a water droplet on SiR polymeric surfaces, where the hydrophobicity is increased with decreasing adhesive tension between water droplet and the surface.

[1] *It can be extended to the distribution network.*

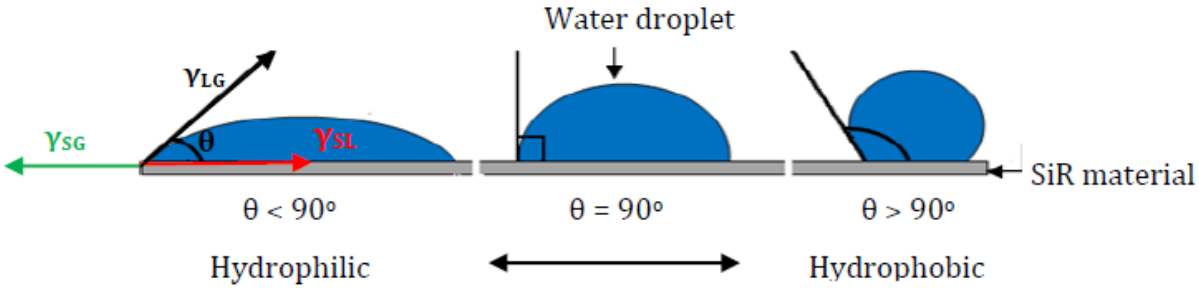

Figure 1.4: water droplets with different degrees of hydrophobicity [8]

Contact angle measurements can be difficult to perform on the surface of complete insulators, or on complex surfaces such as on textured insulators. To overcome this, a simple test for Hydrophobicity Classification (HC) has been developed by the Swedish Transmission Research Institute (STRI) [11].
Table 1.1 shows the STRI criteria for determination of HC.
In this test, the insulator surface is sprayed with water using a hand held spray bottle, similar to those used for domestic cleaning products. The hydrophobicity of the surface is evaluated by comparing the surface with standard photographs and written definitions to give a HC of between HC1, which corresponds to the most hydrophobic surface, and HC7 which corresponds to a completely hydrophilic surface.
Lower contact angles or higher indices of hydrophobicity classification (HC) may occur, due to changes of the surface state, from degradation by electrical discharges or UV exposure. Results published from this research conclude that non-irradiated insulators belong to HC1 or HC2 categories, whereas hydrophobicity of the samples after aging is between HC3 and HC5 categories. Therefore, UV irradiation reduces the hydrophobicity of the SiR insulators measurably.[12]

HC	Description	Picture
1	Only discrete droplets are formed. Their space seen perpendicular to the surface is practical circular. This corresponds to $\varphi_r = 80°$ or larger for the droplets.	
2	The major part of the surface is covered by droplets with a shape, still regular but deviates from circular form. This corresponds to $50° < \varphi_r < 80°$ for the majority of droplets.	
3	Only discrete droplets are formed. The major part of the surface is covered by droplets with an irregular shape. This corresponds to $20° < \varphi_r < 50°$ for the majority of: droplets.	
4	Both discrete droplets and wetted traces from the water runnels or water film are observed. Less than 10% of the observed area is covered by water runnels or film.	
5	Both discrete droplets and wetted traces from the water water film are observed. More than 10% but less than 90% of the observed area is covered by water runnels or film.	
6	More than 90% but less than 100% of the observed area is covered by water runnels or film (i.e. small non-wetted spots/traces are still observed).	
7	Continuous water firm is formed over the whole observed area.	

Table1.1: criteria for the hydrophobicity classification (HC) [11]

1.5 Dry band formation

Pollution Flashover

The pollution flashover mechanism depends on the nature of the dielectric material. In the hydrophilic case, where ceramic insulators belong, when the insulator surface is wetted, a thin film of electrolyte covers the surface whereas in the hydrophobic case, e.g. silicone rubber, the water resides on the surface in the form of discrete beads without the whole surface being wetted.

Flashover mechanism for a hydrophilic case (ceramic insulators)

In the review compiled by CIGRE working group 33.04 [13], the process of pollution flashover is described as follows:
1. Contaminants like soluble salts or dilute acids or alkalis are deposited on the insulator surface and eventually form a pollution layer. There are two cases: the pollution layer can be in the form of a liquid electrolyte or the layer is non-conductive when is dry. In the first case, steps 3 to 6 might take place immediately whereas for the case of a dry non-conductive layer, a process of layer wetting described in step 2 is required.
2. Under conditions of slow humidification such as fog, mist light rain, sleet or melting snow or ice, the pollution layer becomes wet and conductive. A heavy rain could be either beneficial by washing off the pollution from the insulator surface or could lead directly to flashover due to bridging sheds together through water cascades.
3. Under energisation and with a wet conductive layer on its surface, the insulator conducts a surface leakage current which dries out parts of the wet layer due to the current heating effect.
4. The leakage current density is always non-uniform resulting in a non-uniform drying of the wet layer where some parts get dry faster than other, thus creating dry zones, called dry-bands, that interrupt the flow of current on the pollution layer.
5. The dry-bands have a width that may be only a few centimetres and they bear across them the insulator energisation voltage. This creates the conditions for the air breakdown, and the dry-bands are bridged by surface discharges that are electrically in series with the wet layer. Fast current pulses are associated with the spanning of dry-bands by discharges.
6. The resistance of the not dried pollution layer is controlling the discharge current and, if it is low enough, the dry-band discharges remain active and gradually longer sections of the insulator are spanned.
However, this results in a further decrease of the wet layer resistance, elongation of the discharges and finally in the complete bridging of the insulator in the form of a flashover arc.

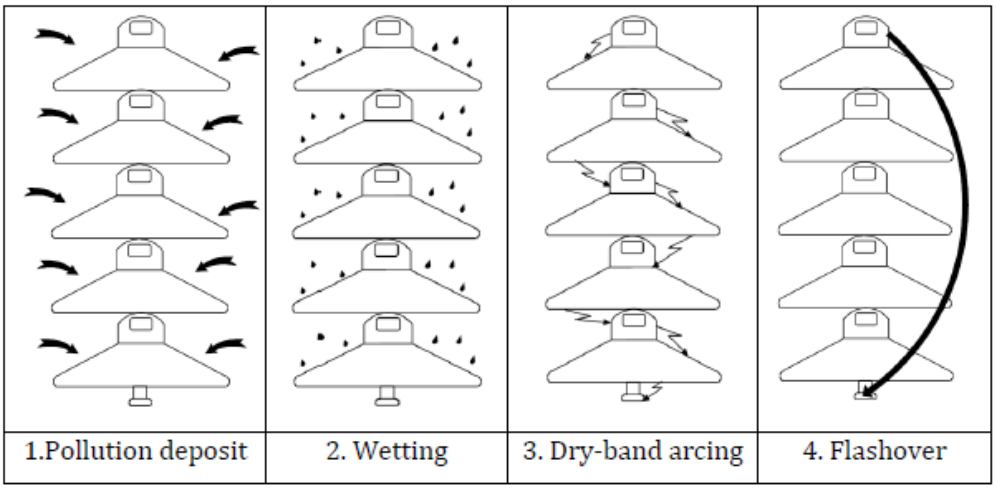

Figure 1.5: pollution flashover

Dry-bands

In general, sustained electrical arcing discharge can cause a deteriorating influence on the silicone rubber housing material can be classified into two categories: dry-band arcing and corona discharges.
The degradation of SiR outdoor insulating materials due to dry-band arcing occurs because of generated heat, chemical reactions, and ultraviolet radiation (UV). It has been observed that prolonged dry-band arcing in a particular region of polymeric insulators, due to their relatively low thermal stability [14] and the impact of UV light, is responsible for initiating degradation before flashover.
The dry-band arc formation on a wet surface can be briefly described as following:

- *Flow of current*. When hydrophobicity is lost due to corona by the effect of UV radiation, pollution with fog, dew, rain or any other form of condensate moisture forming a continuous wet film on the insulator surface. Theoretical models that predict the impact of dry-band discharges on polymeric insulators are described in [15,16,17]. Dry-band formation depends on the surface electrical field E and the surface leakage current density J:

$$E = \rho * J$$

where *E* is the electric field, *ρ* is the surface layer resistivity and *J* is the surface current density. Power dissipation is given by

$$P = E * J$$

that can be expressed as

$$P = \rho * J^2 = \sigma * E^2$$

where σ is the pollution layer conductivity.

- *Drying.* When the leakage current reaches a certain value, in the order of few µA to a few mA, heat is produced due to the Joule effect and the water in the path of leakage current evaporates, thereby, drying portions of the surface and forming dry-band area, which interrupt the current [18].

- *Sparking.* When the LC is interrupted, much of the voltage is applied across the dry area, and if this voltage is high enough, small arcs bridge the areas.

- *Restarting.* As the surface conditions dynamically change, dry-band arcing can stop in one specific location and starts in another on the insulator surface.
If the conditions for the dry-band are sustained with considerable levels, the ultimate effect of dry-band arcing on the material surface is tracking and erosion, and a decrease of the number of LMW that impart hydrophobicity to the polymer, potentially leading to failure and flashover [213], flashovers occur in wet weather conditions, occurring in step sequences as shown in figure 1.6.

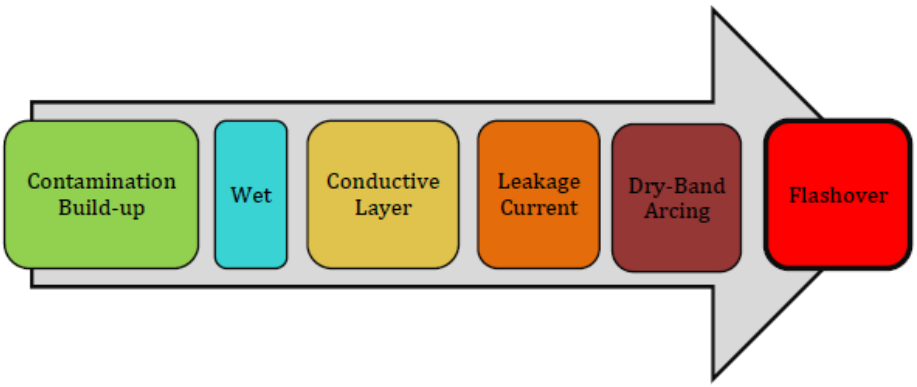

Figure 1.6: flashover mechanism on high voltage insulators

In [19], the authors proposed dry-band discharge modelling called a spark-model as shown in Figure 1.7. This model has been suggested on the premise of that the conductivity of the spark leader is maintained by impact ionisation that occurs at low temperatures, instead of thermal ionisation observed for arc channels at high temperatures. The spark leader channel of length C spans the dry-band. The dry-band might become larger as streamers of combined length S sprouting out the spark leader can penetrate the dry-band [20].

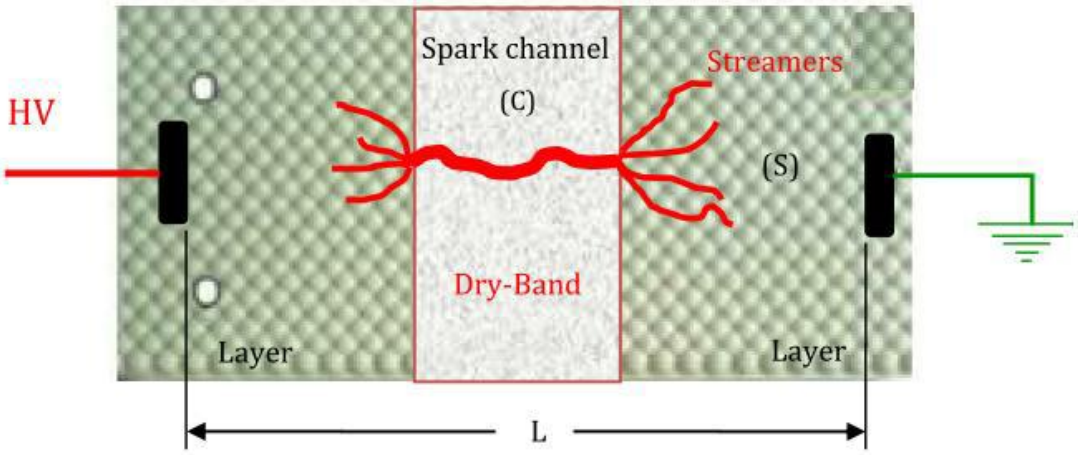

Figure 1.7: the dry-band spark model

Flashover mechanism of a hydrophobic case (polymeric insulators)

Due to the dynamic nature of the hydrophobic surface of polymeric insulators, the flashover mechanism is substantially different from that of ceramic insulators and hydrophilic dielectrics. Generally, non-ceramic insulators show a better flashover performance than ceramic insulators of similar creepage length.
The higher permittivity of water droplets residing on the hydrophobic surface compared with the permittivity of air and the dielectric material acts as an electric field enhancer. Also, the air over the dry part of the insulator surface is shortened by the intervening gaps introduced by the droplets which tend to change shape under the influence of the electric field.
Karady and Shah [21] described a qualitative mechanism for the flashover initiated by water-drops rather than dry-bands of polluted silicone rubber insulators (figure 1.8). The insulator surface gradually gets polluted during service. For both marine and inland pollution, the surface tends to accumulate a uniform pollution layer.
Due to diffusion of LMW chains from the bulk of the polymer, a thin oil-like layer forms on the insulator surface, covering the pollution. Wetting from fog, a morning mist, light rain or the condensation of the air humidity on the insulator, leads to the formation of water drops that reside on the hydrophobic surface (figure 1.8a). At this stage, water by diffusion and through the thin polymeric layer, wets the dry contaminants resulting to highly resistive regions surrounding each droplet (figure 1.8b). At the same time, salt from the pollution layer and through the oily layer is transferred and dissolved in the water beads increasing their conductivity. The droplets change shape and elongate under the influence of the electric field which become more flat and elongated. During this process, neighbouring droplets may merge to form conductive filaments with a highly resistive layer around them (figure 1.8c).

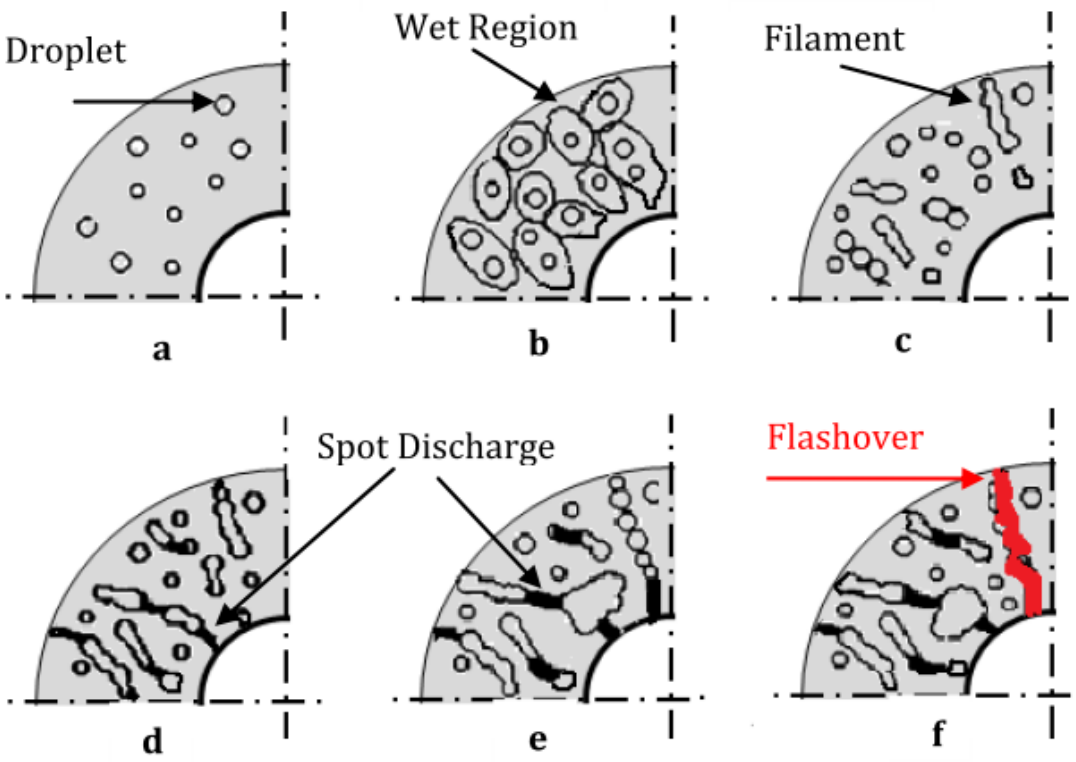

Figure 1.8: flashover mechanism on polymeric insulator [22].

The elongated filaments shorten the distance between the electrodes thus giving rise to even higher values of electric field between them and other neighbouring filaments. Spot discharges are initiated between the filaments (figure 1.8d). The discharge activity leads to a loss of hydrophobicity that favours further expansion of droplet filaments that form wet regions. Such wet regions may form also near the electrodes under the influence of corona and surface discharges.

Unlike the uniform wet pollution film observed for ceramic dielectrics, the wet regions are patched on the insulator surface, and are surrounded by a high resistance layer with discrete droplets (figure 1.8e). The growth of wet areas along with the further elongation of water filaments finally creates a conductive path capable of leading to a flashover when the arc voltage gradient is lower than that of the filament (figure 1.8f). The mechanism described above is indicative of the challenges that are faced for establishing a commonly accepted test method for polymeric insulators due to the dynamic interaction of their surface with the environment.

It is generally agreed that the major cause for polluted insulator flashover is from dry-band formation.

1.6 Overview of possible tests

Polymeric insulators test methods

To assess the performance of polluted polymeric insulators, different artificial test methods are used, such as inclined plane test [1], the tracking wheel test [23], the IEC salt fog and clean fog tests [4].
Artificial pollution testing is described in detail by the Lightning Insulator Subcommittee [24] of the IEEE Working Group on Insulator Contamination. The three basic procedures commonly employed are the clean-fog test, salt-fog test, and wet contaminant test.
In the clean-fog test, dry contaminated insulators are energized and subjected to a fog produced from tap water. This test method represents the condition in which a contaminant accumulated on the insulator surface is wetted by natural moisture, creating a condition favourable to flashover laboratory tests. In the salt-fog test, clean insulators are energized and simultaneously subjected to a fog generated by atomising water of known salinity; this test serves primarily to simulate insulators located in coastal areas, where they are exposed to direct salt spray.
Lastly, in the wet-contaminant technique, which is not accepted as a standard test, voltage is applied to insulators that have a wet conducting coating to simulate re-energisation of a line on which contaminated insulators have been exposed to a wetting agent such as high humidity, rain or snow.
The impact of high voltage source parameters on the behaviour of high voltage tests were among the factors contributing to the variation of test results from different laboratories participating with the studies of IEEE. Despite this, several standards and recommendations for artificial polluted tests exist [4].

1.6.1 Inclined plane test

One of the experiment to test the resistance to tracking and erosion for polymeric insulator is the Inclined Plane Test, in which rectangular samples are subjected to a voltage application and the behaviour of the material is studied.
The reference standard is the IEC 60587[1], in which all the parameters to set the ageing unit for carrying out the test are specified.
A pollutant is dissolved in distilled water and it is applied to the specimens, allowing a surface discharge to develop. The leakage currents from the samples are acquired and a visual monitoring system is set to record the data images.
A software controls the machine and the voltage application, furthermore it stores the data on a PC disk drive.
This test is deeply descripted below in the thesis.

1.6.2 Rotating wheel dip test (RWDT)

The reliability and the safe operation of the power transmission lines and distribution networks are greatly affected by the performance of the outdoor insulation. For this reason, it is crucial to study the influence of outdoor insulators on high voltage systems. The rotating wheel dip test (RWDT) is one of the most commonly used methods of investigating the performance of high voltage insulators.
Based on the standard IEC 62730 [23], RWDT has been considered as a screening test in order to identify any material or design unsuitable for use in overhead transmission lines. The standard also specifies the principal operation and test conditions required to examine four-shed polymeric insulators under the rotating wheel dip test.

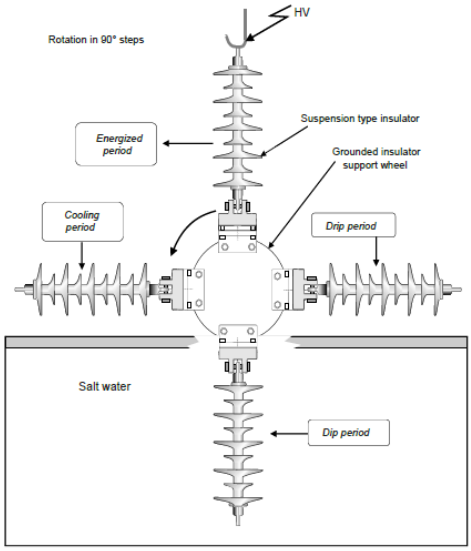

Figure 1.9: RWDT scheme

1.6.2.1 Rotating wheel dip test set-up and facilities

A Rotating Wheel Dip Tester was designed and constructed in accordance with IEC 62730 standards [23]. The apparatus was designed to be able to accept AC and DC voltages.
Figures 1.10 and 1.11 show the circuit diagram and the arrangement setup of the RWDT test.
The Ferranti high voltage 7.5 [kVA], 100 [kV] step-up transformer was fed from the 220[V] mains supply voltage through a voltage controller, an isolating transformer, and a low-pass LC filter. For DC tests, the Glassman WX15P70 Series DC source was utilised to provide 1 [kW] of output power with a voltage up to 15 [kV] and a current of 70 [mA]. A 2 rpm DC permanent magnet motor with a Single Pole Single Throw Normally Open (SPSTNO) relay was used to attain the rotational movement of the test insulators. The tank used for the salt solution was made of a glass reinforced plastic (GRP) material with dimensions of (1.6[m] x 0.25[m] x 0.75[m]). The voltage and current transducers

consisted respectively of a voltage divider with a ratio of 3750:1 and a 200 [Ω] shunt resistor for current measurement. The voltage and current signals were acquired using a computerized data acquisition system. For this purpose, a data acquisition (DAQ) card (MIO-16E series) was used, and its input was protected using a three-stage overvoltage protection system.

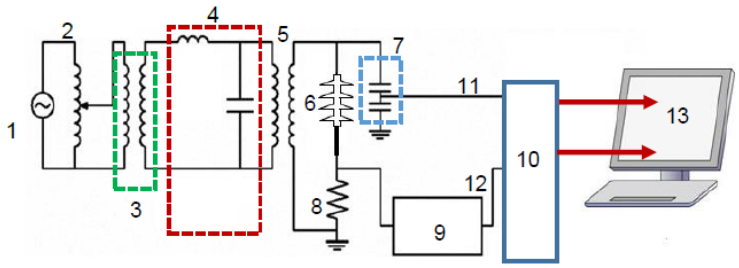

(1) 220V/main supply
(2) Variac
(3) Isolating transformer
(4) (L-C) Filter
(5) 100kV step-up transformer
(6) SiR insulator
(7) Voltage divider
(8) 200 Ω resistor
(9) Over-voltage protection system
(10) DAQ card system
(11) Voltage signal
(12) Leakage current signal
(13) PC

Figure 1.10: Circuit diagram of RWDT.

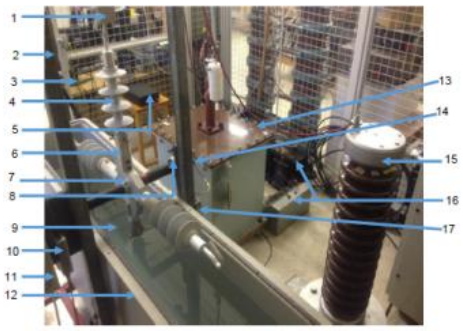

(1) HV electrode
(2) Frame
(3) DAQ card system
(4) SiR insulator
(5) Protection unit
(6) Insulator mounting
(7) Aluminium wheel
(8) Ring
(9) Salt water (NaCl)
(10) (SPSTNO) relay
(11) DC motor
(12) GRP tank
(13) Step-up transformer
(14) Carbon brushes
(15) Voltage divider
(16) (L-C) Filter
(17) resistor

Figure 1.11: Test set-up of Rotating Wheel Dip Test on 11kV polymeric insulator.

1.6.3 Fog chamber test

The most widely used method for evaluating the tracking and erosion resistance of polymeric insulators is the salt fog test. The salt fog test simulates wet and polluted conditions by exposing samples to the combination of high voltage and saline fog.
A salt fog chamber typically consists of a corrosion resistant chamber into which salt water is atomised, usually using compressed air atomiser nozzles as specified in IEC publication BS EN 60507. [4]

1.6.3.1 The fog chamber

The chamber is situated in one of the three high voltage cages subdividing the laboratory at Cardiff University. The safe access to the cage is secured by an interlock system that interrupts high voltage supply until all precaution measures have been followed. The chamber shell is made of polypropylene and the dimensions are 2[m] x 2[m] x 3[m]. An earthed aluminium mesh covers the chamber floor and beneath is a collection sump for accumulated water due to condensation. The sump is drained with the help of a pump. Access to the fog chamber is possible through a transparent door made of polycarbonate. The door has a rectangular opening at approximately the height of the tested sample to allow the visual and infrared cameras to record during the test. Three pairs of spray nozzles supply the chamber with uniform fog: two pairs are located at the opposite corners of the chamber and one pair is situated on the chamber floor. An external control panel situated outside the fog chamber cage controls the fog supply. The panel consists of controls to adjust the air pressure,
the water flow rate and the spray nozzles. Indicators of the air pressure and the water flow are also installed.
The high voltage supply enters the fog chamber from the chamber ceiling. A vertical aluminium tube with stress rings at both ends, serves as the high voltage conductor. Different types of insulator terminals (cap, pigtail) can be mounted by using the appropriate mounting extension. The test sample is earthed by connecting the lower terminal at the earthed mesh. Measurement coaxial cables also have access through the lower side of the chamber walls.

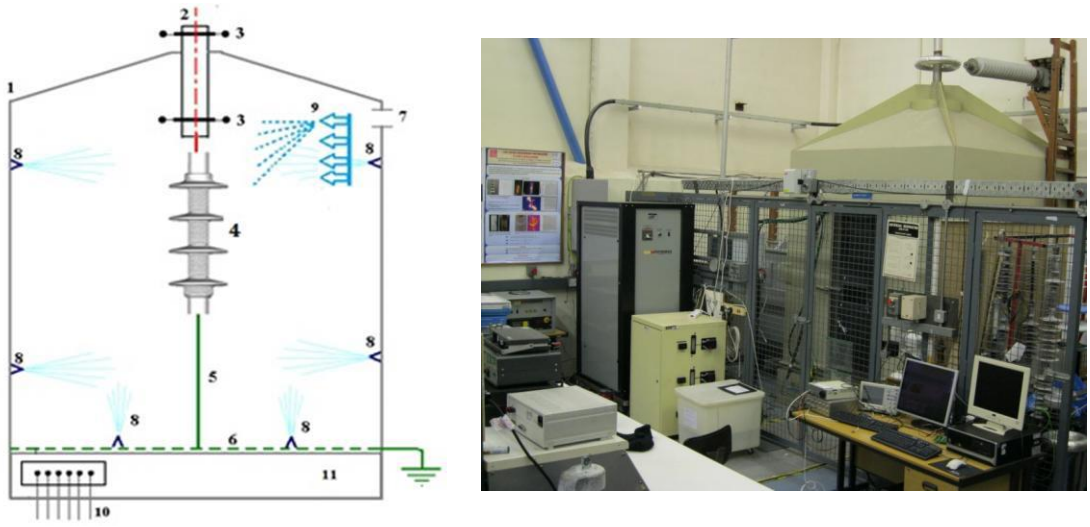

Figure 1.12: schematic layout of Cardiff University fog chamber (left), test set-up of fog chamber tester (Cardiff University High Voltage Laboratory) (right).

CHAPTER 2

Fabrication of new samples

To study this specific argument particular specimens have been used for the tests. The related guideline is the IEC 60587:2007 [1]. In this document adopted by the IEC dimensions and shape of the rectangular samples are specified.
It's reported:
"Flat specimens with a size of at least 50 mm X 120 mm shall be used. The preferred thickness shall be 6 mm. Other thicknesses may be used, but must be mentioned in the test report. The specimens shall be drilled as shown in Figure ##, to attach the electrodes"

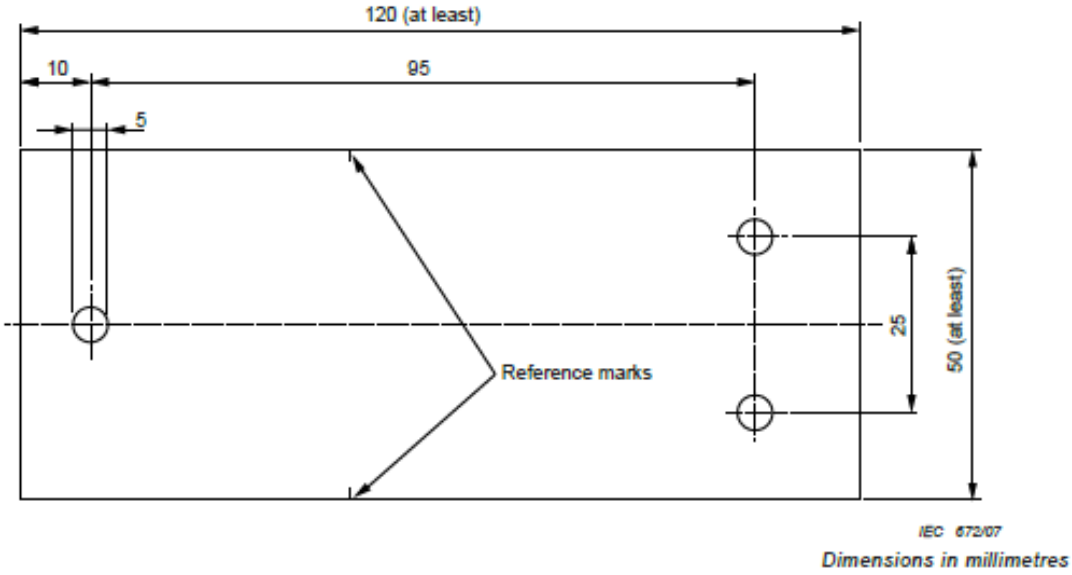

Figure 2.1: sample dimension

All the samples created in this project case had dimensions: 120 x 50 x 6 [mm].
In figure 1.14 are reported the mold ceiling on the left and the depth of 6 [mm] on the right. The material was let flowing through the ceiling thanks to the big central hole that can be seen on the bottom. The two small venting channels above were useful for silicone rubber's leak when the mold was full, ensuring the completely filling of the cavities. The element on the right side was used to ensure the minimum of 6 [mm] for the depth of the sample. It can be seen a cavity used in the past to fill the mold from a vertical position. For my purpose this cavity was closed with a special glue hard stopper avoiding the leak of material from this tunnel, because the mold was filled up in horizontal position.

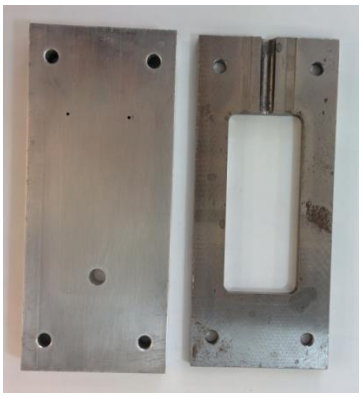

Figure 2.2: mould ceiling and depth

To close the mold several bases have been used in according to the samples type I had to build. More specimens have been realized in according to the study purposes, both conventional and textured.
As reported below in table 2.1 the surface types used for building the different specimens can be seen.
All the mold kinds available in the Cardiff laboratory were manufactured using a computer numerical control (CNC) machine at the Mechanical Laboratory. They are shown below, someone also outside the scope of this work.

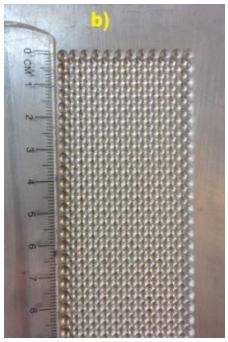

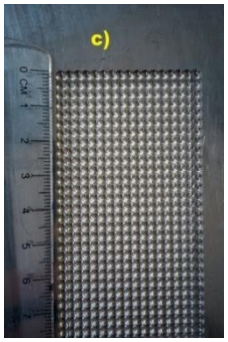

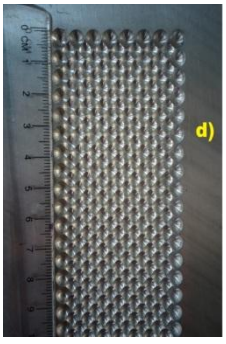

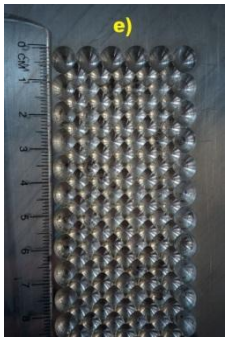

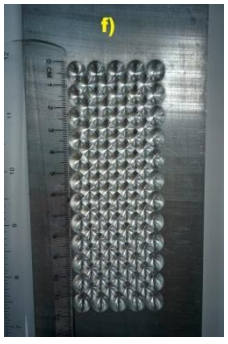

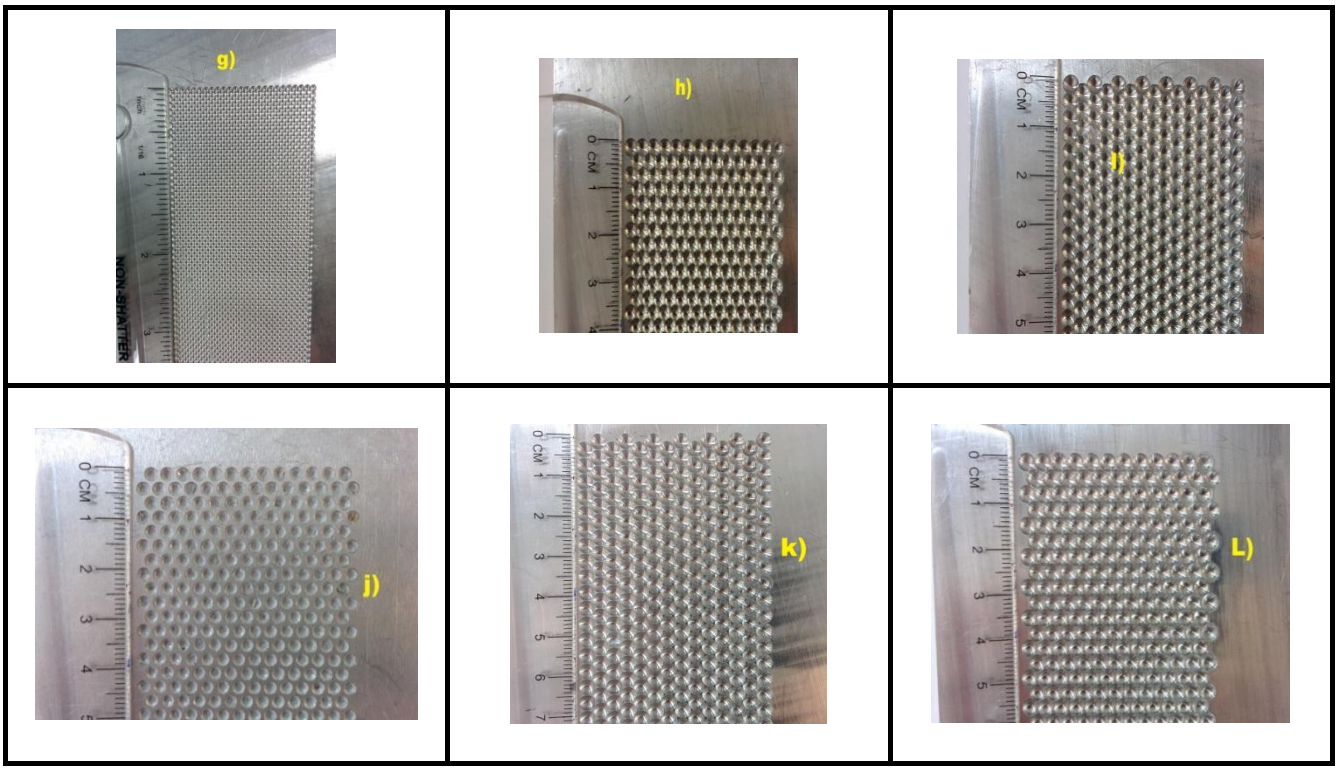

Table 2.1: a) Conventional, b) Square 4 mm type 1; c) Square 4 mm type 2; d) Square 6 mm; e) Square 8 mm; f) Square 10 mm; g) Square 1/16 inch; h) Hexagonal 4 mm type 1; I) Hexagonal 4 mm type 2; j) Round not intersecting 2,5 mm; k) Round 4 mm type 1; L) Round 4 mm type 2.

The mold had to be cleaned with the propan-2-oil before using to avoid impurities go inside because their presence most likely modify the fabrication. The same agent was applied to the specimens before the experiments started in the inclined plane test (IPT) machine to ensure a correct evaluation of the electric parameters without modifications due to impurities.

Furthermore a spray (silicone release agent S3) was applied to avoid the upper part of the mold to paste on the bottom surface and to allow an easily opening at the end of the warming-up in the oven.
After these preliminary operations the mold was closed with four bolts and was ready to be used inside the vacuum casting machine.

2.1 Vacuum casting machine

The MCP vacuum casting machine is the appliance used to fabricate the specimens.
The Advanced High Voltage laboratory at Cardiff University was furnished with the 5/01 model, manufactured in 2006. The operating voltage is 240 [V] single phase and the absorbed current is 7,5 [A]. A touch screen allowed the control of the operations.
With this machine all the samples used during the tests were manufactured.
It has two different chambers which can be connected together or keep them separately by a control valve which isolate them, allowing different pressure levels in the two parts.
Thanks to the touch display it was possible to insert the parameters we need and it

allows us the control of the machine.
In the upper chamber there are two different cups (A and B) for the material restraint. We used only the B one and keep the materials stirred by a palette with three different speeds in according to our needs.
The connection between the upper chamber and the lower one was made possible by a rubber pipe in which the material flowed to join the mold.
The chambers are kept in vacuum (0 [bar]) thanks to a pump controlled by the user through the touch display (figure 2.3).

Figure 2.3: touch display of the vacuum casting machine

The function buttons are described hereafter:

RESET: to reset the machine when it doesn't work or to restart it when it's blocked;

RUN: pressing it the palette starts to mix the material inside cup B, with three different speeds according to our needs;

STOP: the button that allows to interrupt the operations if there are any problems;

UP/DOWN CUP A/B: these four buttons are used to overthrow the cups A in B and B in the mold respectively. With the UP buttons we can restore the initial position of the cups after the material is completely flowed down;

SPEED: to set up the speed of the mixing palette in according to the timing of the operations;

LEAK: touch buttons to restore the pressure inside the chambers. There are two of them, one for the upper chamber (slow) and one for the lower chamber (fast);

PUMP: is the touch button which allow to start and stop the pump to ensure vacuum;

ESC: with this button it is possible to return to the previous page to select the operating mode of the casting machine.

Two timers that indicate the timing of the total operation and the time of mixing by the palette in the CUP B are also present and an indication of the chamber pressure is expressed.
In figure 2.4 the front panel of the machine during operation can be seen: the rectangular mold is optimally positioned thanks to an height regulator.
From this image the two separate chambers and the touch display can be distinguished.

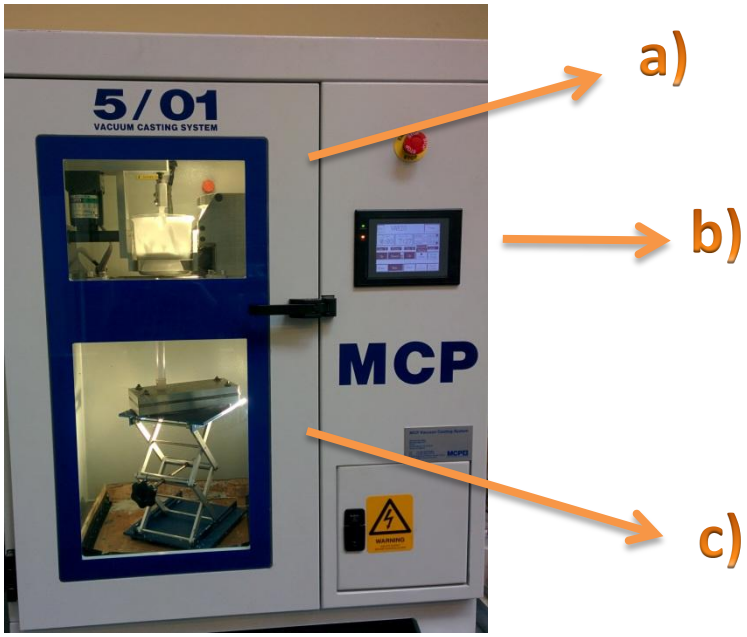

Figure 2.4: a) upper chamber; b) touch display; c) lower chamber.

To set up the vacuum casting machine and to mixing the material a procedure has to be followed to avoid mistakes and to obtain acceptable specimens. The steps are the following:

- Selection of VARIO VAC (Manual Control of Vario Casting) MODE;
- Check that Cup A and Cup B are in UP position and the BALANCE VALVE is OPEN at the beginning;
- Push RUN button to activate the mixer with the palette on the upper chamber in cup B;
- Adjuste the speed to 1 (2 minutes), 2 (5 minutes) and 3 (3 minutes);
- Meanwhile start the PUMP with the dedicated button for the degassing;
- Meanwhile press the DOWN button for cup A (this is done to allow the operations to proceed even if cup A is empty);
- Push the button DOWN for cup B;
- Close the “Balance Valve” (to separate the upper and the lower chambers);
- When the valve is closed set about 42 [mb] of pressure in the upper chamber in order to facilitate the material’s flow;

- As soon as the material flows from the small holes made for the spillage of the silicone, restore the 0 [mb] on the upper chamber;
- STOP vacuum pump;
- OPEN the valve (wait until the blue light is fixed);
- Restore the pressure inside the vacuum machine following the order SLOW UPPER and, after some seconds, FAST LOWER;
- Open the door (when the pressure is restored at 1000 [mb] as the atmosphere pressure) and put the mould in the oven at 50 Celsius for 6 [h].
  In this work during the specimens' manufacturing the material was direct inserted in the cup B avoiding the material losses in cup A cause its stickiness. However the button CUP A DOWN has always to be pressed to enable the following logical steps of the procedure.

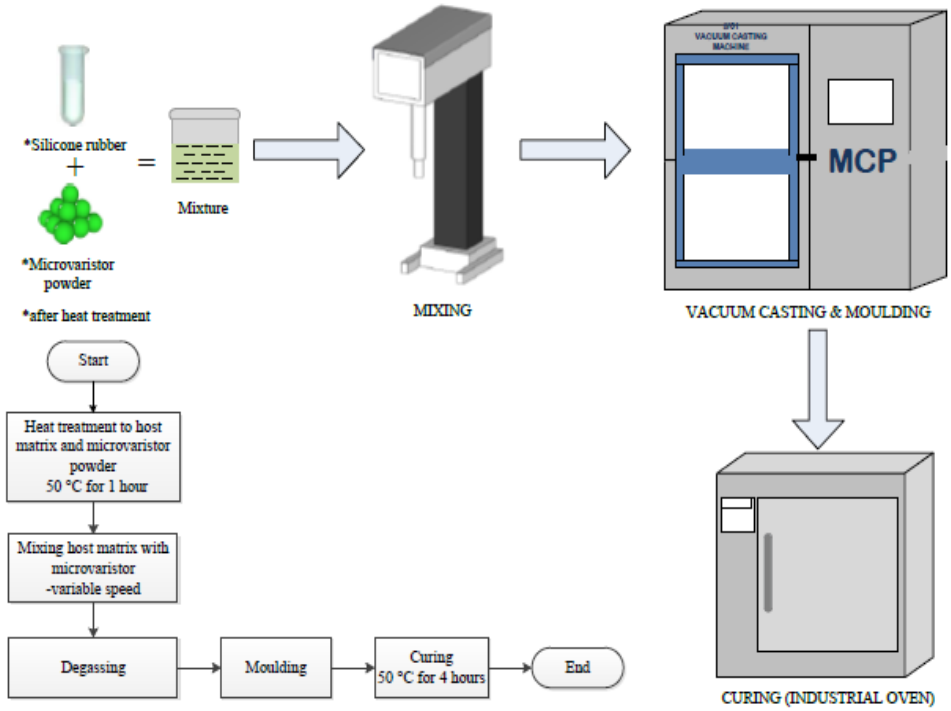

Figure 2.5: operations' schematic to produce the specimens.

The sample preparation process for silicone rubber and catalyst was carried out using a precision digital balance scale (KERN ABJ 320-4 that operates to maximum capacity of 320 [g] with readability of 0,1 [mg]), two iron spoons and various laboratory glasses for weighing and mixing the two materials.



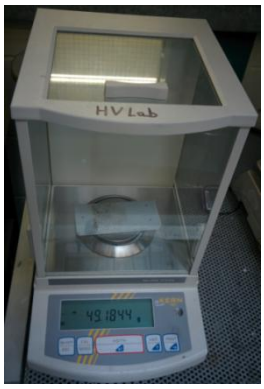

Figure 2.6: a) spoon, b) normal scale, c) precision scale

The first image is reported just for curiosity: from it the silicone rubber property of hydrophobicity can be noted, in fact the spoon has been used to manipulate the rubber for the weighing and its surface was still impregnated with the material. It can be noticed a contact angle greater than 90^{O}.

In the central image the plastic containers used to weight the materials are shown. The internal one was made of light plastic instead the external one of hard plastic to ensure a robust assembly in the machine. The scale shown on the right allowed the precision weighted of the samples after they have been made. In figure a textured sample was weighted (the approximate weight is 50 [g]).

2.2 First sample fabrication

To make the rectangular 120 x 50 x 6 [mm] specimens the white silicone rubber Powersil 600-A type was used, mixed with the catalyst Powersil 600-B (grey color) reported in fig. 2.7.
The main properties of these components are reported in table 2.2 [25], where is also specified the referred inspection method used to carrying out these characteristics.

Materials	Properties	Inspection method	Value
Silicone rubber POWERSIL 600 A/B	Relative permittivity	IEC 60250	2.9 Ɛr
	Density	IEC 1183-1 A	1.13 g/cm^3
	Volume resistivity	IEC 60093	10 x 10^{15} Ω*cm
	Elongation at break	ISO 37	500%
	Viscosity of mix at (shear rate 10 s^{-1}	ISO 3219	10000 $mPa * s$
Hardness Shore A		ISO 868	30
Pot life at 23 °C			70 min
Tensile strength		ISO 37	8 N/mm²
Tear-strength		ASTM D 624 B	22 N/mm

Table2.2: material properties of silicone rubber and microvaristor powder.

The ratio between the materials used to fabricate the samples is 9:1, where for 9 parts of 600A 1 part of the catalyst 600B was added.
It is already supplied in the correct ratio in big containers of 4,5 [kg] for the 600A and 0,5 [kg] for 600B from Wacker Chemie, a German company.

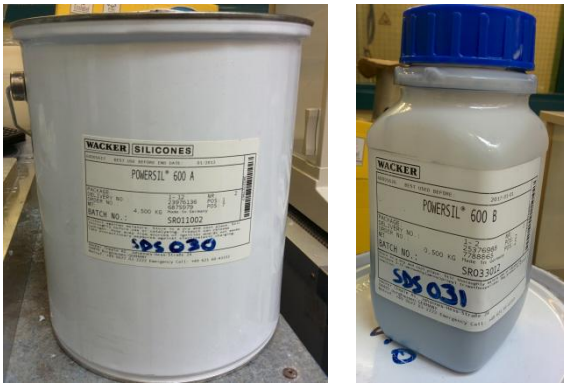

Figure 2.7: Powersil 600A and catalyst 600B

The vases has to be kept correctly close and stored in a dry space avoiding the material to dry and consequently to waste. In figure 2.8 the content components can be seen.

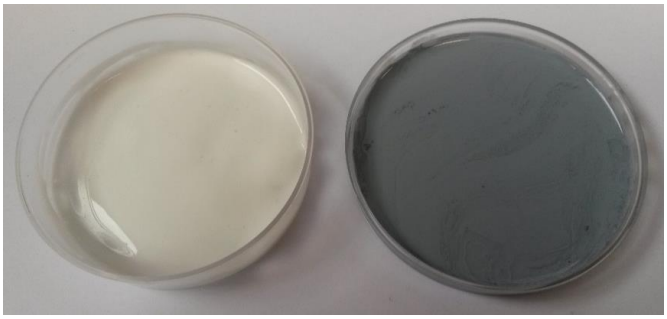

Figure2.8: the white silicone rubber, Powersil 600-A (host matrix) on the left and Powersil 600-B (catalyst) on the right.

Every sample realized during this project was made with the same standard ratio and the materials were mixed together manually with a spoon to facilitate the amalgamation. After the second realization an improvement was carried out heating the cup with the two components in the oven for few minutes at 25-30 [°C] allowing the compound to be less dense facilitating the mixing. The spoons had to be different for the two components to don't contaminate the other material in the vase.
The first specimen has been fabricated with 114 [g] of silicone 600A and 12.7 [g] of catalyst 600B.[2]
To weigh the components a scale with the sensibility of 1 [g] was used (figure 2.6b).

Figure 2.9: first specimen

[2] *This weight also includes the material used to fabricate another sample for different purpose used by a PhD student for his research. The weight of a rectangular sample is approximately 40 [g] for the conventional and about 50 [g] for the textured.*

2.3 Procedure

The process to make the samples is one of the so called *room temperature vulcanizing* (*RTV*)[3] technique.
When the components were weighted and positioned in the vacuum casting machine the standard procedure reported above was followed.
For the first fabrication the palette was let working for 7 minutes at speed 2 and for 3 minutes at speed 3. During all the makings the time was changed varying the speed of the palette and the respective duration with the aim to find the best compromise concerning the final sample result.
It has been noticed that more time the compound was mixed, better was the flowing out from the pipe.
When the material was satisfactory mixed, cup B was overturned and the valve was closed. The pressure in the upper chamber was increased at 42[mb] instead the lower one was maintained at 0 [mb], through the "Slow UPPER" button on the right side. This was performed to push down the material through the pipe in to the mold.
The operation was repeated two or more times after the first increment until the material was flowing through the venting holes in the upper surface of the mold ensuring a complete filling. In fact air bubbles inside the mold at this time would be unacceptable for a good result of the specimen.
To stop the material flowing the connection between the two chambers was restored trough the "Balance Valve" button. To ensure the complete opening of the valve a sufficient time had to be waited until the indication point is fulfilled with a blue color indicating the end of the operation.[4]
At the end of the procedure the mold was put in the oven at a temperature of 50 [°C] for 6 [h] of time: this operation allowed to enhance the speed of the solidification process of the rubber. Later, it was left at room temperature for another 24 [h] to ensure that the silicone cross-linking process has been completed.

[3] *Vulcanisation is a chemical process for converting natural rubber or related polymers into more durable materials by the addition of solfur or other equivalent curatives or accelerators. These additives modify the polymer by forming cross-links (bridges) between individual polymer chains. Vulcanized materials are less sticky and have superior mechanical properties.*

[4] *Another improvement to the standard procedure was to keep the pump "ON" during all the operations turning it "OFF" only when the mold was completely full of material.*

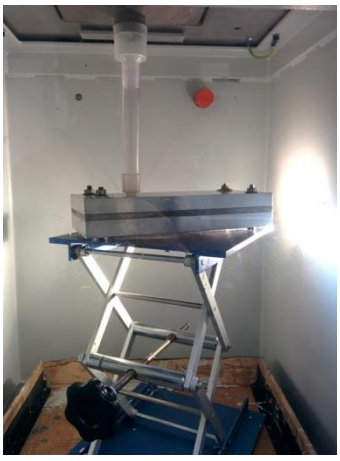

Figure 2.10: mould of 120x50x6[mm] sample during the operation of vacuum casting, lower chamber.

Figure 2.11

The first specimen was a conventional type and the result of the fabrication was very good. The shape was checked and was verified that it didn't present defects or particular irregularities[5] (figure 2.9).
The second specimen is a 4 [mm] textured with a square arrangement realized with another circular sample for a different research project. The employed quantities were the following: 160 [g] of 600A silicone rubber and 18 [g] of 600B catalyst. With this manufacture it has been noticed that we have to control the mold position before the closure because it was not well centered resulting in a non-symmetrical specimen (the space on the right was not the same on the left causing possible different behaviors during the electric test).
However, this was assumed as negligible because the electrodes are positioned centrally in the sample, so the boundary does not influence the test results.
The mold opening was tricky so it was considered that the release S3 spray should have been applied in a different way to facilitate the operations.

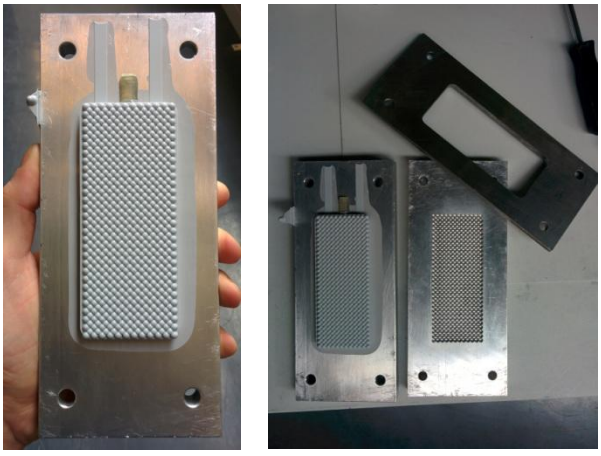

Figure 2.12: mould opening

[5] *The specimen for other purpose built in parallel to this was satisfactory as well, this ensured the correctness of the operations.*

Twelve rubber samples have been made following the same procedure, with the improvements that were discovered increasing the experience.
A brief description of them is reported below.
The third sample was a 6 [mm] textured square arrangement type realized with (figure 2.13):

- 110 [g] of 600A;
- 110/9≈12 [g] of 600B.

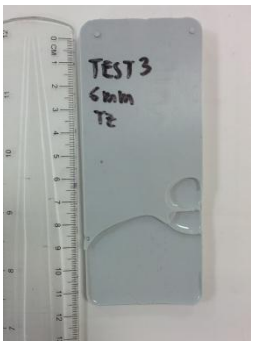

Figure 2.13

The alterations of the quantities were set up to use as less material as possible for the high cost (200£/box) of it avoiding big wastes.
During the production of this piece the air bubbles flowed inside the casting bringing to a bad result on the sample surface.
Operations such as opening the door of the machine and not extracting all the air must be avoid. Another error would be setting up the pressure in the upper chamber too high in respect of the 42 [mb], since it would result in pushing down air bubbles through the pipe inside the casting.
All these operations have to be carefully carried out because an error could produce an imperfection or a cavity that brings to reject the sample making it useless for the inclined plane test.
It would represents also a waste of time in case is required a big number of samples to be tested together because every specimen produced requires at least one day to be ready for the tests.
The fourth sample was a 6 [mm] textured square arrangement type with (figure 2.14):

- 70 [g] of 600A;
- 70/9=7.78 [g] ≈8 [g] of 600B.

Figure 2.14

The fabrication result was a specimen not completely full of material, presenting a lack on the bottom part of it. This is due to an error on the calculation for the material weight which was used to fabricate the sample, with the purpose to find the lower amount of material to reduce the waste.
It was the first specimen realized alone.
The fifth one was again 6 [mm] textured square arrangement type with (figure 2.15):

- 140 [g] of Powersil 600A;
- 140/9≈15.5 [g] of Powersil 600B.

The result was acceptable, the mold was full without irregularities.

Figure 2.15

The sixth was a 6 [mm] textured square arrangement type composed by:

- 145 [g] of 600A;

145/9≈16 [g] of 600B (figure 2.16).

Figure 2.16

Also this realization was performed good and the result was acceptable.
The seventh specimen was a conventional type with (figure 2.17):

- 100 [g] of 600A;
- 100/9≈11 [g] of 600B.

Figure 2.17

The eighth was a 4 [mm] textured square arrangement with (figure 2.18):

- 145 [g] of 600A;
- 145/9≈16 [g] of 600B.

Figure 2.18

The result was a specimen with a small hole on the back surface caused to an air bubble that flowed inside the cast during the operations.
For this reason was decided to keep it apart and not testing it soon.
Eventually, testing that piece was possible, but it has to be reported at the end of the experiment specifying location and depth of the cavity.
This gave the idea to test it in the IPT apparatus as a modified analysis that could be encountered from an isolator in service.
The ninth was a 4 [mm] textured square arrangement with (figure 2.19):

- 105 [g] of 600A;
- 105/9≈11.5 [g] of 600B.

Figure 2.19

Also this sample was affected by an air bubble on the back surface probably because the time for the casting degasing was not sufficient.
The tenth was a conventional one with (figure 2.20):

- 120 [g] of 600A;
- 13 [g] of 600B.

Figure 2.20

In this case the time left for the material degasing was increased resulting in a good final result: all the surfaces were perfectly graven.
The eleventh was a 6 [mm] textured square arrangement with (figure 2.21):

- 105 [g] of 600A;
- 105/9≈11.5 [g] of 600B.

Figure 2.21

The twelfth sample was a 4 [mm] textured square arrangement without other molds casting together.
It was composed by (figure 2.22):

- 100 [g] of 600A;
- 100/9≈11 [g] of 600B.

Figure 2.22

Also this specimen was acceptable and ready to be used in the electric inclined plane test appliance.

The initial procedure has been improved so far, resulting in better samples produced. The main change is the degasing time, which has been increased of about 4 minutes for a rectangular specimen, avoiding air bubbles inside the cast. The other important improvement is that all the procedure has to be performed with the pump "ON" and not only during the mixing: this helps the extraction of the air from the material, also from the lower chamber, when it is on the mold.

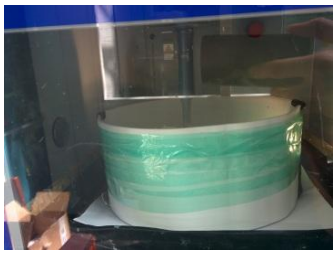

Figure 2.23

The improvements were reached also thanks to the large number of castings we made. Just for curiosity it's reported the manufacture of an entire brain for a bio engineering purpose.
This had been helpful for learning some tricks about the casting of the full insulators I performed because to build big pieces it is needed to make more castings restoring the atmosphere pressure more times and always avoiding air bubbles inside. The main difficulty is when the pressure is restored the air flows inside the material which is already in the mold, the subsequent extraction requires more time to end up with an acceptable insulator.

CHAPTER 3

Inclined Plane Test

3.1 Standard IEC 60587:2007 [1]

According to IEC 60587, the inclined plane test is one of the classical methods to evaluate the resistance of rectangular silicone rubber samples to tracking and erosion under HV stress in severe ambient conditions at a power frequency of 50 [Hz].

The standard, after the specifications regarding the shape and the dimensions of the test samples that brought to the previous fabrication, specifies the electric apparatus and the contaminant which has to be used to fix a standard and allow comparisons among experiments made in different laboratories around the world.

The contaminant should be composed by:

– 0,1 % ± 0,002 % by mass of NH4Cl (ammonium chloride) analytical quality;
– 0,02 % ± 0,002 % by mass of isooctylphenoxypolyethoxyethanol (a non-ionic wetting agent) in distilled or de-ionized water.
This contaminant shall have a resistivity of 3,95 [Ωm] ± 0,05 [Ωm] at 23 [°C] ± 1 [°C] and shall be not more than four weeks old and its resistivity shall be checked before each series of tests.
Eight layers of filter-paper with a thickness of 0,2[mm] ± 0,02[mm] are clamped between the top electrode and the specimen.
The rate of application of contaminant shall be that within ± 10 [%] specified in Table 3.1 in relation to the applied voltage.

The steel electrodes are descripted with particular attention to the dimensions and the shape to allow a perfect installation on the specimens. The upper one has an arrow shape and has to be curved to ensure the fitting of the filters, instead the ground electrode is flat with several semi-circular irregularities on its border.

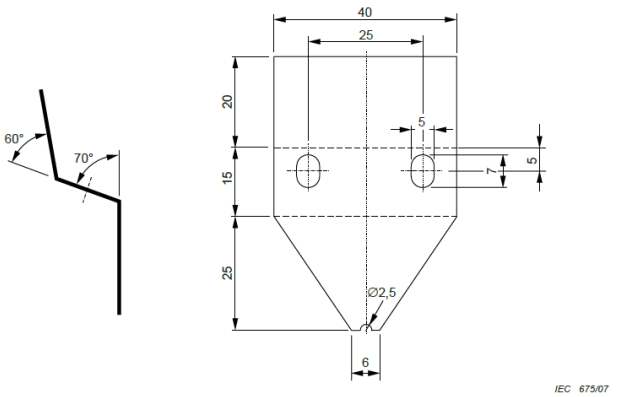

Dimensions in millimetres

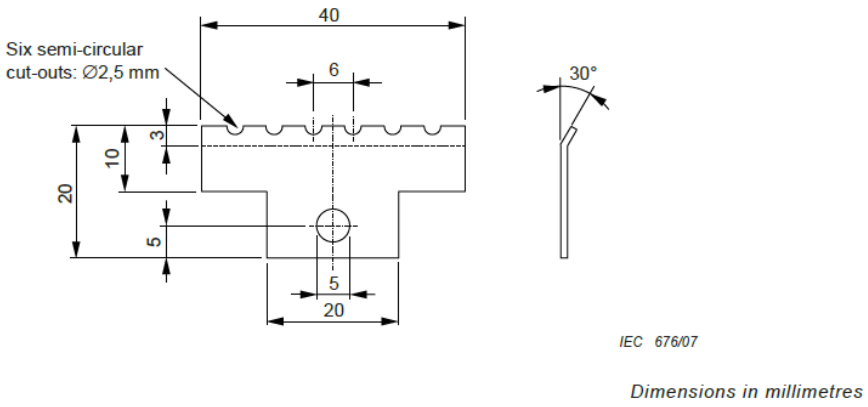

Figure 3.1: electrodes dimensions, a)upper, b)lower. [1]

The leakage current we're interested to measure will flow from the top electrode to the lower one through the silicone rubber surface.

In the high voltage electrode eight filter papers has to be installed. Their shape is indicated in figure 3.2 and they serve to act as a reservoir for the contaminant ensuring a constant limited flow of the water with the pollutants as specified in Table 3.1.

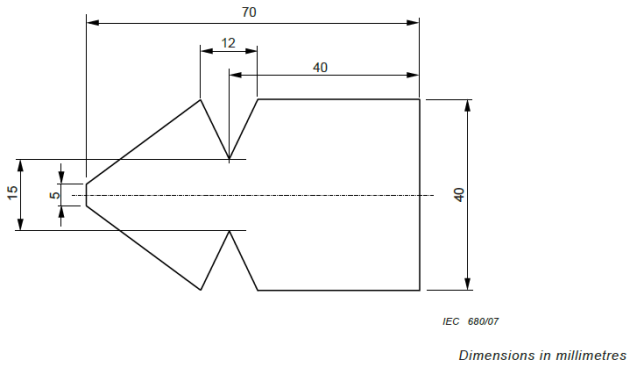

Figure 3.2: filter paper dimensions [1]

Unless otherwise specified, the test shall be carried out at an ambient temperature of 23 [°C] ± 2 [°C] on sets of at least five specimens for each material.
Mount the specimen, with the flat test surface on the underside, at an angle of 45° ± 2° from the horizontal as shown in figure 3.3, with the electrodes 50[mm] ± 0,5[mm] apart. The test for further five specimens can be achieved either simultaneously or respectively.

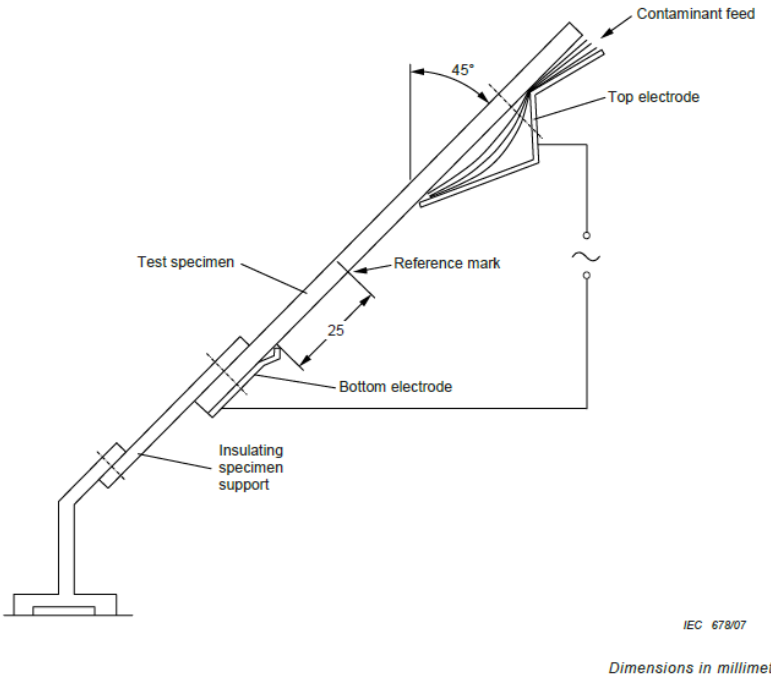

Figure 3.3: sample assembly on the test bay at inclined position of 45° [1]

If the specimen is not self-supporting an insulating mounting support for the specimen must be used.

The mounting support shall be such that the heat dissipation from the back of the sample is not hindered and the material shall be heat resistant and electrically insulating (e.g. PTFE).

An example of a mounting support is shown in Figure 3.4.

Start introducing the contaminant into the filter-paper pad allowing the contaminant to wet the paper thoroughly.

Adjust the contaminant flow and calibrate to give a flow rate as specified in Table 3.1.

Observe the flow for at least 10 min and ensure that the contaminant flows steadily down the face of the test specimen between the electrodes.

The contaminant shall flow from the quill hole of the top electrode and not from the sides or the top of the filter-paper.

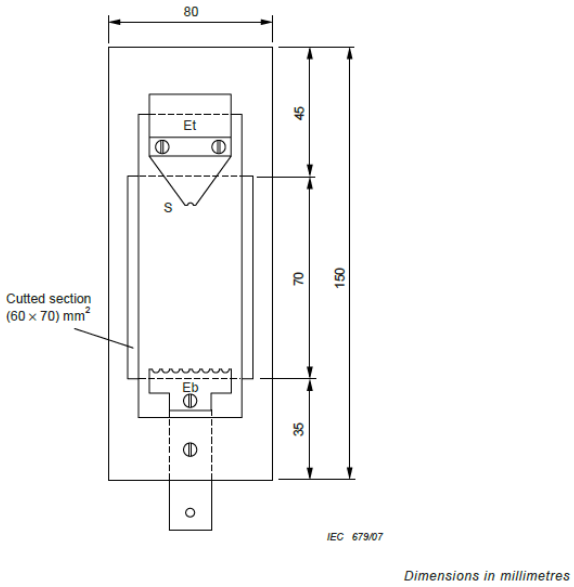

Figure 3.4: mounting support [1]

Tests have to be conducted following one of the two methods specified:

- Method 1: application of constant tracking voltage;
- Method 2: application of a stepwise tracking voltage;

and must be reported which one has been used.
The first implies to fix a constant voltage among the available values 2,5-3,5-4,5 [kV] reached in a maximum of 10 [s], apply it on the samples and keep it constant until one of the end point criteria is reached.
The second implies to apply an initial voltage on the sample and increasing it of multiples of 250 [V] for each hour until failure.
This method involves also an adaptation in the machine parameters increasing the voltage. Two end-point criteria are descripted:

- Criterion A[6]: the end point is reached when the value of the current in the high voltage circuit through the specimen exceeds 60 [mA] (an overcurrent device then breaks this current not before 2 [s], but not later than 4 [s]) or when a specimen shows a hole due to intensive erosion or the specimen ignites.
- Criterion B: the end point is reached when the track reaches a mark on the specimen surface 25 [mm] from the lower electrode or when a specimen shows a hole due to intensive erosion or the specimen ignites.

At the end of each test a report has been made: it shall include the material type, the details of specimens with thickness, orientation, the voltage application method and the maximum depth of erosion.

[6] *The A criterion without burning is the preferred criterion.*

3.2 Inclined plane test facilities

The inclined plane test facilities consist of three main parts: an accelerated ageing unit, a voltage and current measurement equipment and circuit, including an acquisition system (DAQ) consisting of a LeCroy digital oscilloscope (DSO) and a desktop computer with National Instruments PCI-6254 data acquisition board for running and controlling the LabVIEW program, and a monitoring system including a Sony Handycam visual camera, a thermal infrared camera and a fast camera to visualize the sparks slow motion movement on the silicone rubber surface.

3.2.1 The accelerated ageing unit

The accelerated ageing unit is a metal enclosure consisting of a test compartment at the top of the unit and the equipment for the high voltage supply and saline contaminant delivery located on the lower shelves of the unit.
The ageing unit is shown in figure 3.5.
In the top the test bays are equipped for holding up to five samples, at a 45^{o} inclined from the horizontal.
The test conditions which are set up in this machine serve to accelerate the production of the effects, not to reproduce all the conditions encountered in real life.
To achieve this scope a repetition of continuous discharges are favorites on the surface samples.

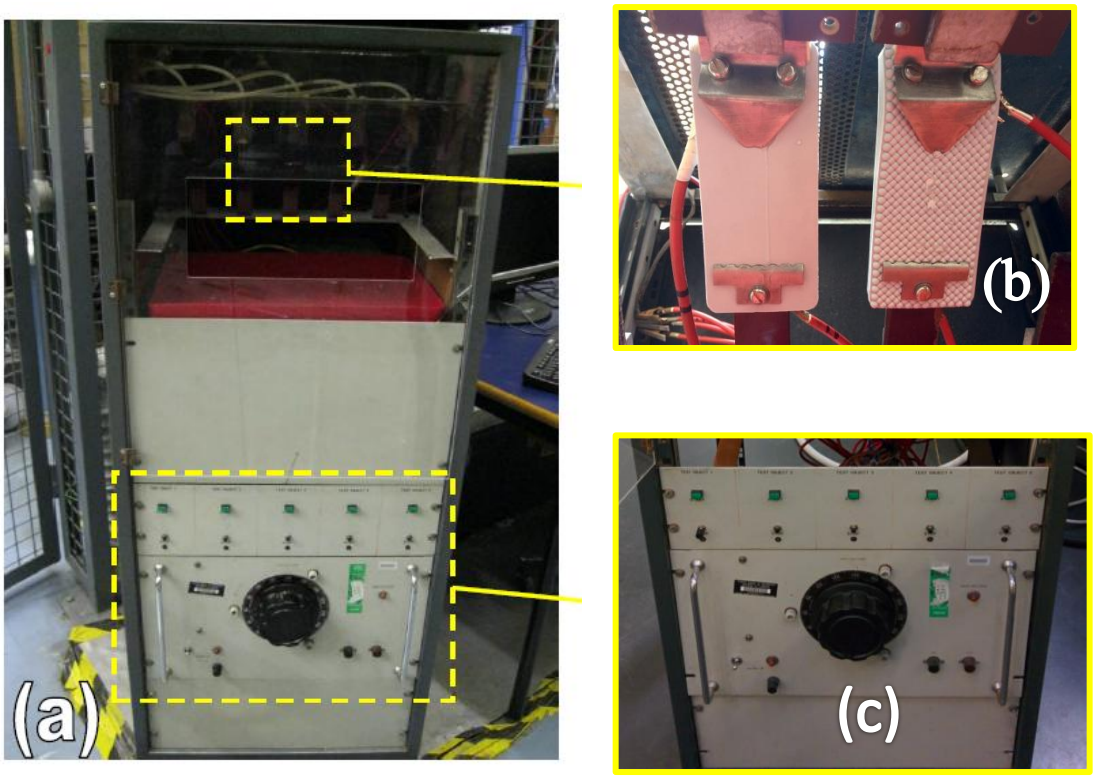

Figure 3.5. The accelerated ageing unit (a), a close-up of a rectangular sample in the test compartment during a test (b) and the HV supply control panel (c).

The photo shows the frontal part of the machine used to perform the IPT. The unit has been developed following the characteristics explained in the related norms.
As can be seen in (b) picture the supports for the 5 testing samples and the respective wirings are positioned in parallel spaced each other to avoid mixtures of the measured currents. The upper red cable, which is connected to the high voltage electrode is the high voltage supply, instead the lower one which is connected to a different shape electrode is the connection to the ground. Under this a tray is positioned for keeping the contaminant and for the eroded material which is deposed during the test. In the same plane the protection box is present. It is used for the connection between the negative electrode cables and the coaxial cables for the leakage currents measurement.
As shown in figure 3.9c the red thick cables which come from the negative electrodes are connected with the quick-blow fuses (250 [mA] – 250 [V]) and the series resistors of 33 [Ω] ± 0,10% (B). In parallel to the resistors the 10 [V] metal oxide disk varistors (MOV) with a breakdown voltage of 22 [V] are connected. If there is a surge voltage they decrease their resistances and all the current passes through them to the ground protecting the resistors of the measurement circuit. The voltage is chopped off at the breakdown level avoiding that dangerous signals are acquired by the SCB-68 card which is projected to work within ±10 [V].
The output (which comes from the upstream connection of the resistors) is connected to the central pin of the coaxial cables.
The shields of these cables are connected together and downstream to the resistors at the ground potential. With this connection we're measuring the voltage drop across the 33 [Ω] resistors to calculate the leakage current thanks to the Ohm's law because in the SCB-68 we can acquire only voltage signals.
Placed under this box there are the power resistors of four different values for each of the five specimens in according to Table 3.1, which is Table 1 in IEC 60587: 1 – 10 – 22 – 33 [kΩ] (figure 3.9f).

Table 1 – Test parameters

Test voltage kV	Preferred test voltage for method 1 kV	Contaminant flow rate ml/min	Series resistor, Resistance kΩ
1,0 to 1,75	-	0,075	1
2,0 to 2,75	2,5	0,15	10
3,0 to 3,75	3,5	0,30	22
4,0 to 4,75	4,5	0,60	33
5,0 to 6,0	-	0,90	33

Table 3.1: Test parameters of the Inclined Plane Test [1]

The switching among these has to be done according to the test voltage applied (2,5-3,5-4,5 [kV]). The set of values are obtained with the parallel/series connections of 1 [kΩ], 5.6 [k Ω] and 6.8 [k Ω] resistors 50 [W] ±5[%]. These are aluminum housed axial wirewound fixed type for chassis mount placed on two different horizontal layers.

These kind of resistors are used for applications which require high precision current measurements due to their high cost. They aren't adapt to transport high power but they are stable ensuring a correct measure of even small current values.
All the connections are moved to a vertical panel that allows us to select the desire resistance by the banana connectors.
The top of the test compartment is slotted to allow natural ventilation and avoid dangerous internal atmosphere with the sparks produced by the current. The ventilation hasn't to be forced because this could modify the test results, inducing a cooling effect on the sample surfaces.
The lower part of the ageing unit is used to place the main board for the operations control and the supply of the machine. A peristaltic Watson Marlow 205S/CA pump [26] and the tank for the contaminant are also present (figure 3.9i).
The pump provides a constant flow of the contaminant from the tank to the surface of the test samples through five parallel pipes. The flow rate can be set from 0,6 [µl/min] to 22 [ml/min]. These two components have been moved outside the vessel to avoid dangerous contact between electricity and liquids.
The contaminant consisted approximately of 1[g] of ammonium chloride and 0.2[g] of Triton-X100 non-ionic wetting agent diluted in 1000[g] of distilled water.
The volume conductivity of the contaminant should be adjusted to 0.253[S/m] and the suspension in the contamination tank was renewed before 4 weeks elapsed.
The pipes bring the pollution to the HV electrodes at the specified rate [ml/m] in Table 3.1 which is modified by the pump speed.
The flow control is possible thanks to the buttons and the display in the upper part of the pump. After some attempts, a linear relation between the rotation speed and the contaminant flow rate has been found, as reported in table 3.2 and in the graph (figure 3.6).

Speed [rpm]	Contaminant flow rate [ml/min]
25	0,6102
23,8	0,577
12,5	0,31405
6	0,14075
6,5	0,1545
6,25	0,146

Table 3.2: contaminant flow rate in relation to the peristaltic pump speed.

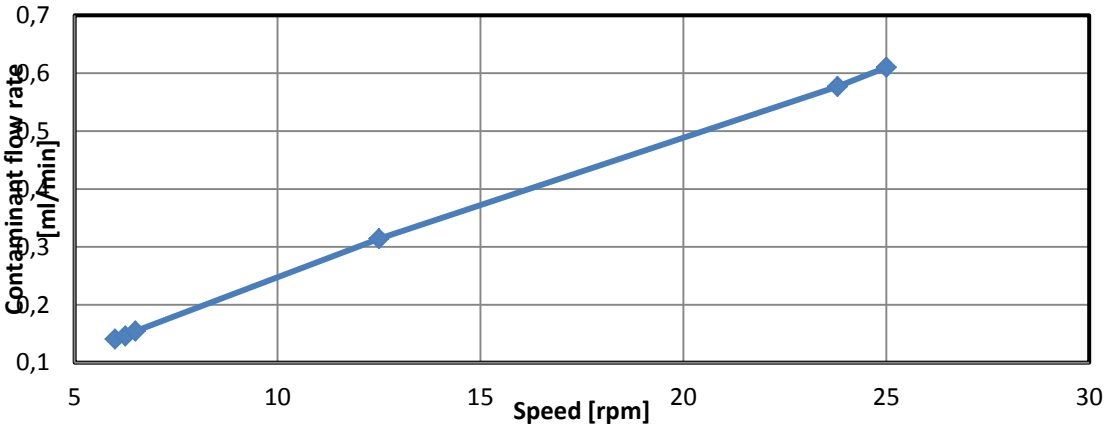

Figure 3.6: graphic visualization of the linear combination between speed and contaminant flow rate.

To find out these values I used two channels of the pump for each measurement.
Afterwards the average between the two has been made and reported in the table.
This to have a medium value because the length of the pipes was different, as well as the resistance encountered by the water in service.
The measurement of the flow rate was possible thanks to the same precision scale used to weigh the silicone rubber (figure 2.6c) which has a sensibility of 0,0001 [g].
Subsequently the weighted values have been converted in [ml/min] according to the table in BS EN 60587:2007.
In the machine front panel (figure 3.5c) there are the old buttons to start and stop the tests on the specimens, now these are bypassed by using the LabVIEW software.
A variac autotransformer allows to modify the voltage supplied by the high voltage transformer connected directly to the electrodes. This was not used during my experiments because the voltage was modified externally to the cage thanks to an HIPOTRONICS control power unit (figure 3.9a) which permits to set up continuously the voltage level to apply to the test system.
Two types of control settings were possible, Manual and Automatic.
The control unit regulates the 240[V]/10[kV], 20[kVA] transformer which supplies the voltage to the IPT unit.

The electric circuit used to carry out the test is the following:

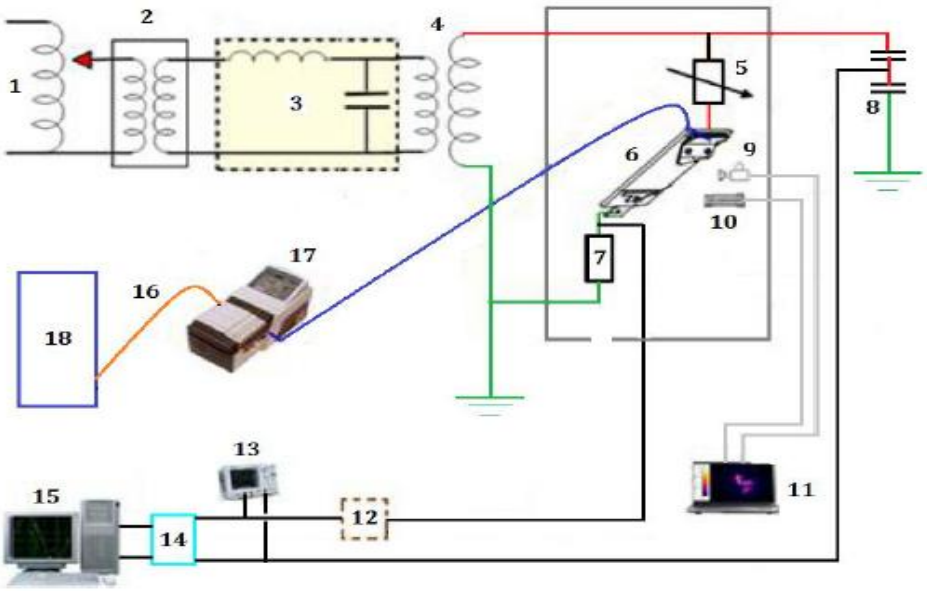

(1) Variac
(2) Isolation transformer
(3) (L-C) Filter
(4) 240/10kV transformer
(5) Variable resistor (1kΩ)
(6) SiR sample
(7) 33Ω resistor
(8) HV probe
(9) Digital video camera
(10) Infrared camera
(11) Laptop
(12) Overvoltage protection circuit
(13) Digital oscilloscope
(14) DAQ system
(15) PC
(16) Orange/White tube
(17) Peristaltic pump
(18) Contaminant tank

Figure 3.7: IPT electric circuit

The power is coming from the main transformer 240[V] / 10[kV] in which the secondary voltage can be regulated external to the interlocked cage.
With an high voltage cable (red in figure 3.7) the resistors are supplied by the connector panel according to the voltage applied (ex. 22[kΩ] for 3,5[kV]), while the output is connected with the high voltage electrode on the higher part of the specimens.
The lower electrodes are connected with the 33[Ω] measurement resistors (7) and from here to the ground as reported in the protection box circuit.
From this point the leakage currents on the specimens can be read and from a Ross Engineering high voltage probe (VD150, VD45-8.3-A-LB-AL, Divider) having 2000:1 ratio (8) the voltage applied on the bays can be read.
This measurements have been acquired as voltage signals from the DAQ system. A PC1 (15) was used to control the tests with LabVIEW and a PC2 (11) to acquire the images from the ThermaCAM and the fastCAM thanks to the FLIR and the Photron softwares installed in this computer.
From the graph the contaminant circuit for one specimen with the peristaltic Watson Marlow 205S/CA pump can be noticed.
More precisely the internal connections of the accelerated ageing unit can be represented in the following scheme:

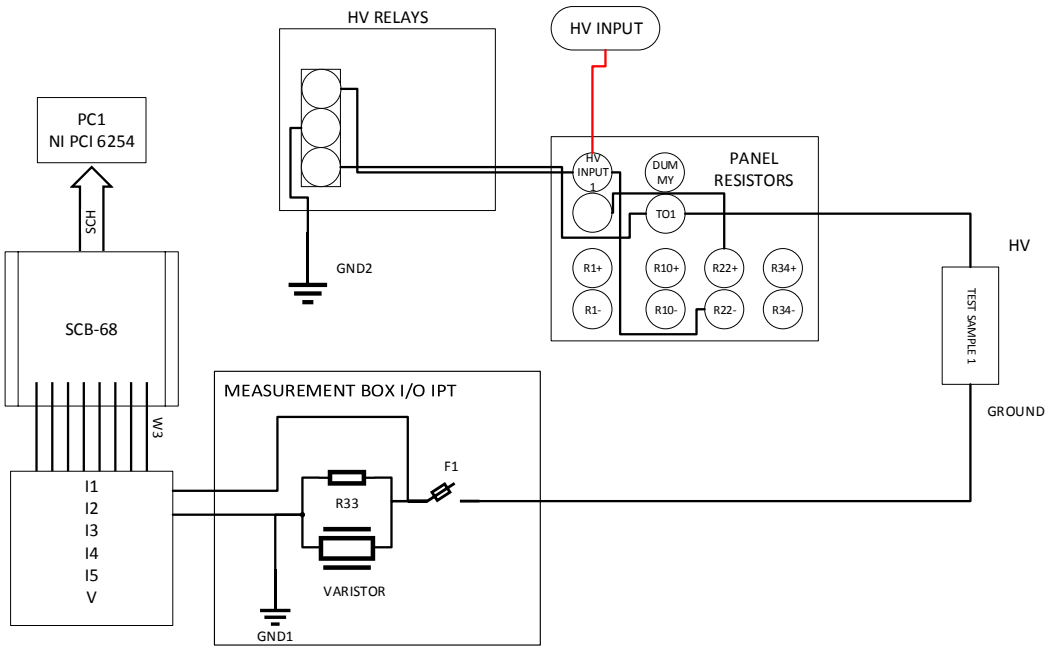

Figure 3.8: internal connections of the IPT ageing unit.

Figure 3.9: main components of the inclined plane test ageing unit. a)Hypotronics control unit, b)HV relays, c) measurement protection box, d) vertical panel resistor, e)coaxial cables connections, f) HV power resistors, g)LeCroy oscilloscope, h) SCB-68 board, i) Peristaltic Watson Marlow 205S/CA pump.

3.2.2 The data acquisition system

The DAQ system represented by block 14 in the general scheme of figure 3.7, is the second part of the IPT facilities. The scope of this arrangement was to record and store the data acquired during the experiments to allow a post processing useful to study the electrical parameters and make some considerations. The intent was focusing our attention on short time tests but exploiting the maximum power of the boards we had, to ensure the maximum speed sampling of information extracted for each period of time. In figure 3.10 the way to acquire data is represented.

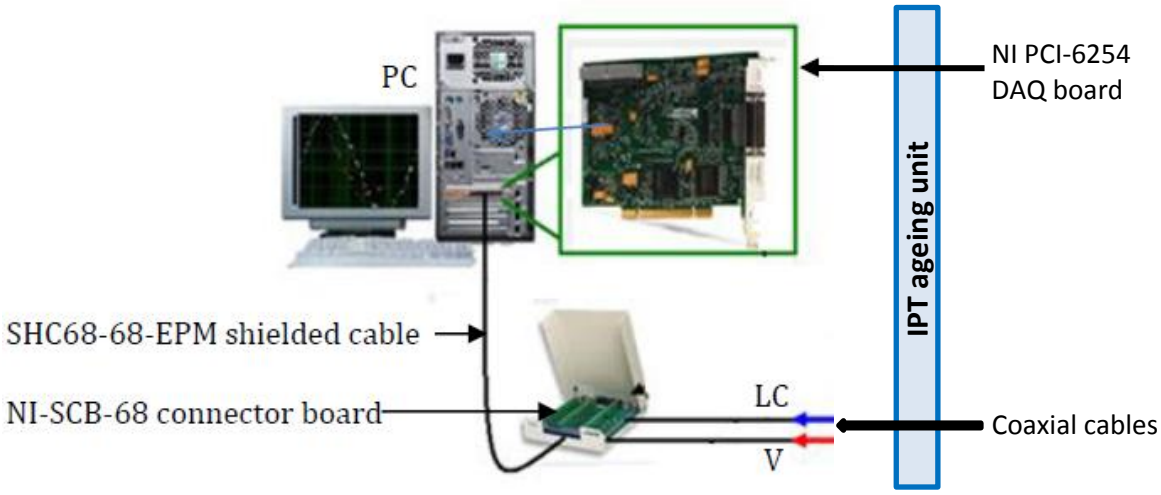

Figure3.10: DAQ circuit

A National Instruments M series PCI-6254 data acquisition board was installed in a personal computer. The card maximum sampling rate is 1.25 [MS/s] for one channel acquisition and 1 [MS/s] for multichannel acquisition. The data board could receive 32 single-ended analogue inputs or 16 in differential mode with a 16 bits resolution.
The maximum input range was -10/+10 [V].
The board could also receive/generate digital signals through 48 digital inputs/outputs. [27]
The physical connections arriving from the ageing unit carrying the voltage and current signals were achieved through a SCB-68 68-pin shielded connector block.[28]
The connection between the connector block and the DAQ board was conducted with a SHC68-68-EPM shielded cable.
Cable Design Advantages National Instruments provides many different high-performance shielded cables that have been designed for specific NI multifunction DAQ devices.
Each type of cable features improved signal integrity using the following technologies [29]:

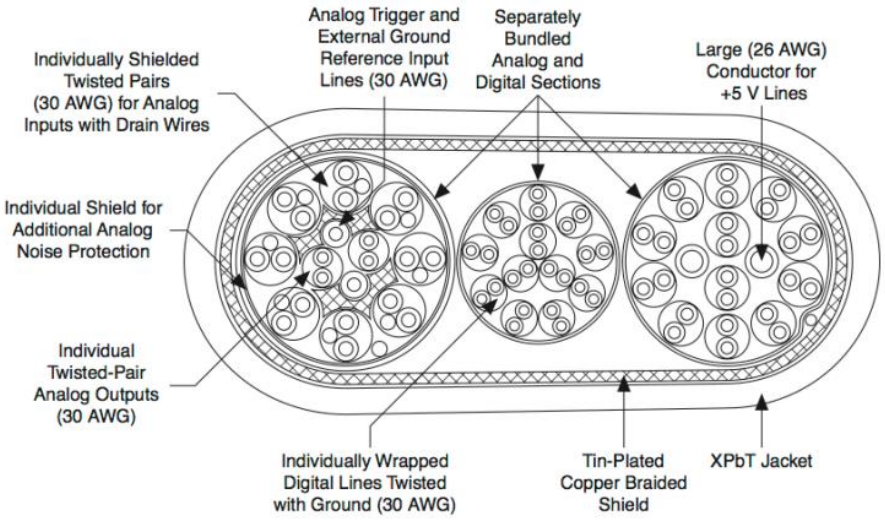

Figure 3.11: shielded cable design [29].

A software already present in the Cardiff University utilities was required to build a data acquisition (DAQ) software that would meet the inclined plane test requirements.
The DAQ software was based on National Instruments LabVIEW program and it undertook the tasks of acquiring, monitoring and storing the waveforms of applied voltage and leakage current. Moreover, by utilising the digital signalling capabilities of the DAQ board, the program controlled the ageing unit high voltage relays (figure 3.9b). The board would send a digital high-state signal in a TTL logic to the relays as soon as the programme was initiated, allowing them to be ready for manual switching.
If the leakage current exceeded 60[mA], the programme would automatically interrupt the power supply from the failed sample without disturbing the rest of the specimens. A relay power supply could also be switched off through the software interface.
This program was developed according to the standard, so once 6 hours of testing were elapsed, the software would switch off all relays, terminating the test.
In this project work was necessary only starting the test and have the possibility to stop it when required, without testing for 6 consecutive hours, but the same program was suitable so it has been used.
Figure 3.12 shows the front panel of the data acquisition software.
At the top, five graph indicators present the history of RMS leakage current during the test for each sample. Below its graph, a virtual push button was used to interrupt the power supply to the corresponding test bay. Lower on the left, another graph indicated the waveform of voltage along with indicators of RMS value. Next to it, there is information about the saving of acquired data and the elapsed time with a warning indicator in case the programme has been set not to keep data records.
The panel is completed with information about the state of the high voltage relays (on or off) and the execution of LabVIEW graphical code in the background.

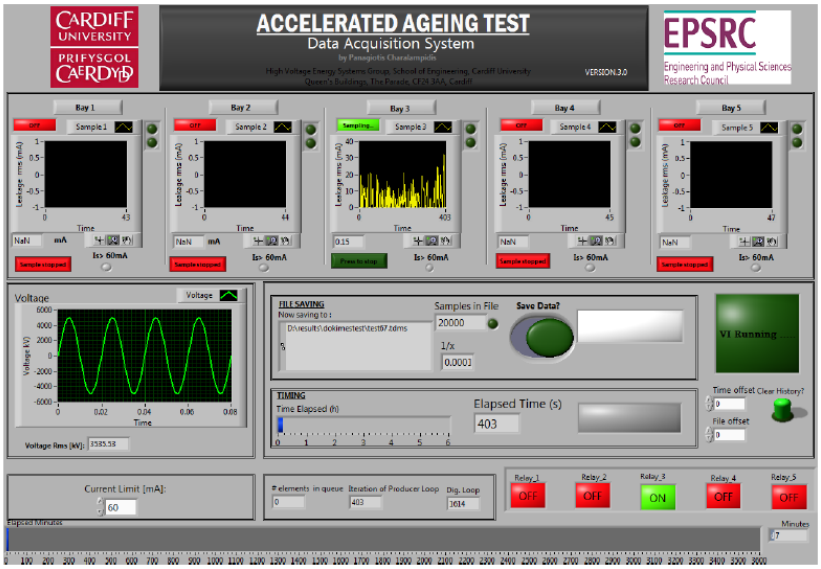

Figure 3.12: front panel of the DAQ software.

The sampling rate for all material tests was the maximum as specified above for the purpose of this work: 1 [MS/s] per channel (because more specimens were tested each time and furthermore the voltage had to be acquired).
For the power frequency of 50[Hz], which has a period of 20 [ms], that corresponded to 20 [kS/cycle].
The waveform signals of voltage and current were stored in TDMS (Test Data Management System) files.
The high speed and high resolution acquisition was achieved by implementing producer/consumer programming architecture and fast data streaming TDMS files.
The saving function of the programming code was based on a State Machines programming logic. This file saving code opened a file and saved data at a high speed. As soon as the file had stored 60 [ksamples] for each channel, the file closed automatically and a new file opened, ready to store the new incoming samples.
The use of LabVIEW features like the queue/dequeue functions secured the reliable and continuous saving during the transition of closing one file and opening a new one.
As these records were segments of voltage and current waveforms, a separate post-processing programme was used to assess and analyse the information acquired during testing.
For a data set which depends to the time range, several TDMS files were stored, and the amount of memory required was used. For a 6 hours test 3600 TDMS files should be saved, equivalent to approximately 9 gigabytes of data.
This necessitated post-processing of these segmented data which was achieved using DIAdem, a post processing software developed by National Instruments which involves many advantages.
Figure 3.13 shows a snapshot of the LabVIEW programming code, called block diagram, for the file saving and data processing functions.

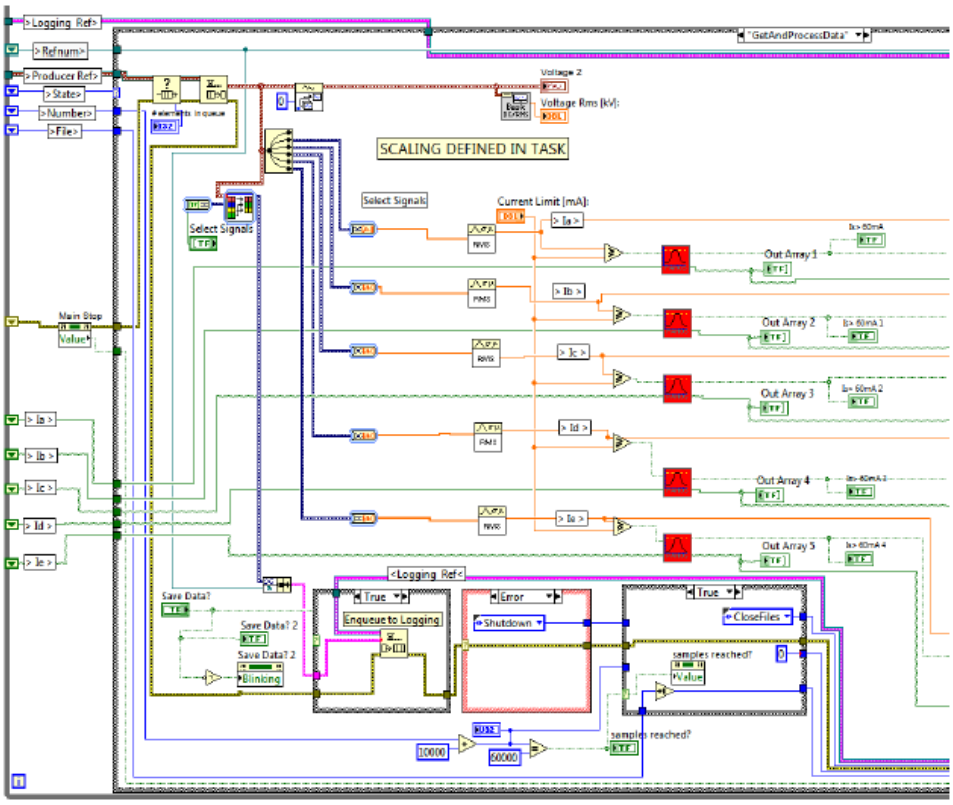

Figure 3.13: snapshot of LabVIEW block diagram.

LabVIEW is a graphical programming language in which, instead of using code lines, the program is developed with a visual interface in which there are connections, ports and transformations which allow it to be more user friendly compared to the text code.
This permitted to have a complete overview of data movement from acquisition to post processing and a general control of the entire program visualizing it.
From the base developed by a previous PhD student [30], the goal of this work was modify the structure of the program to acquire the data at the maximum speed in according to the maximum sampling rate of the board.
Furthermore, the instantaneous values of currents and voltage needed to be represented instead of the RMS values. This was made to have a comparison between the software and the signal visualized in a Teledyne LeCroy oscilloscope. A second oscilloscope (figure 3.9g) was used to visualize the voltage signal applied as input on the IPT machine. This was helpful to see if there were problems with the source, as for example a short circuit between the active parts and the shell of the machine thanks to the waveform shape. All the signals were conducted through coaxial cables to shield as much as possible the noises from the external environment and to ensure a good quality measurement. In fact the leakage current values were very weak, so this needed a precise measurement system avoiding other signals to be measured in common with the same cable.
Moreover this consideration is valid because the setup of the machine involved many cables in parallel, increasing the danger of this contamination.
Some tips have been applied, as installing the cables far from other electric power

sources as general electric boards present in the High Voltage laboratory.
During the experiments was noticed that also another transmission, as for example an electric high voltage discharge in the same laboratory even far from the test location, causes a temporary change in the voltage waveform applied and in the measured leakage current, which was the fundamental parameter acquired during the tests.
For these reasons the attention about the shielding has been massive.

3.2.3 Camera recordings

The third main part of the IPT arrangement consisted in the cameras used to have a real time monitoring system during the tests.
This was part of the goal of this research project because it allowed to put in parallel different kind of data and make helpful considerations about the SiR material.
Three cameras have been used to record images at the same time on the same samples to allow a correlation among them.

- **Sony Handycam visual camera**

A Sony Handycam has been used to have a visual record during the tests. It was mounted on a tripod and placed outside the machine monitoring the insulators through the rectangular opening of the IPT frontal door.

Figura 3.14: Sony handycam

The data were stored in a memory card inside the camera, avoiding a physical connection with a PC during the test. The quality of the images were good enough to allow a satisfactory view of the physical phenomena of discharge.
This camera have been used to have a general understanding on what was happening, in particular in case of fire on a test sample, the test would have been stopped as soon as possible. A remote control allowed to start and stop the camera from outside the cage, avoiding dangerous direct contacts with the machine. In fact the camera was placed inside the cage but the interlock system would have stopped the test voltage if the door was suddenly opened.
It was equipped with a 1/5.8 (3.1mm) back-illuminated Exmor R CMOS sensor type and ZEISS Vario-Tessar lens. The filter diameter was 37 [mm] and it had a 30X optical zoom which allowed to decrease the observation area focusing on the arc discharges.
Thanks to a touch screen 7.5cm(3.0 type) Clear Photo LCD display (460-800 dots) in 16:9 it was possible to set the image definition.

Furthermore it was equipped with an optical SteadyShot w/ Intelligent Active mode(5-axis) stabilisation system which ensured an adaptable focus even after a light change.
The recording format video was AVCHD, version 2.0, compatible with all the main formats readable from a PC as :MPEG4-AVC/H.264, MP4, XAVC S format MPEG4-AVC/H.264, hence no particular software has been required.
The video resolution in AVCHD was adjusted to the maximum 1920x1080 with 50[fps] ensuring a satisfactory quality on a PC screen.
The tripod material was plastic, so it hasn't been necessary to ground it to the reference potential.

- **SC 7600 infrared camera**

The second recording device was a FLIR SC7600 infrared camera [31], which is part of the FLIR SC7000 family. Since this camera was a diamond tip of the technology in the sector of IR images, an expert technician helped with the setup and with the proper recording way for the purpose of these tests.
The scope was mapping the thermal stress on the specimen surfaces during the IPT test and detect the formation and development of dry-bands and subsequent spark discharge activities.

Figure 3.15: FLIR infrared camera

The camera detector was a Indium Antimonide (InSb) type with a spectral range 1.5 – 5.1 [µm] with an infrared resolution of 640x512 [pixels]. The maximum imaging frequency was increased if we used the windowing function.
Windowing allows a subset of the total image to be selectively read out with user adjustable window size at a much higher frame rate. The sub-sample window sizes and locations have been arbitrarily chosen and have been defined using the camera control software.
The SC7600 model with the InSb detector can deliver thermal images up to a speed of 3,425 [kHz]. This value could also be adjusted to a lower, user-defined level.
For this recordings the frequency has been varied during the several tests to find a good compromise between the frames per second and the window chosen as optimal to observe the process.

An optical focal lens of 25 [mm] has been used, with a FOV (field of view) solid angle of 22°x 17°, f/3.0. The lens modified the spectral band to 3.7 – 5.15 [μm].
The standard camera calibration range was maintained, so the measurement interval was 5[°C] to 300[°C] for spectral thermography.
It has been decided that was appropriate for this kind of tests thanks to the previous literature available in this field area, in fact the maximum temperature recorded was about 300°[32].
An Ethernet link with a personal computer established the communication with the FLIR ResearchIR Max software that processed and stored the captured infrared records and also allowed control operation of the camera.
This software has been developed for intuitive viewing and advanced processing of the thermal data provided by the camera.
The file format was '.ptw' that could be dynamically post-processed retrieving most real-time data. As soon as the data have been acquired the conversion in '.avi' and '.wmv' have been made.
In this way a first visualization could be possible and some adjustments have been carried out to increase the quality of the recordings correlated to this test type. In figure 3.16 a snapshot of the ResearchIR Max software can be seen. On the right a column shows the real time temperature in relation to the colour gradation.
In this way hotspots and dry-band arcing can be detected.
On the left the source information specify the camera type, lens and filter used and a segmentation allows to select the time range of which we wanted to save the data.
The lower part of the software interface shows which directory is used to store the data and several settings to enhance the image quality.

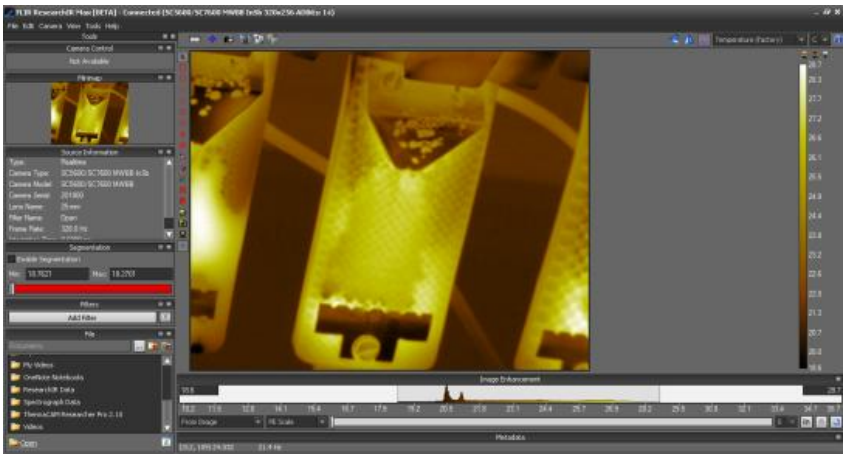

Figure 3.16: snapshot of the ResearchIR Max software for the infrared imaging

The data in .ptw format were big (up to 15 [GB] for 50 [min] recording), so for the visualization and the primitive considerations the converted versions have been used. With 10 [min] video in .avi format the file dimension was about 5 [MB].
This camera substituted the previous FLIR A325 infrared thermal camera, which has been used from the previous students during similar tests on SiR material.

It has a spectral range from 7.5 to 13 [μm], an image resolution of 320x240 [pixel], and a variable imaging frequency up to 60 Hz.
This change allowed to reach better performances and increase the imaging frequency, even focusing on a small section of the insulator where the activity had origin.
The imaging quality was also excellent and ensured a good recording to extract the temperature from the images.

- **Photron SA5 ultra high-speed camera**

The camera in figure 3.17, as for the infrared SC7000 operated in parallel, was available in the "Morgan-Botti Lightning Laboratory" at Cardiff University, hence it has been borrowed to perform the test when it was not used for lightning tests.

Figure 3.17: ultra high-speed camera

The high performance permits the SA5 model [33] to be applied to areas of research once dismissed as unsuitable for digital high-speed imaging.
Our camera had 32 [GB] of internal memory to store the data and it can achieve up to 775.000 [fps] with an exposure time of 1[μs]. This huge frame rate is possible only if there is a decrement on the resolution (both horizontal and vertical).
The camera was equipped with a Nikon lens and it can be used in an event markers way: up to ten user entered event markers mark specific events within the image sequence in real time and are immediately accessible through the software.
In these tests one of the main problems was that we didn't have an event marker, so the camera had been used with the synchronisation at the GPS time code, correlated to the other cameras and the PC local time.
The scope of this synchronisation was allow a post processing study in which the same moment could be showed by the three cameras together.
This is one of the advantage of exploiting the DIAdem software and it would have conducted to a complete representation of the physical phenomena.
In this research area this was the first time an high speed camera with these performances has been used to monitor the IPT test.
Previous similar tests operated a low performance Nikon high-speed camera that was sufficiently powerful for their purpose (to have a general understanding of the surface discharges).

In this case a more performing camera allowed to record what was happening on the surface SiR materials in the test bays and how it was developing.
The scope was achieving a better comprehension about the movements of the dry-band arcing on the samples and how it modified its behaviour in according to the textured size of the surface.
The old camera image showed in figure 4.2 was unsuitable for the scope of this work because the resolution was too low for looking at the arc movements around the protuberances of the SiR material because it was affected from the sunlight which in the laboratory couldn't be avoided.
The snapshot from the Photron SA5 while recording a discharge is showed in figure 3.18. It can be noticed the dry band which is going from the top electrode to the lower one. There are many streamers which are deviated by the surface protuberances.

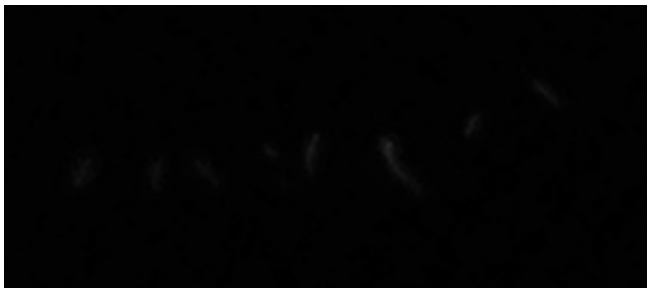

Figure 3.18: image acquired from the high-speed camera during dry-band discharge

The electricity branches are not well defined because the image is taken from a common .avi video before post processing, but a general understanding of the behaviour can be achieved.
Since it was the first time this kind of camera was utilised, several attempts at different frame rates and resolutions have been made to find the best one related to our purpose. Even if the quality of the images was not so good, the sparks can be noticed and where they occurred revealed the formation and the development of the dry band arcing, in which we were interested.
For example a recording at 30.000 [fps] with a maximum resolution (without windowing) of 768x320 [pixel] brings to a record duration of 3,11 [s] and a total of 93.189 frames. This is valid for our camera with 32 [GB] of memory to store the data. What previously mentioned represented a limitation during the test because no more than a specific amount of time could be registered, so the time range was very short.
To register a dry band formation and development we needed a time up to 20 [s], which is the time required at the sparks to reach the ground electrode, but it wasn't possible so another tip has been adopted. Thanks to a direct inspection on the specimen it could be observed when the dry band began and when it stopped. The camera presented the possibility of a backward recording, so putting a mark when the sparks finished their path, it could be selected the time range precedent to that moment. In this way the arc discharge recording on the surface has been achieved. Since the time to reach the lower electrode was bigger than the possibility to store all in the same file data, more of them had to be saved. To do this the entire set of data was divided selecting the desired

frames and saved part by part. In the post processing work, the entire video was merged to have the complete dry band discharge on the test sample.
A huge amount of data have been stored, for example a recording at 31000 [fps] with a resolution of 320x352 pixel for a 6 [s] test represented 18 [GB] of storage data.
To ensure the safety necessary to carry out high voltage tests, the two cameras mounted on the iron tripods have been electrically grounded avoiding dangerous floating potentials which could come in contact with the user.

3.3 Inclined Plane Test setup

The inclined plane station has been built with consideration of user safety during testing as well as protection of test equipment and samples. An interlock safety system interrupts power supply in the event of the cage door being opened during the test.
A modified test station door has been made of transparent PVC allowing monitoring of the test sample using visual, infrared and fast cameras. The top of the test facility has open holes providing ventilation for smoke resulting from the material erosion. Once a steady flow of the contaminant is established on the test surface, the high voltage is supplied to the sample. All the components have been checked and substituted where necessary considering the long inactivity time of the ageing unit. Some of the power resistors were completely replaced, as well as several high voltage cables, the insulation between the shield and the active parts has been restored. A black epoxy potting compound was put on the power resistors. It protected against moisture and corrosion and improved insulation resistance and mechanical strength. Furthermore the peristaltic pump has been extracted from the shell and kept outside to enhance the operations security avoiding dangerous contacts between electricity and liquid (figure 3.19). The internal control constituted by the variovac autotransformer has been bypassed modifying the original circuit, becoming controllable by the LabVIEW software. The protection box and the scb-68 block were in good conditions, so they have been just checked and recalibrated.

Figure 3.19: the IPT ageing unit.

To set up the IPT machine many elements had to be prepared and checked before starting the test.
The ageing unit which represents the hardware had to be set with the parameters specified in the relative norm. The software had to be organized following the correct specifications reported in the manuals. Furthermore, the samples have been previously prepared and the complete arrangement has been made. This involves all the connections with the coaxial cables and the internal connection of the IPT shell, through the high voltage red cables. These cables allowed a secure connection between the components thanks to their design. In fact in all applications, the insulation of the cable must not deteriorate due to the high-voltage stress, ozone produced by electric discharges in air, or tracking. The cable system must prevent contact of the high-voltage conductor with other components or persons, and must contain and control leakage current. Cable joints and terminals inside the IPT machine are designed to control the high-voltage stress to prevent breakdown of the insulation. The high-voltage cables has a metallic shield layer over the insulation, connected to the ground and designed to equalize the dielectric stress on the insulation layer.
As already specified the peristaltic pump has been set to bring the contaminant in the correct amount and the rectangular samples of different texture have been fabricated in the vacuum casting machine. The contaminant flow rate was a critical parameter since it determines the nature of observed arcs and discharge activity. It was, therefore, necessary to ensure uniform contamination along the centre of the underside of the sample, with contaminant flow rates as a function of the applied voltage defined by Table 3.1. It should be noted that the rectangular samples have been weighed before and after the tests, to calculate the material weight loss.
The steel electrodes have been cleaned or restored with new ones and new screws have been used. After a general new arrangement all the components have been checked to ensure the machine was working properly. This was fundamental for the security of the test operations.
To set up the software for the DAQ in LabVIEW, it has been previously necessary to calibrate manually the acquisition thanks to a National Instrument environment developed ad hoc. The NI MAX DAQ program has been used.
A screenshot of the interface is reported in figure 3.20.

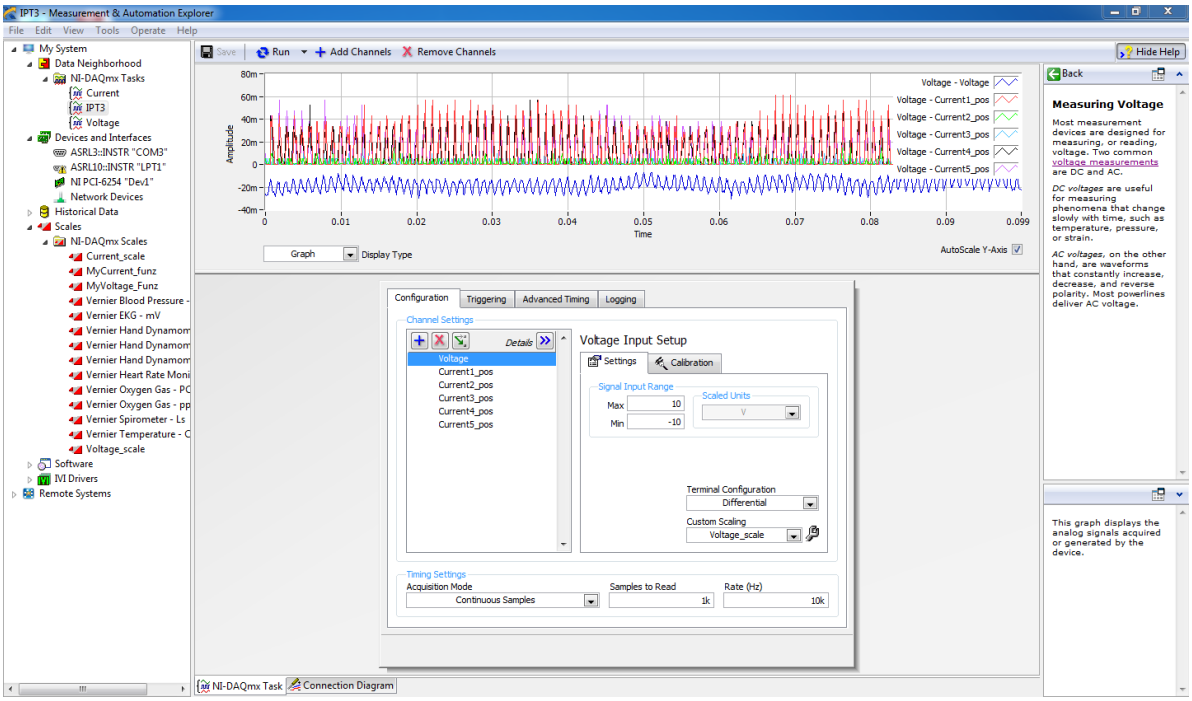

Figure 3.20: NI MAX DAQ interface. The test signals acquired are shown in the graph.

The software is developed by NI to initiate the DAQ ensuring a correct acquisition of the values needed during the operations. As for this project the leakage current was the desired parameter, the first thing done was set up the board and the connector block to acquire the right currents from all the channels connected.
The interface allows, on the left, to select which task has to be used and which device it recognizes installed on the PC.
The task has to be created by the user specifying some parameters as:

- Number of channels and create them in the list;
- The signal input range;
- The terminal configuration: it can be chosen between DIFFERENTIAL, NRSE and RSE modes;
- The scaling factor adopted;
- Timing setting: acquisition mode, samples to read and rate (Hz).

The definitely task created for the scope and used for all the IPT tests performed was called “IPT3”. It had six channels physically connected to the input of the SCB-68 which came from the six coaxial cables connected to the measurement box. Every physical connection had to be manually related to a pin of the connector block selecting in the software interface the correct name, as reported in the following scheme (figure 3.21a):

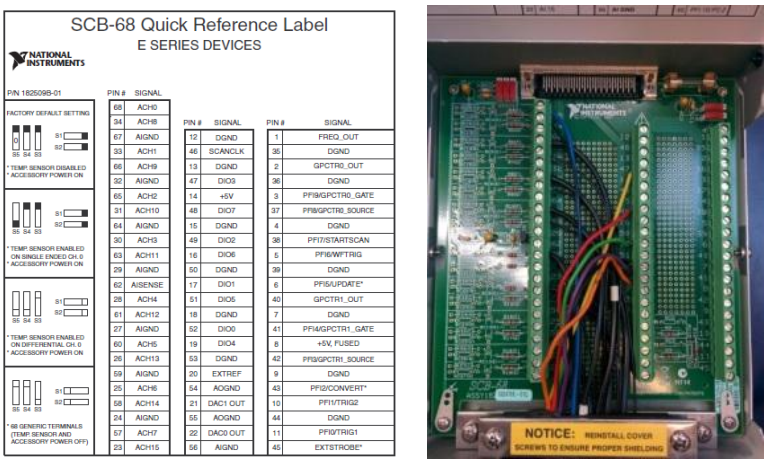

Figure 3.21: a) pins connections for the E series devices, b) physical SCB-68 board.

This represent the internal connection description of the board in figure 3.21b.
The first column represents the analog inputs available, while the second represents the digital outputs connected to the relays of the respective test bays.
The third column brings other useful functions not used for this project.
The signal input range was set at ±10[V] because represented the maximum limits for the SCB-68 board. An higher signal could ruin the expensive board.
Every analog signal was acquired in DIFFERENTIAL mode, ground referenced.
A differential connection is one in which the DAQ device AI signal has its own reference, or signal return path. These connections are available when the selected channel is configured in DIFF input mode. The input signal is tied to the positive input of the instrumentation amplifier, and its reference signal, or return, is tied to the negative input of the instrumentation amplifier. On DAQ devices that support both single-ended and DIFF input modes, using DIFF input mode commits two channels, ACH<*i*> and ACH<*i*+8>, to each signal.
The use of differential input connections is recommended for any channel that meets any of the following conditions:
• The input signal is low-level (less than 1 V).
• The leads connecting the signal to the DAQ device are longer than 10[ft] (3[m]).
• The input signal requires a separate ground-reference point or return signal.
• The signal leads travel through noisy environments.
Differential signal connections reduce noise pickup and increase common-mode noise rejection. Differential signal connections also allow input signals to float within the common-mode limits of the instrumentation amplifier.
This acquisition way calculates the difference between to connector block pins, so it requires two connections for each measurement.
This halves the maximum number of signals can be acquired.
The RSE mode is used for floating signal sources. In this case, the DAQ device provides the reference ground point for the external signal. The NRSE input mode is used for ground-referenced signal sources. In this case, the external signal supplies its own reference ground point, and the DAQ device should not supply one.

Every signal acquired was ground referenced because the return of the circuit was electrically connected to the ground through the machine shell.
The scaling factor adopted has been calculated by several pre-tests after the hardware and software setup has been achieved. The initial purpose was to measure a DC current supplied from a current generator, with a digital Fluke multimeter (figure 3.22).
The results of this setup could be transferred to the AC case, which effectively was the waveform applied during the test.

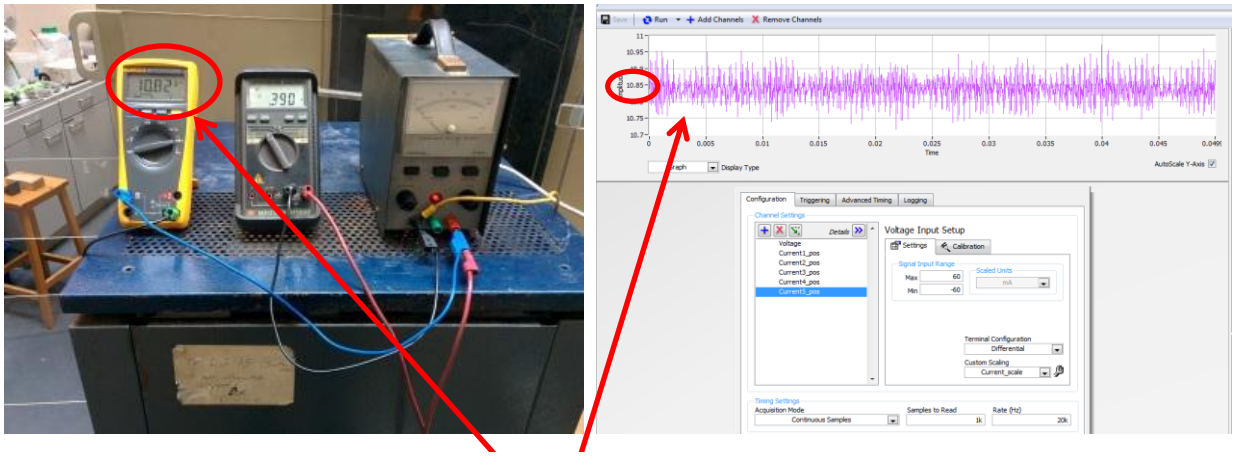

Figure 3.22: DC test to set the signal acquisition

This has been done to be sure that the current and voltage values collected from the machine were exactly visualised by the software.
If this wasn't checked all the post processing calculations would give unphysical results.
A second possibility adopted in the second IPT test has been scale the signals after the acquisition thanks to the DIAdem software. It has been seen that the result is equivalent.
The electric circuit designed for this attempt (figure 3.22) is descripted. A voltmeter is connected in parallel to the generator power supply to have information about the voltage applied. A series circuit is built to measure the current imposed by the generator and allowed to flow in the high voltage cables simulating the test.
The lower potential is grounded to the ageing unit shell.
Several measurements have been done varying the potentiometer on the power supply. The current values are reported forming a table in the NI MAX program to construct a mapped scale for this signal. Since the board could acquire only voltage signals, they have to be converted into current values. From this ratio a linear relation with a factor of 30,1657 has been found interpolating the mapped measurements.
The output current values were expressed in [mA], while the input voltage in [V].

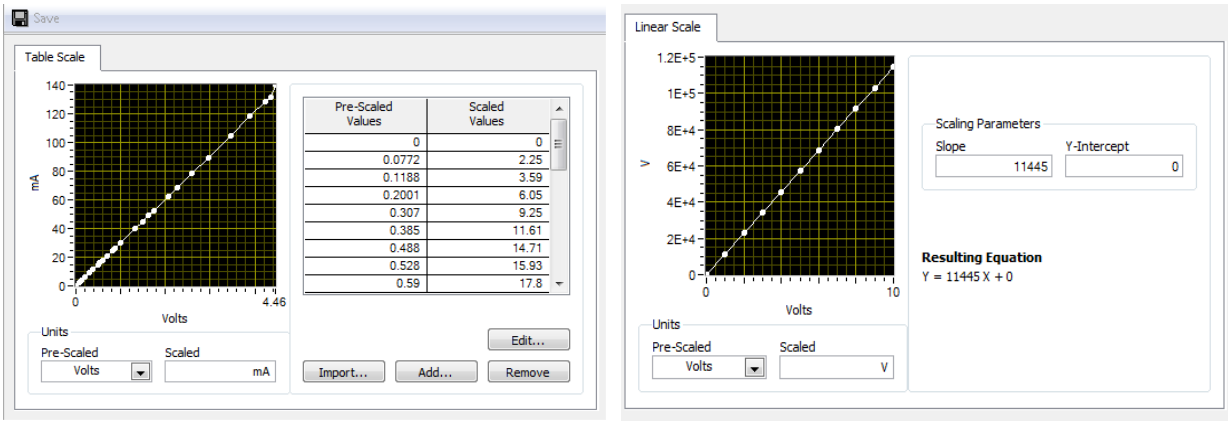

Figure 3.23: mapped scale for the current and linear scale for the voltage

The same has been done for the voltage signal. Even in this case a linear relation between the signal measured by the multimeter and the values visualized in the NI MAX brought to a linear scale with a ratio of 11445.
Many scale functions have been created before finding the most appropriate one in which the equivalent values were found both in the multimeter and in the PC screen.
The last section to arrange was the time setting. A continuous mode was imposed to ensure that the acquisition was not stopped after an event as a peak of current of after a short period of time.
The number of samples to read and the acquisition rate (Hz) were modified until a good comprehension and visualization of the phenomena has been reached.
The signals with their amplitude and waveforms can be seen in the upper graph of figure 3.20. This allows to see if there are some errors in the setting and correct them. For example in figure can be noticed that the current signals are chopped keeping only the positive part. This wasn't correct because the negative part is not negligible, since it contributes to the erosion of the test samples. Another thing can be observed from the graph is the offset value around which the voltage signal is floating. This is due to the fact that the software wasn't enabled to acquire in that moment, when it would be connected the voltage signal has to float around the "0" value to ensure the correctness of the measurement.
The currents represented are negligible because the values indicated in the vertical axis are very small: this indicates that there is a small noise in the environment, proving that the noise shielding is crucial in this application. Furthermore, it can be observed that there are channels which are more disturbed as CH1, CH4 and CH5. Instead CH2 and CH3 are cleaner, so it has been decided for the first test to use these two channels to acquire the leakage currents from the specimens.

CHAPTER 4

The experimental tests

4.1 Test Day 10th April

The first test was carried out to set-up definitively the inclined plane test and have a general comprehension of the operating unit with the devices, verifying that all were working properly. In this test the less performing high speed camera and the FLIR IR A325 camera were used, discovering that the FLIR IR had a connection problem to store the data in the PC and the high speed Nikon camera wasn't suitable for our purpose.
In fact the camera should be used with as little light as possible allowing a good visualization of the leakage current in the silicon rubber.
The environment should be dark, so the lights in the laboratory have to be turned off.
Since the previous observations, the goal of this test day was to concentrate the attention in the correct setup of the machine.
The test was carried out at 3,5 [kV], the contaminant flow and the resistances have been set in according to the relative standard. The pump speed was 12,5 [rpm] and the resistors inserted in the circuit of 22 [kΩ]. The samples used were a conventional and a 4[mm] square arrangement types. The aim of the test was to see the different current behavior on the surfaces and try to see how these leakage currents were flowing, recording the electric parameters by a software acquisition. The specimens have been drilled with a punch plier in the correct positions to allow the mounting of the electrodes. The punch plier had six different sizes to make the holes and the 5-sized has been used. Furthermore, the specimens have been weighed on the precision scale to be able to measure the difference with the weight at the end of the test (this in accordance to the standard for the six hour test and, even if our purpose was different, it has been done for completeness with the procedure). The weights are reported below in table 4.1.

SAMPLE N.1 Conventional	SAMPLE N.2 4 [mm] textured square arrangement
39,2174 [g]	**49,2637 [g]**

Table 4.1: weights of the two tested samples

To carry out the test the channels CH4 and CH5 have been used respectively for the conventional and the textured samples.
The contaminant was made up with 1000 [g] of distilled water and the impurities added. The volume conductivity measured at a temperature of the liquid of 18 [^{O}C] was 2,3 [mS/m], which correspond to a resistivity of 434,78 [Ωm]. This is not compliant with the standard because it specifies a value of 3,95 [Ωm], or an equivalent conductivity of 0,253 [S/m]. The pump has been started at a speed higher than 12,5 [rpm] to decrease the

time to fill the pipes. When the contaminant reached the top electrode the speed was adjusted to 12,5 [rpm] which was the correct speed to operate the test. The contaminant flow was controlled and has been noticed that the solution was not reaching the lower electrode in the textured sample because the shape of the surface wasn't ensuring the sufficient adherence. The drops were falling from the midpoint of the specimen.
To avoid this behavior the sample has been wetted until the lower part to drive the drops. The slope has been increased with a thickness of 2 [mm] for an angle of 3[^{O}]. In this way the flow was adjusted and the drops could reach the lower electrode following the central axis of the specimen. When an acceptable flow was reached the voltage has been applied and the test started. The following figures 4.1 represent two frame of the contaminant flow observed before the test. As can be seen the drops after the adjustment were flowing regularly in the central part of the specimen as desired.

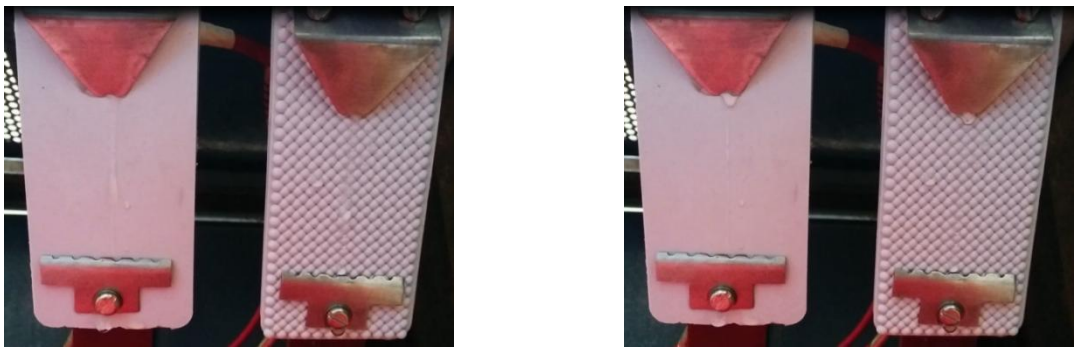

Figure 4.1: flow of the contaminant after the adjustment

The high speed camera has been set up with these specifications:

- Frame rate 750 [fps];
- Resolution 1280x684 [pixels];
- Shutter speed 1/750 [sec].

The figure 4.2 shows the visualization through the software interface, used to capture the leakage current in the material.

Figure 4.2: Nikon high-speed camera software imaging

The poor quality pointed out before could be addressed to the fact that increasing the frame rate the portion visualized in the window is smaller and the resolution becomes lower. In consideration of this the new Photron SA5 camera has been adopted for

following tests.
The first experiment failed also because a loss of insulation has been discovered between two strings of resistors and the ageing unit shell, which was grounded to the earth reference potential. This fact happened because the epoxy potting compound was old and ruined by previous overvoltages occurred. It lost the insulation property but the machine needed to operate in safe conditions. After have replaced the eight resistors that were damaged, the problem was totally fixed applying a new potting compound on them. This was necessary because during the tests, some sparks generated in the test bays could fall in the panel resistors which is positioned under the test specimens.
A future work on the IPT unit will be completely changing the machine design, installing the panel resistors in a vertical position avoiding this kind of problems.
The troubles we had were regarding the 22 [kΩ] resistors of CH1 and CH4 of the IPT unit, so the 3,5 [kV] couldn't be operated.
The test could be restarted when the indications effectively reported the problems resolution. This was proved by the visualization of the sinusoidal voltage shape on the LeCroy oscilloscope. When this waveform is a "clean" sinusoidal, it means that there are no insulation losses on the machine components. If the shape is sparking, represented by a sinusoidal with peaks and holes, it means that a short circuit is present. A leakage current is flowing between the HV circuit and the ground potential, even in a not continuous way. A double check is possible through the Hipotronics control unit by applying the voltage and verifying which is the current that is flowing in the open circuit, when the test bays are disconnected. This value should be zero if all the circuit components are well insulated from the machine carcass. When the insulation have been restored and all the problems have been solved the definitive tests could be performed.

4.2 Test Day 10th May

When the machine has been set up and was working, the inclined plane test has been carried out in two test days spaced of one month each other. This long time was necessary to post process the data acquired from the first test and to organise the second full day test, borrowing the cameras from the lightning laboratory and preparing the ageing unit to be used again.
Meanwhile some full insulators have been built, as we will see forward in chapter 6.
Starting from the knowledge acquired during the machine setup and from the first unsuccessful test, the IPT ageing unit has been prepared with the improvements gained.
The slope of the textured rectangular specimen has been kept constant and equal to 45 [^{o}] because the direct continuous observation for more time indicates that the drops would follow the path adherent to the sample.
The difference compared with the conventional one is the longer time required to reach the lower electrode, approximated in about 2 [min].
A total of five experiments have been executed, mixing different kinds of texturing which characterized the surfaces. In this way good considerations could be done comparing the

different behaviors on the test bays.
Two tests have been carried out in May and the others three in June, when the experience grade about the machine and the procedure was improved.

4.2.1 Test A

On the first entire test day two complete experiments have been performed. A total of three samples have been used (numbers 7, 12 and 2 referred to the initial fabrication). The setup has been carefully prepared in every part. The pollution prepared in 1000 [g] of distilled water had a resistivity of 4,08 [Ωm] at a temperature of 18,5 [^{O}C], very close to the standard specification.
The board has been calibrated with the parameters it required as temperature and humidity and the software has been initialized for the acquisition.
For test A, the first of the two performed during the day, a conventional specimen with a flat surface and a 4[mm] square arrangements one in parallel have been used. Two bays and the relative channels for the acquisition have been used. The cameras were positioned in front of the IPT ageing unit inside the cage (figure 4.3). Since it was the first time three cameras at the same time have been used to carry out this experiment and the opening in the PVC front barrier of the unit didn't allow a good arrangement of them, it has been kept opened during the test. The cables for the image acquisitions were conducted under the door with the interlock system activated.
All the metal parts of the devices used during the experiment have been grounded.

Figure 4.3: cameras installation for the test setup

After 7 minutes the pump has been powered, the pipes were filled with the contaminant and as soon as the liquid was flowing on the surfaces, a voltage of 3,554 [kV] was applied.
The high voltage potential was taken from the fog chamber appliance, for which the cage in use has been designed. The Hipotronics control unit allowed the constant inspection

of the voltage level and its regulation, even if during all the experiments it has been kept constant in according to method 1 in BS EN 60587:2007.

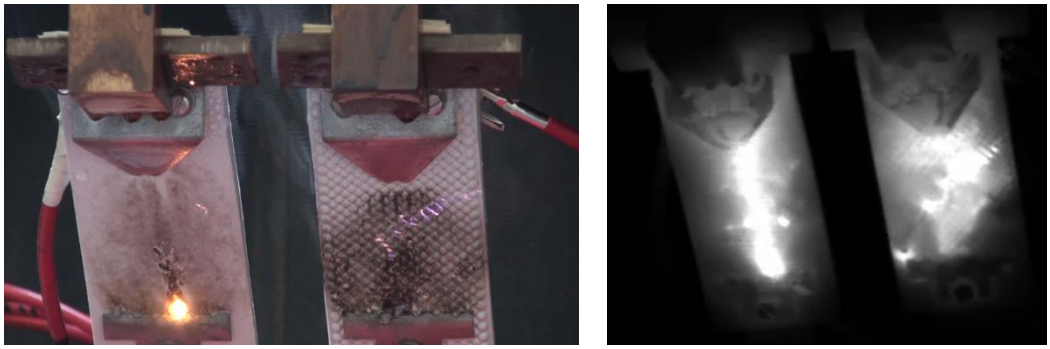

Figure 4.4: a) visual image during IPT test, b) infrared recording at the same moment

What can be observed during the experimental test is that the current in the two samples had a completely different behaviour. On the left the current is concentrated in the central part of the conventional specimen, while on the textured insulator on the right it is divided in several ramifications. In fact the blackish indicates where the current passed and shows this behaviour. The smoke was present while the test was going: it is composed by the contaminant, which has been evaporated from the heating effect of the current flow. In figure 4.4b, on the right, the infrared recording at the same moment has been reported.
Lighter is the colour, higher is the temperature in a specific point. In fact the emitted waveform has a different wavelength in according to the body emitter temperature.
The Photron fastcam SA5 model has been initially set to record at 60.000 [fps], with a resolution of 512x224 and an exposure time of 16,4 [μs]. After the first attempt, it has been set to 7000 [fps] increasing the resolution. The data have been acquired and converting the videos the sparks can be distinguished, but it will require another deep post processing to achieve useful information from these recordings.
The test terminated after 7658 [s], in which as many camera recordings as possible have been stored. This two hours test can be considered one third of the standard inclined plane test as the IEC 60587 specifies.
The aim of this project has been put in parallel the different data types acquired from several devices to permit a coordinated comparison among them, with the scope to achieve new knowledge about the behaviour of the tested material under stress. To do this DIAdem has been used. The software developed by National Instrument allows to correlate different kinds of data and visualize them in the same program.
It has been profitable for the post processing, both for the exportation of the visual data and for the mathematical calculations.
Some parameters has been calculated because considered important to describe the performance of these insulators. The current RMS values, the power dissipated and the accumulated energy have been assessed (table 4.2).
The test timing was not as long as the standard specifies, so the parameters in this study

case can't give a direct comparison with previous IPT experiments, but they give a roughly understanding on what is happening.

Sample	Conventional	Textured 4 [mm] A
Voltage [kV]	3,554	3,554
I rms [mA]	5,64	6,51
I min [mA]	-27,73	-27,99
I max [mA]	28,82	27,69
Range [mA]	56,55	55,68
P max [W]	144,85	143,71
P mean [W]	20,04	23,14
Dissipated energy [J]	4089,09	4719,85

Table 4.2: result parameters of the test A

Since the purpose was to combine together the different data acquisitions, a study of the available storage data have been executed. It has been found that for 204 [s] of the experiment all data were available, so the values in the table are referred to this time range. The same time period has been used for test B of the same day to allow a good comparison between the different specimens used. This has been done selecting the desired TDMS files stored by the acquisition software and post processing them.
Every file stored 6 [s] of recording data, containing voltage and currents of the samples, so 34 files have been used for a total of 2.040.000 points evaluated.
The correct range time has been used putting in parallel the recordings and extrapolating the period in which all data were available. To do this the next graph has been applied.

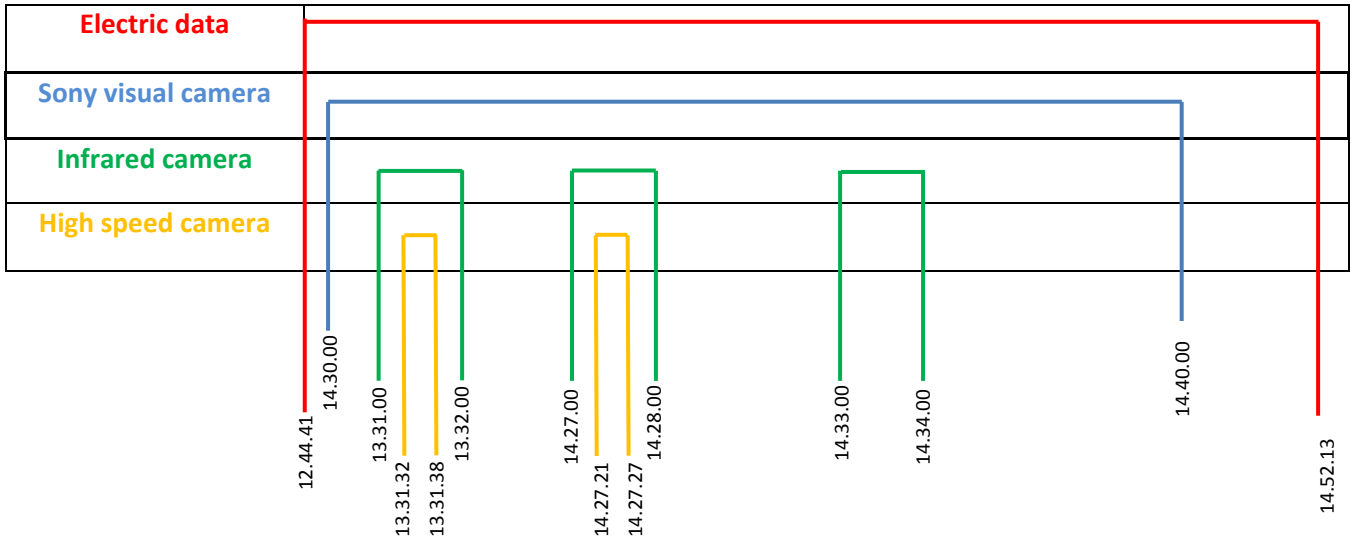

Figure 4.5: the graph shows where the different kind of data are simultaneous

It can be noticed that the fast cam (orange) has the most restrictive time range among the acquisitions because the amount of data stored was huge. Only few seconds of the total experiment was available to study in parallel with the other sources. For this reason the focus of the recordings has been applied to the dry band formation in which we were interested more. The goal was understanding how the streamers move inside the textured sample. The two ranges in which all the data kind were available have been used for visual experimental considerations.
The values in the table doesn't show a huge difference between the two test samples, but this is referred to the fact that the time range analysed (204 [s]) is not so long and the consequence is that the integral of the mean power along time can't show a big difference in the dissipated energy.
The current waveforms are reported below. It can be verified that the peaks for the first minutes testing are very similar. The same can be red also for the RMS values, noting that the current in the flat specimen is also lower than the current in the textured one.

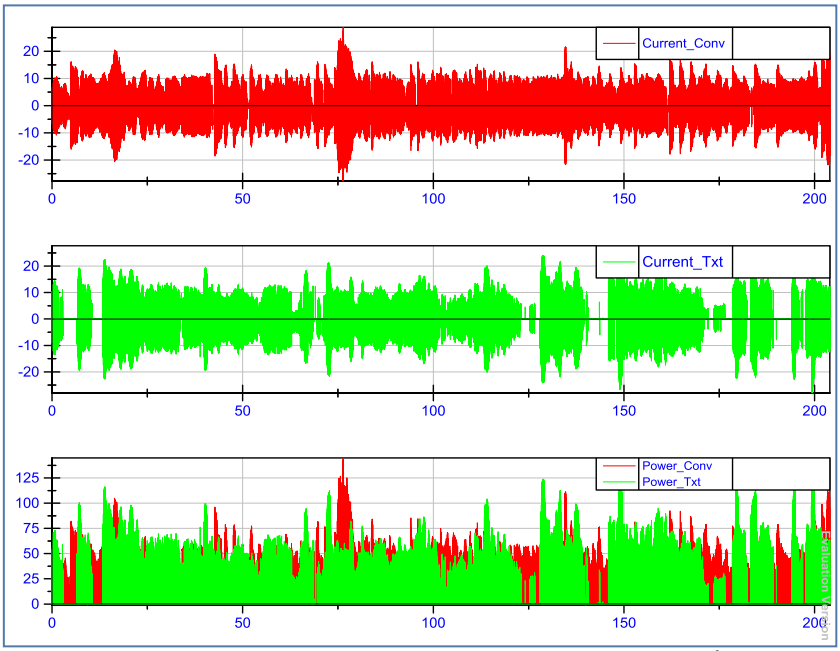

Figure 4.6: current waveforms for test A, May 10th

In the first graph the recorded current on the flat specimen is showed in red instead the green one in the second graph represents the current on the textured surface. The shapes are very different showing a different behaviour in the two cases. In the third graph the powers dissipated are visualized, respectively in red and green as for the currents. Even in this case the shapes are very similar proving that the time range was too short for a comparison of this type. It has been chosen that the last parameter calculated was the energy, because it summarised the convenience of one insulator in respect of another. In fact, also in the transmission lines and hence in service, this parameter is important to know how much energy is lost due to the insulation between the conductor and the pylon.

4.2.2 Test B

The test B during the same day has been done after the textured sample has been removed from the ageing unit. It was substituted with another textured sample with protuberances of 4[mm] in a square arrangement configuration.
The flat sample was not removed and so tested again in parallel to the textured 4[mm] B. This has been done to allow a new recording with the fast camera on a virgin specimen, while the conventional has been kept to study the behaviour if the test was going on for more time. This allowed to make some considerations which were closer to the literature in which the IPT test has been fully operated.
The same range time is studied, so 204 [s] of data have been analysed.
The TDMS files contained 3 [s] of real time data because the sample speed was incremented with this acquisition. 68 files have been merged for a total of 4.080.000 points evaluated.
The same parameters were acquired and studied to develop the table below.

Sample	Conventional	Textured 4 [mm] B
Voltage [kV]	3,412	3,412
I rms [mA]	12,05	7,16
I min [mA]	-57,64	-22,04
I max [mA]	57,75	22,04
Range [mA]	115,39	44,08
P max [W]	288,54	110,48
P mean [W]	41,11	24,43
Dissipated energy [J]	8387,38	4983,70

Table 4.3: result parameters of the test B

In this case it can be seen that all the values from current to power to the energy are higher in the conventional sample. This is obvious because the flat sample hasn't been substituted, so we were testing the 'old' specimen. The values increased from the previous as expected showing an initial linear relation considering that the test time was double and the energy dissipated doubled as well. Regarding the textured 4[mm] A and the textured 4[mm] B the values are very similar, ensuring a good success of the experiment. The voltage applied was not the same but very similar (3,412 [kV]), within the specification of the standard. The waveforms studied in DIAdem are reported to show how they changed increasing the experimental time.

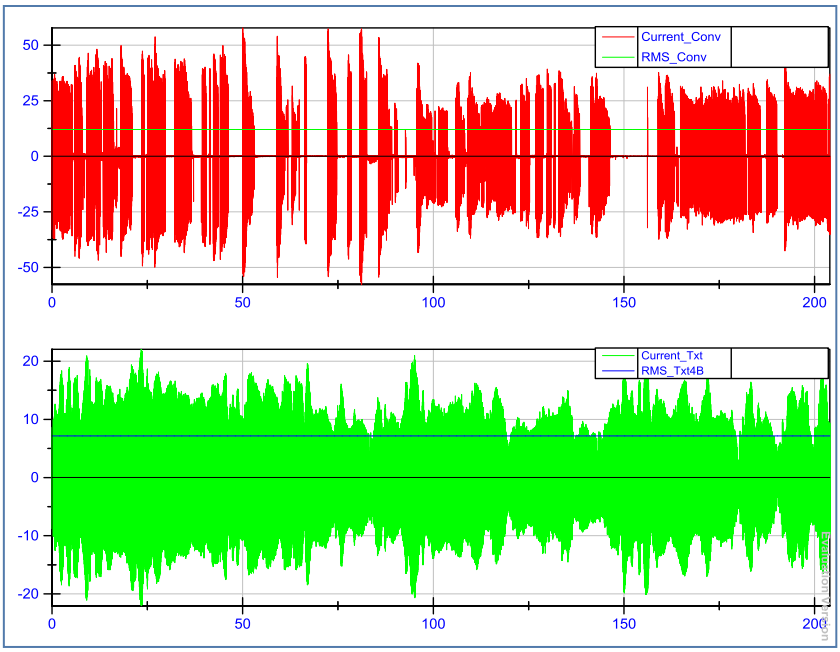

Figure 4.7: current waveforms for test B and relative RMS values, May 10th

The currents and the respective RMS values are showed. In red the flat samples is studied instead the green colour is reserved for the textured specimen. The main difference is the different shape of the waveforms. In the first case the current has some peaks and subsequent holes in which there is no discharge from one electrode to the other, while the other current is smoother and continuous. The reached peaks are lower and the current range is limited. In blue the RMS value can be noticed. The maximum current peak in the flat case reached 57 [mA] which is just under the limit fixed by the norm at 60 [mA]. Projecting this trend would bring to discover that soon the flat specimen fails the test much earlier than the six hours of the inclined plane test.
This high peaks brought to a visible material erosion in the specimen, ensuring that this rectangular sample suffers quite soon after the voltage application.

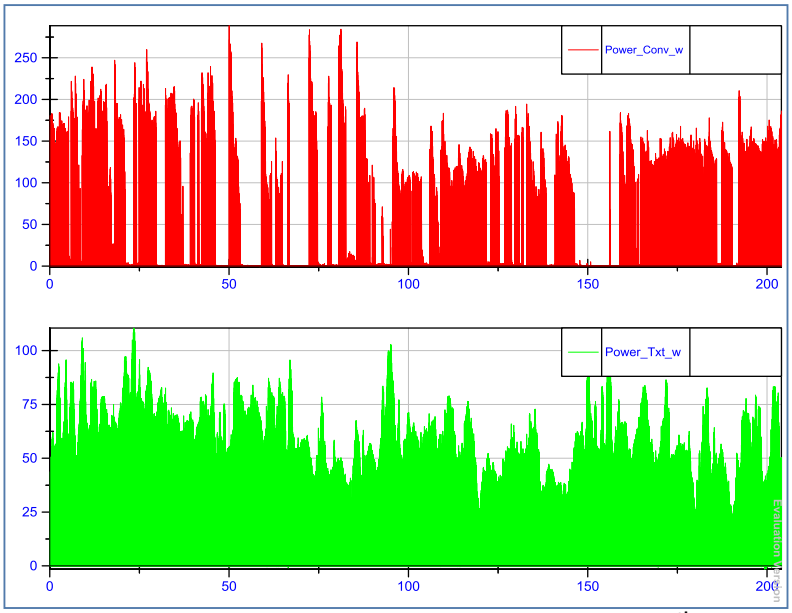

Figure 4.8: power waveforms for test B, May 10th

Previous graphs show the power dissipated in the test samples. The first in red is referred to the flat sample and shows that the peaks reach almost 290[W], compared to the 110[W] of the textured 4[mm] one. Even in this case the shapes are different with the same visible considerations of the respective currents. These evaluations conduced to the energy considerations with which the general behaviour is summarised.
While the test was going on the integral of the power in time increased and it describes how much of the input energy is lost during this test period.
First of all the test B proved the correctness of the first experiment. Furthermore, it allowed a consideration about the flat specimen increasing the range time using the energy parameter. Lastly it allowed a video recording comparison between the currents movements in the two different surfaces.
It has been tried to put in parallel the videos to the electrical data with DIAdem to see what was happening when the sparks were visible and how the electrical data were constituted.
The picture of the three test sample soon after the experiment is reported in figure 4.9. The photo has been taken before washing and cleaning the surfaces. The left one is the conventional and it can be seen that the central part is eroded by the AC current, in particular a deep cavity is scraped from the surface close to the central part of the lower electrode.
This verified the previous literature tests [20] ensuring the same visible results.
The central specimen is the textured 4[mm] A in which the blackish typical of this surface kind can be noted. The black parts denote where the current flowed. This shows that the current has been split in several branches, in particular the experimental test showed that two visible channels has been formed on the textured surface. The first one was in central position along the rectangular specimen, while the second one was present on the left part until the lower electrode. This fact could be addressed to a not symmetrical mounting of the upper electrode, causing a deflected liquid contaminant flow. The current was attracted from the contaminant, so it followed this liquid path. The discharges amount which was visible depended from the flow rate of the pollution, in fact increasing it the current which was flowing raised.
The last specimen (textured 4[mm], test B) has been used only to allow other camera recordings, so the limited time range of voltage application can't permit a blackish formation, but from this observation can be extracted something as well. In fact it has been verified that the first tracking on a rectangular specimen is developed close to the lower electrode, where the contaminant is concentrating.
This proved that particular attention has to be put on this location area.

Figure 4.9: tested samples

In general a different involvement of the surfaces is verified. While for the flat sample the current tends to follow the contaminant flow directly from one electrode to the other in central position, the textured ensured a more homogeneous exploitation of the total surface. This brought to a smaller concentrated erosion, scraping less material from the outer surface.
The specimens have been weighed before the test, soon after and after they have been washed, to see if the amount of material lost was considerable.

Samples	SAMPLE N.1 Conventional	SAMPLE N.2 4 [mm] textured square arrangement A	SAMPLE N.3 4 [mm] textured square arrangement B
1st weight [g]	39,2882	49,5253	49,7969
2nd weight [g]	39,1308	49,3090	49,7237
3rd weight [g]	38,8535	49,2720	49,6225

Table 4.4: weights before and after the test, distinguishing before or after washing.

The weights in table 4.4 haven't showed a big material erosion from the textured samples, while about 1% of the silicone rubber from the flat specimen has been scraped after the material cleaning. It was eroded but still attached to the surface. If the test would be performed for six hours the weight reduction would be around 6-8% [20]. These considerations about the material losses in a rectangular 120x50x6 [mm] specimen, could be extended to the study of the full insulator, which will be used in the practical applications.

During the progress of this test the features of the DAQ system have been assessed. Since it was continuously recording the parameters for which it has been used, some theoretical considerations can be done.
One of the main issues when a fast acquisition recording is going is that the acquisition board should be shielded from the external noises and the environment should be as clean as possible. This fact would bring to a correct data acquisition and the stored data can be directly post processed. If this is not possible a filter should be imposed to study the signals we are effectively interested. In particular in this project the board was not immune to external noises and the laboratory was used also for other experimental tests. During one of the presented IPT tests, an electric arc in the same room has been created and the data acquisition system have acquired it. What can be seen from figure 4.10 is that not only a fluctuation is visible, but it's also bigger than the desirable signal which became negligible compared to the noise. This would bring to a wrong evaluation of the parameters causing a false qualitative representation of the physical phenomena.

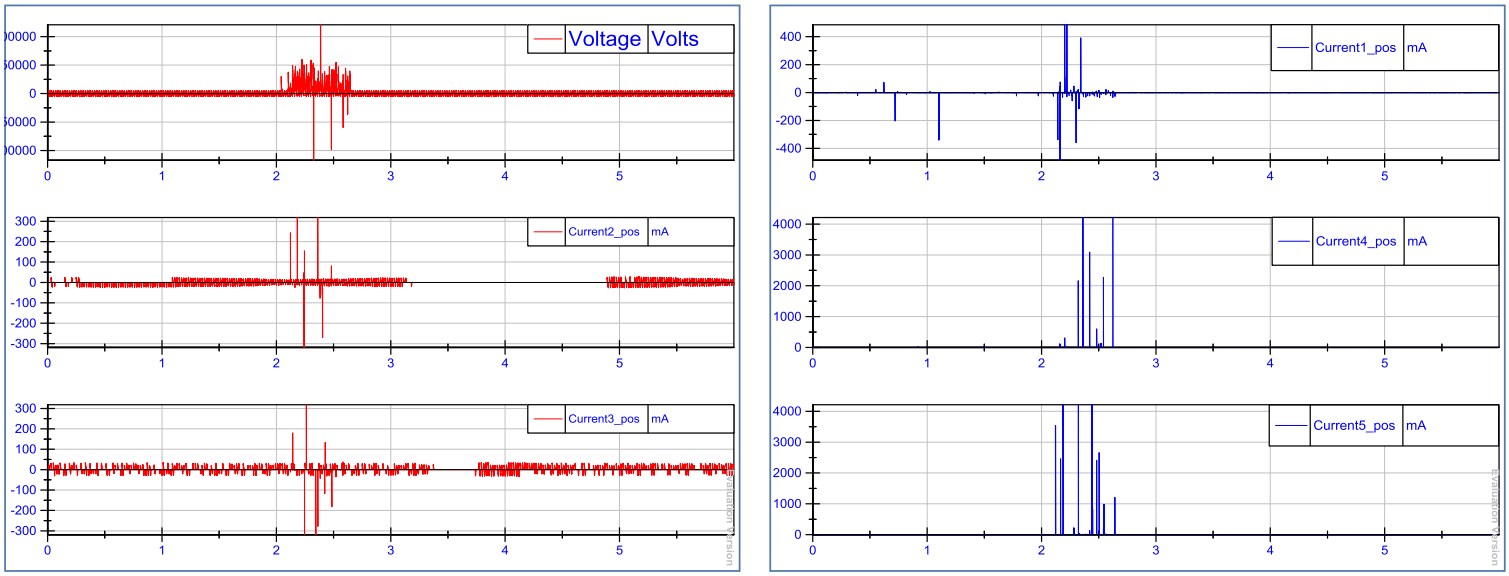

Figure 4.10: spark in the same room which brought to a noise in the acquisition.

In the first graph the noise is visualised on the voltage signal and on two channels used for the currents acquisition. In blue the noise has been acquired also from the channel which weren't used for the data acquisition. The induced values have been so high that the desirable signals can't be valued if the original scale is maintained. The turbulence lasted for less than one second but the system was able to acquire it as a fast change in the input parameter applied to the electronic board. To clean the signal a post processing filter should be used or, as in this case, the six seconds range should be removed from the data to analyse.
These considerations have been done here to focalise the attention on the difficulties encountered while testing, showing all the aspects which have been kept in consideration before, during and after all the experiments.

4.3 Test Day 6th June

The second test day has been set several days after the first one allowing a better comprehension about how the cameras were working and which was the best way to acquire the videos. Furthermore this time has been used to post process the data and to decide in which parameters we were more interested. The accumulated energy has been confirmed as the key parameter of this study, finding confirmation in the literature about this research field.
The tests have been carried out in the same way as the previous ones. The experience gained and the dexterity with the ageing unit allowed to decrease the preparation time of the specimens and the setting time of the appliances. Also in this case the acquired signals have been scaled after the tests because the scaling coefficient was varied. In fact, during this experiment, a LeCroy oscilloscope has been used in comparison with the acquisition LabVIEW software, to double check the acquired signals. This addition modified the total impedance of the electric circuit, so the scaling factor was not previously known.
In particular, the current factor has been kept at 30,1657 as the first day test, while the voltage coefficient has been calculated starting from the real value applied on the specimens and indicated by the Hipotronics power unit and the RMS values calculated in the post processing analysis.
The same TDMS files stored from LabVIEW have been used and each one of this has been merged with the adjacent to build the total observed waveforms. A simple MATLAB code has been developed to do this, a short version of it is reported below.

```
close all;
clear all;
clc;


tic

load -ascii test0.txt
load -ascii test1.txt
load -ascii test2.txt
load -ascii test3.txt
load -ascii test4.txt
.
.
.
load -ascii test33.txt

%%

t = linspace(0,34*6,34*size(test0,1));

table = zeros(34*size(test0,1),size(test0,2)+1);
table(:,1) = t;
for i = 1:1:size(test0,2)
   table(1:60000,i+1) = test0(:,i);
   table(60001:120000,i+1) = test1(:,i);
```

```
   table(120001:180000,i+1) = test2(:,i);
   table(180001:240000,i+1) = test3(:,i);
   table(240001:300000,i+1) = test4(:,i);
.
.
.
   table(1980001:2040000,i+1) = test33(:,i);
end

%plot(table(1:end,1),table(1:end,4))
%xlim([0,6*34])

save thomas3.txt table
table1 = table(1360001:2040000,:);
xlswrite('testdata3.xlsx',table1)

toc
```

In the first program section the data, previously saved ad .txt files, are loaded. A timeline is created with the linspace command to ensure that all the points are evenly spaced from the others. After this a matrix is built: in the first column the time is inserted, the second represents the voltage values and the other three columns bring the current values in the tested specimens.
MATLAB has been used also to double check that the waveform graphs were correct, plotting every time the desired parameter versus time.
The second test day can be divided into three experiments, everyone subsequent to the other. The same three specimens have been tested on the incline plane machine. Since a basic knowledge about the main difference between a conventional sample and a textured one has been achieved, the purpose has now been to study deeper the performances of more textured samples. To do this a flat specimen in parallel with two textured samples have been tested. The two textured had different surface type: a 4[mm] and a 6[mm] square arrangements have been compared. Now the focus has been concentrated on the rough surface because it has been verified being the best solution against leakage currents.
A rigorous description of the tests is now presented, leaving the common comments at the end of the explanation.

4.3.1 Test 1

The first part of the experiment involved the setup and the check of the unit and the preparation of the relative components.
The contaminant resistivity of the solution has been measured and the value was 2,55 [mS/cm] at 19 [°C], that corresponds at 3,92 [Ωm], so very close to the standard value of 3,95 [Ωm]. The contaminant has been renovated after the first test day.
The DAQ system has been set with the desired parameters to increase the sample rate bringing it to the maximum the card could acquire:

- Rate sample per channel/s: 20000 [s/cycle];

- Samples per channel: 30000;
- Task/channel: IPT3, that was the function created ad hoc to acquire in parallel the voltage and 5 different currents, one for each bay.

The saving path had to be specified, otherwise the program wasn't correctly initiated. For this test the bays 2-3-4 have been used to put the specimens as closest as possible to allow a good visual recording. The acquisitions have been achieved through CH 2, CH3 and CH5, because they resulted the most shielded in respect to the others (figure 4.11).

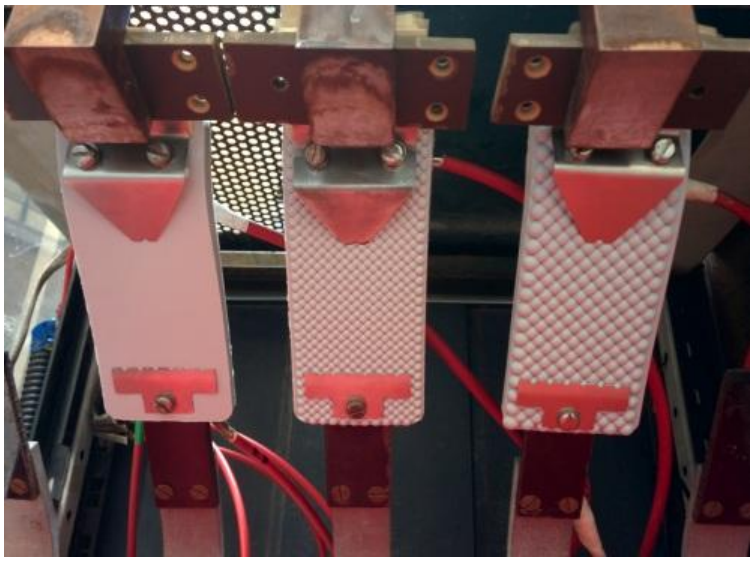

Figure 4.11: IPT, 6th June

The software has been set to acquire in differential mode without scaling factor. It has been added after the acquisition exploiting the post processing analysis. The maximum limits have been imposed to ±10 [V] to cut the signals over these values and protect the board (figure 4.12).

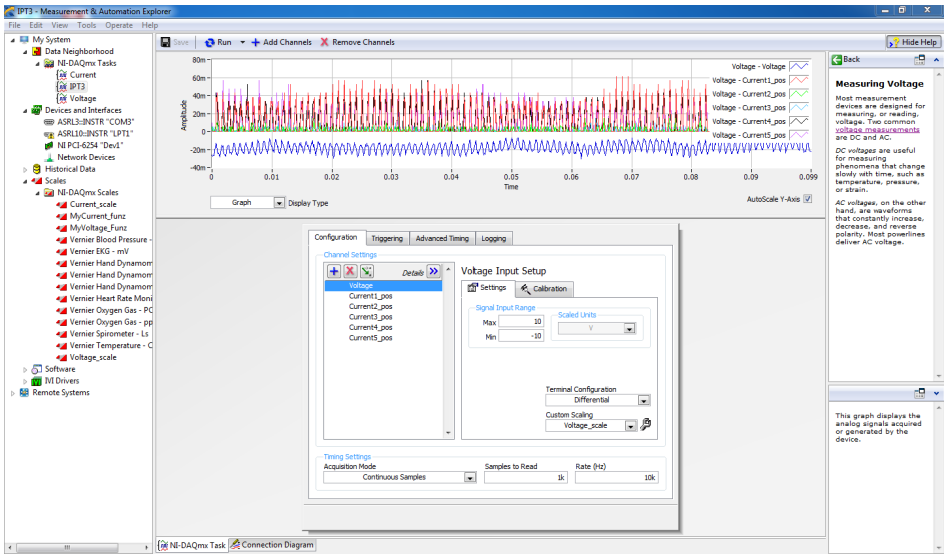

Figure 4.12: setup of the ±10[V] voltage limits for the board.

The pump has been started and after the pipes have been fulfilled after about 7 [min], the voltage has been supplied. The first test has been operated at 3,412 [kV] and it takes about 10 minutes in total. In figure 4.13 the voltage waveform can be seen: the peaks reach almost 5000 [V], so all the circuit insulation has to keep at least this potential.

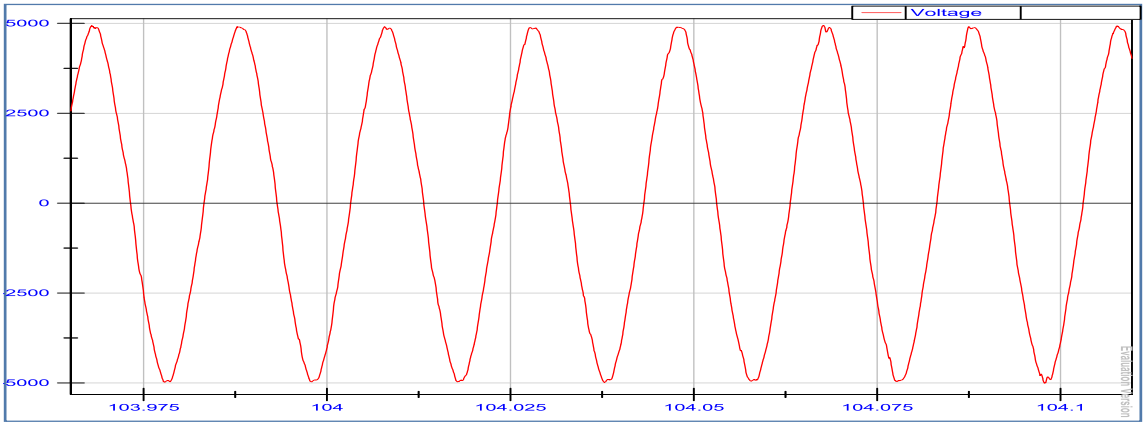

Figure 4.13: voltage signal applied to the specimens

The voltage scale which has been used was 12028,84 and the current scale the previously reported 30,1657.
The stored files have been divided by LabVIEW in parts of 3 seconds with 60.000 measurement points for each one. The voltage and three leakage currents were contained.
For the analysis it has been followed the same concept already applied for the first day test. Where the signals have been considered acceptable, they have been studied. The starting point was set when the voltage reached the regime.
From test13 to test197 have been considered, which corresponds to 185 files * 3 [s] = 555 [s], i.e. 9 [min], 15 [s]) for a total of 11.100.000 points evaluated.
The merging of these files have been executed, creating only one file easy to handle and to visualise. The time column has been added in first position[7] and a matrix was completed by the voltage in second column and the three currents respectively in third, fourth and fifth columns.
Importing this file in DIAdem a post processing analysis has been possible: the leakage currents in which we focused our attention are plotted below (figure 4.14).

[7] *This allowed to show the waveforms versus time in graphs, where time is represented by the x-axis.*

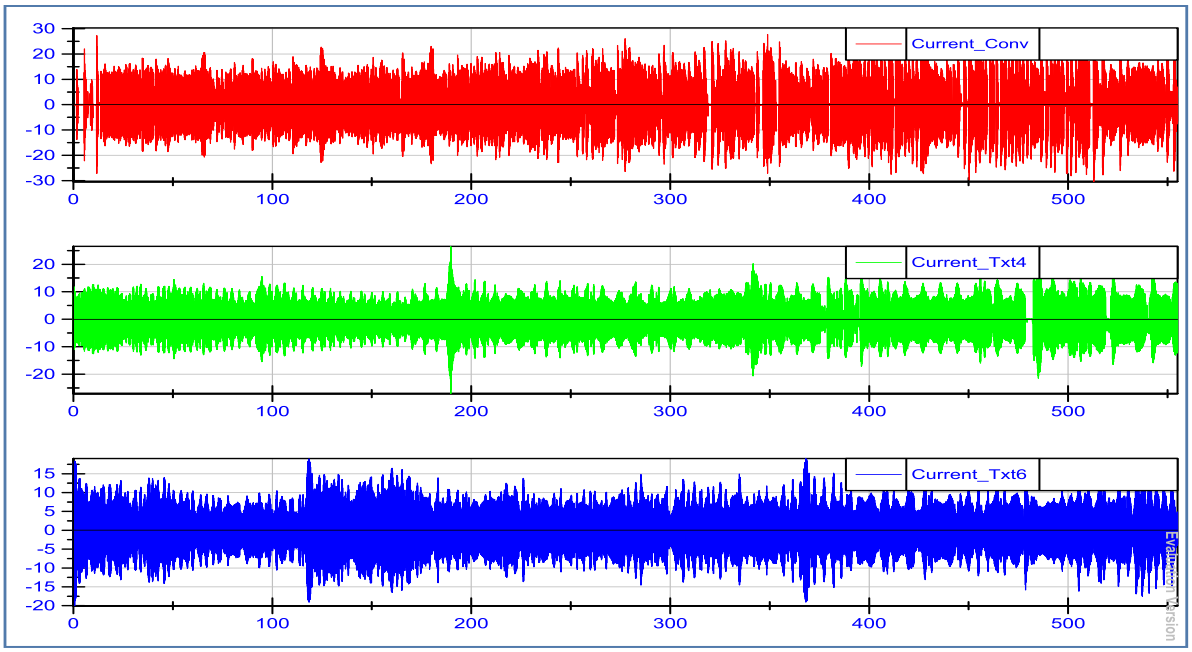

Figure 4.14: leakage currents of test 1, 6th June

The current in red flowed on the conventional specimen surface, while the green one through the textured 4[mm] and the blue through the textured 6[mm] sample.
It can be easily distinguished that the shapes are very different. In the first case the current has higher peaks and valleys with some intervals in which the current level is zero or close to it. Instead for both the textured, the current waveform is smoother ensuring less and lower peaks.
The power is also represented in figure 4.15, showing a different behaviour according to the surface type. In the first case the leakage current brings to a greater dissipated power, while for the textured specimens it is limited under 100[W] for the 4[mm] (excluding an exceptional peak above 125[W]) and for the 6[mm].

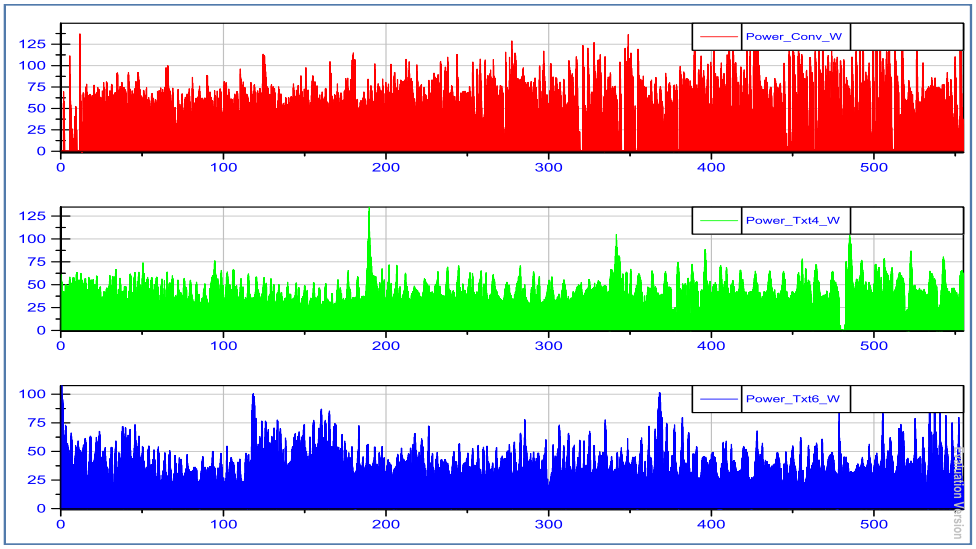

Figure 4.15: power waveforms of test 1, 6th June

These visual considerations of the electric data brought to summarise the values in a table, which will be compared with the other tests further in time.

Sample	Conventional	Textured 4 [mm]	Textured 6 [mm]
Voltage [kV]	3,412	3,412	3,412
I rms [mA]	6,42	5,31	5,15
I min [mA]	-30,38	-27,07	-20,03
I max [mA]	30,31	26,54	19,03
Range [mA]	60,69	53,61	39,06
P max [W]	149,47	134,88	107,56
P mean [W]	21,91	18,12	17,57
Dissipated energy [J]	12157,3	10055,33	9752,35

Table 4.5: result parameters of the test 1, 6th June

In this case test, which has been applied to a virgin material, the energy dissipated in the conventional surface is greater than the energy in the 4 and 6[mm] textured samples. This is confirmed from the previous tests and similar results have been already achieved in earlier experiments carried out in [20] and in [12].
A quite long time has been left for the data saving from the fast camera. After that the test has been performed again with the same specimens.

4.3.2 Test 2

The machine has been set with the same parameters as for the test 1. The scope was not only increase the testing time for each specimen but also allow more acquisitions from the cameras. The voltage applied for the second test has been 3,761 [kV], with a linear scale of 12158.89[8] and a current scale fixed at 30,1657.

Since the speed rate was not modified from test 1, the saved files have been divided by LabVIEW in parts of 3 seconds, with 60.000 points of measurement for this period of time.
The same criteria has been applied to select the correct records for the analysis. The voltage level was at regime from test12 to test212, which corresponded to 201 files * 3 [s] = 603 [s] (10 min 3 [s]) for a total of 12.060.000 points evaluated.
A matrix with all the values has been created and every physical quantity has been plotted.
The leakage currents are visualized in figure 4.16:

[8] *The scaling coefficient is different from the previous one because an oscilloscope is connected in parallel to the acquisition to visualize the waveforms. This modified the total impedance of the electric circuit.*

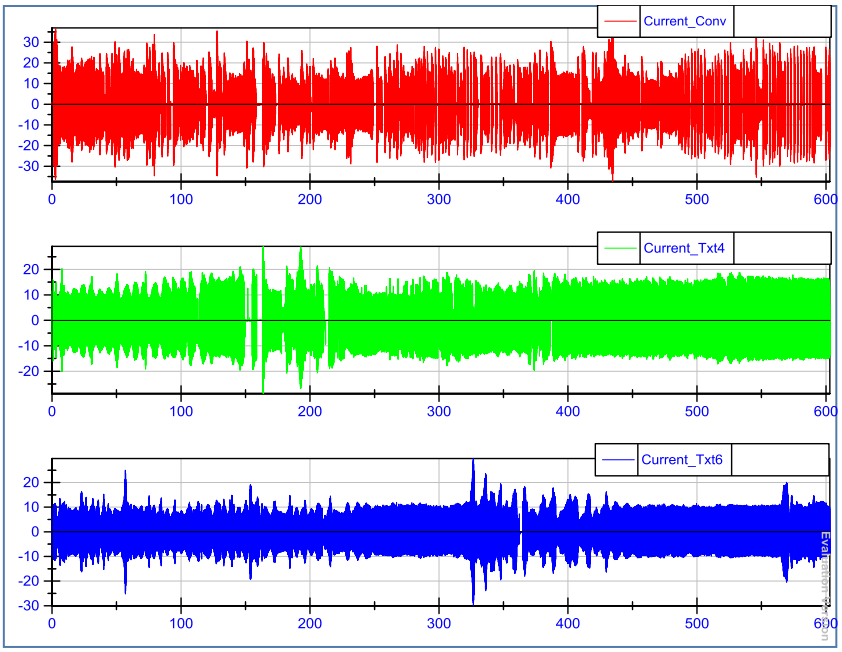

Figure 4.16: leakage currents of test 2, 6th June

Even if the time was going on, the behavior was the same as the firsts nine minute testing. Many peaks can be observed from the red graph, which indicates the leakage current on the flat specimen. The peaks values are even two times bigger than the ones reached in the textured specimens, both 4 and 6[mm]. This shows that increasing the time for which the samples are tested, an incremental difference can be noted. The RMS values are raising for each specimen, but in the flat case the speed is greater. This fact denotes a rapidly worsening of the surface insulation property which can be visually verified directly on the specimen.
The instantaneous power has been plotted below in figure 4.17.

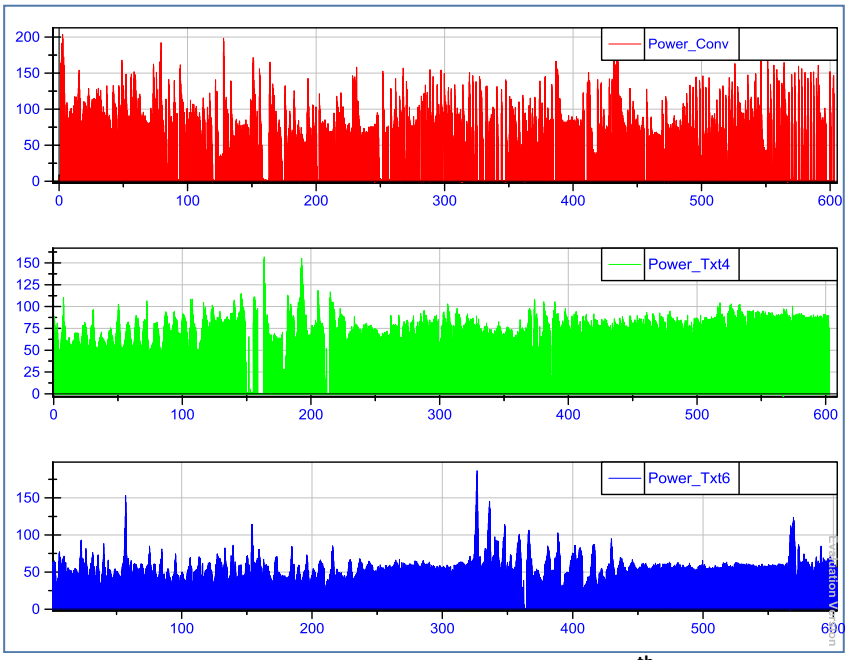

Figure 4.17: power waveforms of test 2, 6th June

The graph shows a trend similar to the test 1, in this case with a bigger difference from the two textured specimens. In this set of 10 minutes the 6 [mm] textured sample seems to oppose itself better to the current flow. The consequence is less power dissipated and an accumulated energy of about 2 [kJ] lower.
In table 4.6 the electrical analyzed results of the second test have been reported.

Sample	Conventional	Textured 4 [mm]	Textured 6 [mm]
Voltage [kV]	3,761	3,761	3,761
I rms [mA]	7,20	6,37	5,57
I min [mA]	-37,43	-28,79	-30,03
I max [mA]	36,93	29,07	29,74
Range [mA]	74,36	57,86	59,77
P max [W]	203,46	156,97	186,52
P mean [W]	27,08	23,96	20,95
Dissipated energy [J]	16328,76	14446,41	12632,11

Table 4.6: result parameters of the test 2, 6th June

A common consideration can be done after the last test, when a general behaviour of the specimens has been compared.

4.3.3 Test 3

The last test of the second day has been performed without changes. The electric connections and the software parameters have been kept equals to the earlier ones.
The voltage applied at the bays during the third test has been 3,761 [kV]. After the signals have been acquired with DIAdem a scaling factor of 12101,73 has been applied. For the currents the same coefficient has been used: 30,1657.
The stored files have been divided by LabVIEW in parts of 3 seconds, with 60.000 evaluation points for this period of time.
The files analyzed in this post processing were from test3 to test172, which correspond to 170 files * 3 sec = 510 [s] (8 min 30 sec) for a total of 10.200.000 points evaluated.
The plots for this test case are shown below, in figure 4.18 and 4.19.

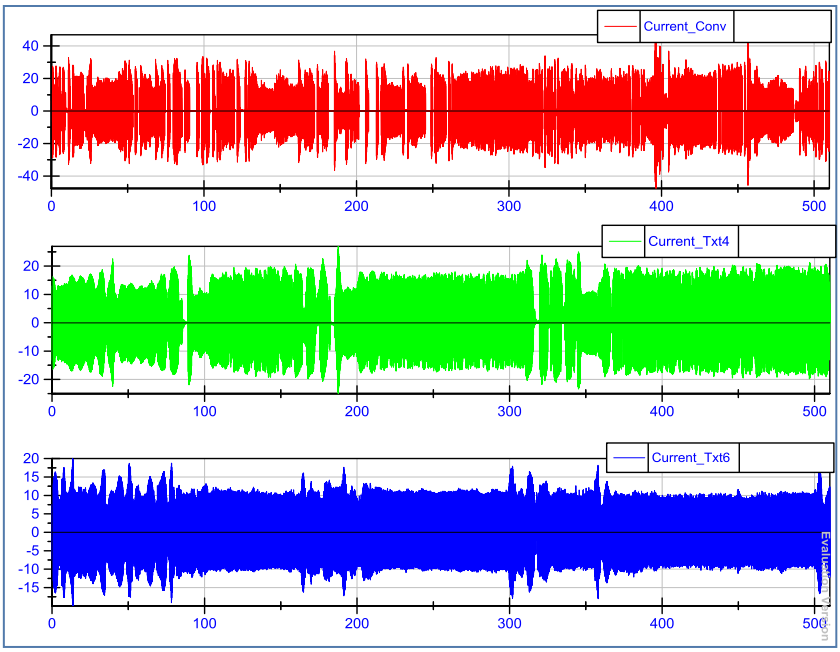

Figure 4.18: leakage currents of test 3, 6th June

Also in this case it has been verify a different behavior of the current on the surfaces. Several peaks are still present in the flat specimen, with a double amplitude in respect of the ones for the textured samples. The 6[mm] seems to perform better than the others. In the blue graph in fact, there are no evident valleys in the current waveform. This doesn't allow a subsequent high peak, which could be deleterious for the specimen or for abbreviate the insulator lifespan.

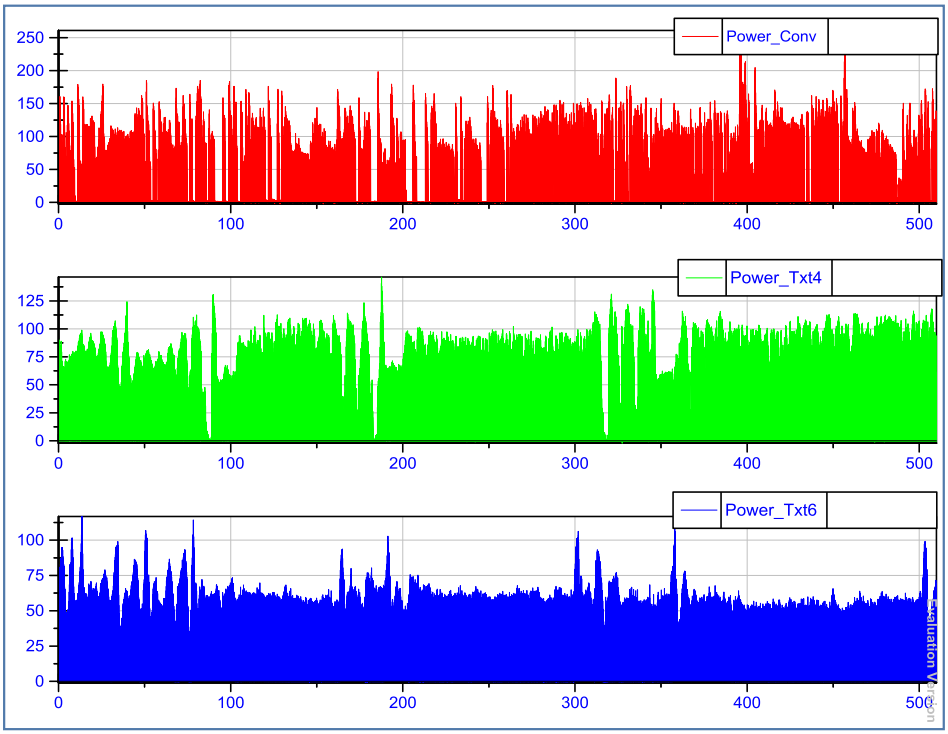

Figure 4.19: power waveforms of test 3, 6th June

From the power graphs analysis it can be noticed that the lowest power peak is guaranteed by the 6 [mm] square arrangement sample, with a difference from the flat specimen of more than 140 [W].
The mean power shows a divergence of about 10 [W], which is reasonable if we consider the limited time range in which the test has been performed.
As previously done, also for the third test the electric collected data have been summarise in table 4.7.

Sample	Conventional	Textured 4 [mm]	Textured 6 [mm]
Voltage [kV]	3,761	3,761	3,761
I rms [mA]	8,12	6,90	5,81
I min [mA]	-47,65	-25,00	-19,93
I max [mA]	46,9	26,95	20,01
Range [mA]	94,55	51,95	39,94
P max [W]	260,96	146,35	116,74
P mean [W]	30,54	25,95	21,85
Dissipated energy [J]	15575,05	13234,96	11144,22

Table 4.7: result parameters of the test 3, 6th June

Going forward with the tests, the gap between the RMS value of the leakage currents increases. This can be achieved observing in succession the tables. After half an hour test this gap increased to about 1,2 [mA] from the flat to the 4[mm] specimen and even at more than 2,30[mA] if we consider the flat and the textured 6[mm] surface. The result is a lower energy dissipation in the textured samples confirming what we were interested to prove with these tests. This will result in lower losses during the future applications in real cases, as overhead lines and substations.

A comparison between the three specimens have been now analised. To help with this analysis a visual and an infrared images for each tested type have been showed.

- **Conventional**

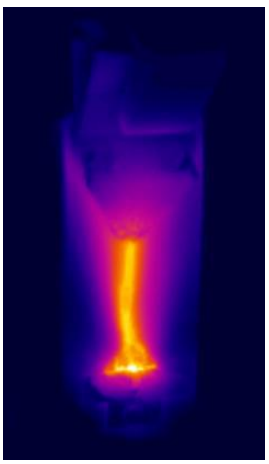

Figure 4.20: Non-textured sample during the inclined-plane test. The visual record showing anchored metal-arc discharges at the ground (left) and infrared record showing the narrow contaminant stream and the arc discharging near the ground electrode (right).

In the flat specimen the contaminant flow remained narrow on the sample surface throughout the test (figure 4.20). The first few minutes of the test, discharge activity was random all over the test surface. Soon, however, dry-band formation was concentrated near or at the ground electrode region where unstable metal-arc discharges tend to anchor at a specific location, causing severe erosion which eventually would bring to a failure of the six hours inclined plane test as specified in IEC 60587. This can be extended to all the non-textured samples [20].

- **Textured**

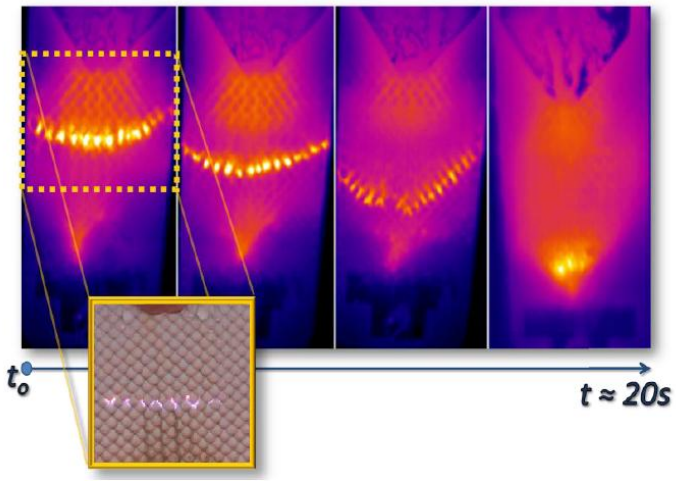

Figure 4.21: dry-band arcing in the 4[mm] textured sample

The dynamics of surface discharges for textured samples were significantly different than the case of non-textured samples. Arcing at the ground electrode was drastically reduced, and stable and controlled dry-bands formed which could be seen with a naked-eye and were also detectable with the infrared camera. Due to the geometry of the upper high-voltage electrode, dry-band formation was first detected in the adjacent area, and it was characterised by three main features. The development of a line of short parallel and dynamic streamer discharges, that gradually spread across the width of the sample were visually observable. The onset of these surface discharges was associated with a fall rather than an increase of current. This 'necklace' shape of discharges along with the dry-band, moved in the direction of the contaminant flow, reaching the ground electrode after some seconds. The time required for the discharges to traverse the sample surface was greater than the time needed for the contaminant to move from the top to the lower electrode. This discharge activity pattern was repeated throughout the test. While, in the beginning, the contaminant flow remained narrow, it was later spread on the sample surface as indicated by the infrared records (figure 4.21). Occasionally, the line of

streamer discharges would extinguish while moving along the sample surface but most of the time they would reignite. Whenever the line of discharges reached the ground electrode, the discharges would transform to metal-arcs that would be localised, causing limited erosion.

- **Textured 4[mm] sample**

In particular in the 4 [mm] textured sample a line of parallel streamers spread across the width of the sample and advanced towards the ground electrode. A close inspection of these faint discharges revealed that the discharge channels formed along the intersecting edges of the hemispherical protuberances. In the square pattern, all intersections are aligned at 45 degrees to the electric field direction. (Figure 4.21) shows the dry-band discharges on a 4[mm] square sample along with the timeline. These discharges, as seen with the naked-eye, are rich in UV, which is typical of streamers growth. As the discharge approached the proximity of the lower ground electrode, the discharges got elongated and tend to jump over the protuberances rather than following the intersections paths. The IR records and the temperature profiles show obvious similarities with the dry-bands observed for silicone rubber insulators which were also maintained by streamers spanning the dry-bands at the insulator shank. [20]
With the help of a high-speed camera operating at 7000 [fps], it has been observed that not more than 3 discharges bridged the dry-band per half-cycle of current. The onset of the faint discharges were again associated with a fall of current and the time required to traverse the sample surface was slower than the time required for the contaminant to reach the ground electrode.
Figure 4.21 shows IR records of a line of discharges advancing towards the ground electrode. During this transit, the streamer discharges of the moving dry-band could briefly extinguish only to resume few seconds later. It took approximately 20 seconds to cross the whole length of the sample. Near the ground electrode, the discharges got elongated and took the form of metal-arc discharges but these were very mobile, thus erosion and material loss were greatly alleviated.
This repetitive pattern could be interrupted by periods of no activity. These ‘dark periods’ were associated with the erosion of the sample around the ground electrode that sometimes inhibited contaminant flow continuity.

- **6[mm] intersecting square samples**

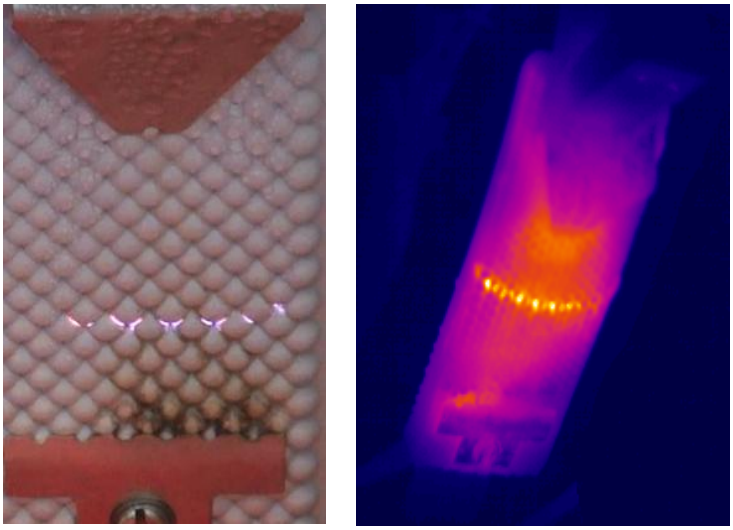

Figure 4.22: dry-band arcing in the textured 6[mm] square arrangement sample

The line of streamer discharges traversed the sample surface and the onset of these discharges was associated with a fall of leakage current. The 6[mm] intersecting square pattern had overall a very similar behaviour to that of the 4[mm] intersecting square configuration, with the material loss due to erosion being slightly smaller than the 4[mm] intersecting square pattern. In fact the samples have been weighted before the test, after the test with the eroded material attached and at the end, after the samples have been washed and cleaned.

Samples	SAMPLE N.1 Conventional	SAMPLE N.2 4 [mm] textured square arrangement	SAMPLE N.3 6 [mm] textured square arrangement
1st weight [g]	39,2217	48,8482	53,7131
2nd weight [g]	39,0354	48,8288	53,6540
3rd weight [g]	38,8535	48,6455	53,6146

Table 4.8: weights before and after the test, distinguishing before or after washing.

As we can see the weights are quite similar if we consider before and at the end of the test with the material adherent (considering in total about 40 [min] test). The weight after washing is a little bit lower, showing that some parts of the specimens were eroded, but also these are negligible (we respectively have a reduction of 0,93[%], 0,4[%] and 0,18[%]).
Furthermore, a naked eye observation of the specimens has been carried out. This was done to verify the results achieved with the first day test and to see the behavior of the 6[mm] textured. The comparison brought to a similar physical ruin of the surfaces

already experimented in the earlier tests (figure 4.23)[9].

Figure 4.23: specimens conditions after test, 6th June

While in the flat sample the deeper erosion was concentrated on the lower electrode, in central position, both the textured samples gave a blackish homogeneous production on the surface. This ensured a lower concentrated tracking and a smaller eroded material, as verified with the weights.

[9] *The figure shows the specimens soon after the test execution.*

CHAPTER 5

Post-processing analysis and comments to the results

To study all the presented graphs, tables and especially for the coordination between different data types, DIAdem has been used in this way.
To put together visual, IR and electric data the software has been set to visualise three windows in which the desired data have been imported (figure 5.1).
The hardest part of the work was exactly synchronize videos and data. In this project a trigger event as a lightning was not present, so the synchronization has been achieved using the GPS of the cameras, which connected to the same time, allowed to relate the information. In this way a correct study has been possible, visualizing the same physical phenomena in three different data types. The high speed camera recording could be addressed to the same way of studying.

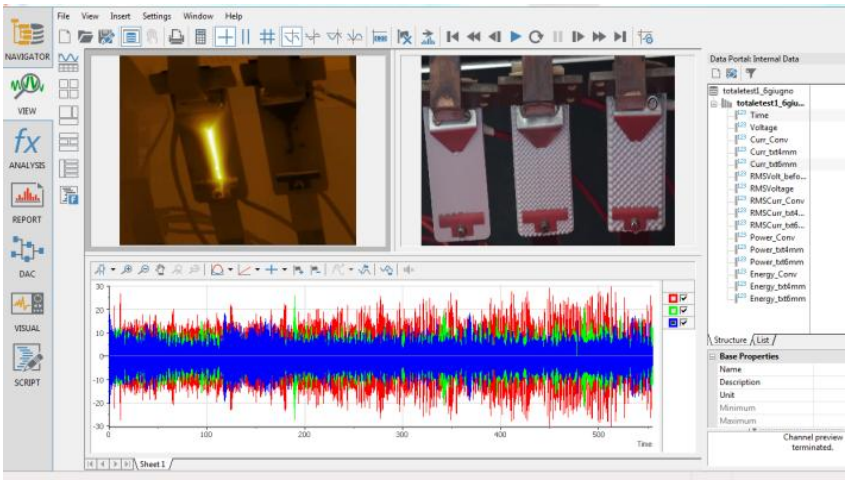

Figure 5.1: post-processing analysis in DIAdem

In the "VIEW" section the signals visualization was possible, to allow a direct comprehension of the selected data. In "ANALYSIS" the tools to calculate the values reported in the data tables were present and with the "REPORT" section it has been possible to export the desired information in form of graphs or tables in different formats.
Thanks to this a deeper comprehension of the physical phenomena has been achieved. Figure 5.2 shows the leakage current waveform during the progression of a line of streamer discharges of a textured sample from their inception at the upper electrode until the phenomenon ends with metal-arc discharges at the lower ground electrode. The graph is accompanied by the infrared records corresponding to different instants during the discharges progression.

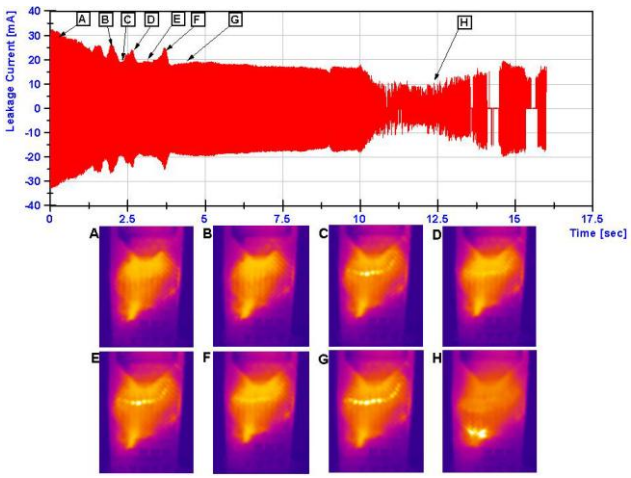

Figure 5.2: leakage current waveform decay associated with the progression of streamer discharges and corresponding infrared images. The onset of streamer discharges is associated with leakage current valleys (C), (E) and (G) while current peaks (B), (D) and (F) occur when discharges extinguish. The event ends with metal-arc discharges (H).

Data analysis showed that the onset of the discharges spanning the dry-band is associated with a fall of leakage current. The correlation of IR records showing active discharges spanning the dry-band corresponds to points of minima (valleys) of the leakage current waveform whereas when the discharges extinguish during progression, they correspond to points of maxima (peaks).
Figure 5.3 shows another current waveform record of the dry-band progression. In this case, the dry-band traversed the sample surface from its inception at instant A until it reached 8.5[s] later the lower ground electrode at instant E. The waveform showed the characteristic decay shape with peaks and valleys. At the lower electrode, the current was further reduced and the discharges took the form of metal-arcs (instant F) until they self-extinguished and a new cycle of progression began.

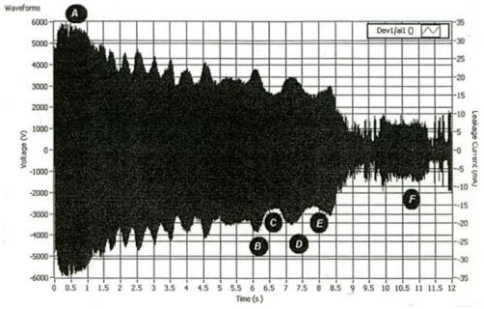

Figure 5.3: data-logging of leakage current during the traverse of a dry band. Vertical scale: 5[mA/division]. Time scale: 12[s].

Peaks, like those at instants B and D, were followed by current valleys, like those at instants C and E. Visible streamer discharges matched current valleys whereas intervals of no visible discharges were correlated with instants of peak currents.
These intervals were attributed to a temporary re-wetting of the dry-band by the

contaminant stream.
Figure 5.4 shows current waveform cycles corresponding to the three main instants observed during the progression of the line of discharges for a textured sample: peaks, valleys and discharges. The waveform starts as a sinusoid for the points of maximum indicating conduction current in the polluted layer, while it became more distorted with nearly flat sections around zero when streamer discharges appeared. The wave shape got even more distorted when the discharges turned from streamer to arcing type at the lower electrode.

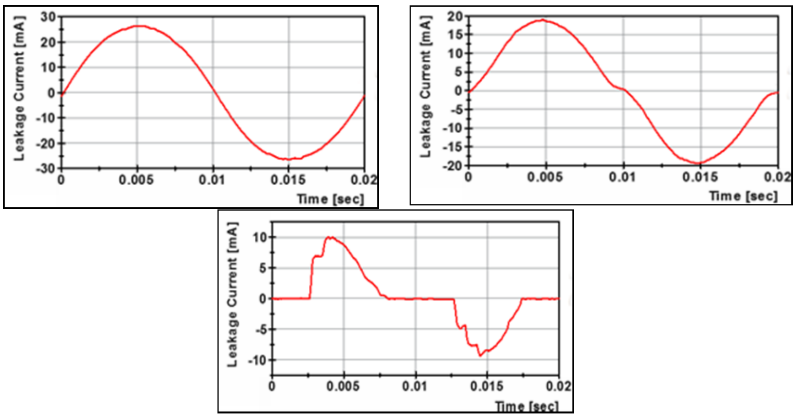

Figure 5.4: current waveforms of leakage current during the advance of a line of discharge corresponding to (a) peaks (b) valleys of leakage current and (c) arcing-like discharges.

These current logs suggested that the discharge channel conductance was less than the conductance of the pollution layer. From figure 5.3 and the data points corresponding to peak values, the pollution layer conductance decay can be approximated by:

$$i_L\,(t) = 32{,}5e^{-0{,}075t}\ [mA]$$

The combined conductance of the pollution layer and the discharges also decayed during the dry-band progression. From the valleys data points:

$$i_{LD}\,(t) = 26{,}6e^{-0{,}08t}\ [mA]$$

Figure 5.5 presents the decay of both the pollution layer and the combined pollution layer and discharges current conductance for the case of figure 5.3. [20]

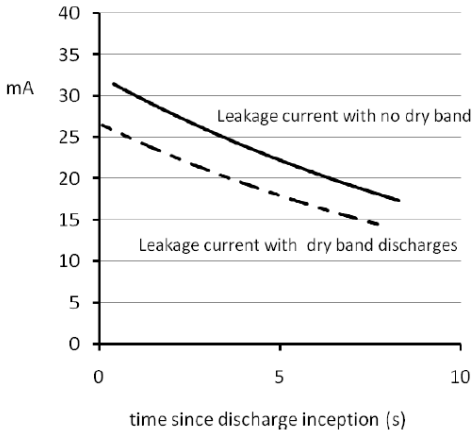

Figure 5.5: current decay trendlines for the case of Figure 5.3.

In addition to this analysis, a snapshot (figure 5.6)[10] represents that the voltage waveform has a fluctuation where there discharges start, so where the current increases from zero to its value.

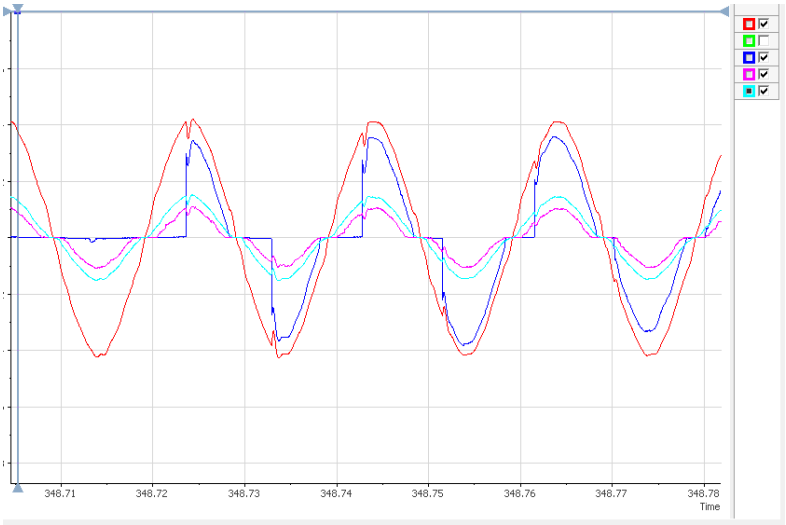

Figure 5.6: fluctuation of the voltage sine wave

This could be referred to the fact that the power supply hasn't an infinite short circuit power, so when the leakage current is present and the short circuit from the electrodes is established, the voltage waveform is no longer a "clean" sinusoidal.

[10] *The current scale has been changed to show the behavior referred to the voltage in red. In blue the conventional current, in purple the textured 4[mm] current and in cyan the current on the textured 6[mm] sample.*

Contaminant layer conductance

The current decay is a result of the reduction of the conductance of the pollution layer. The layer conductance is reduced due to evaporation caused by the ohmic heating on the sample surface as revealed by the IR records.
If we assume that the evaporation rate, and thus the layer conductance, is proportional to power loss, then

$$\frac{dG_L(t)}{dt} \propto -U^2 G_L(t)$$

which would indicate

$$G_L(t) = G_L(0)e^{-kU^2 t}$$

This is consistent with the current logs and the observed decay of current. For a test voltage of 3.5 [kV], the measured leakage current displayed in Figure 5.3 gives an initial conductance value of 6.6 [μS] that falls to half-value after 8 [seconds].

Combined discharge-layer conductance

The ratio between the leakage current during the presence of discharges and the current when the discharges are absent is

$$\frac{i_{DL}(t)}{i_{L(t)}} = 0{,}82e^{-5*10^{-3}t} \approx 0{,}8$$

The ratio is, therefore, constant and equal to 0.8 for the duration of 8 [seconds].
This means that the combined conductance of the contaminant layer and the discharges, GDL, is lower than the conductance of the layer alone, GL, and it falls from 5.4 [μS] to 2.7 [μS] during this time.
If we represent the combined conductance as the conductance of the layer in series with the conductance of the discharges (figure 5.7) then

$$G_{DL} = \frac{G_L * G_D}{G_L + G_D}$$

and the discharges conductance will be

$$G_D = \frac{G_{DL} * G_L}{G_L - G_{DL}}$$

The discharge conductance, therefore, falls from 29 [μS] at t=0[s] to 13[μS] at t=8[s].
If there are several discharges bridging the dry-band, these values are the sum of the

conductance of each individual discharge spanning the dry-band.

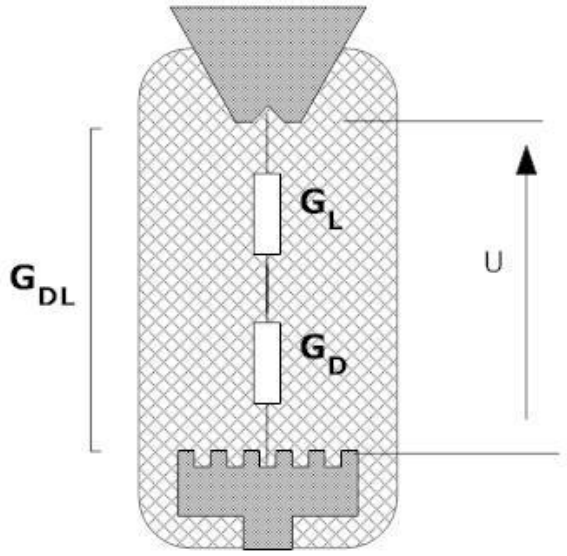

Figure 5.7: the combined conductance of the pollution layer with the presence of dry-band discharges represented by the conductance of the layer in series with the conductance of the discharges.

Modelling of the discharges

The voltage UD across the dry band when bridged by the discharges is

$$U_D = \frac{G_L}{G_L + G_D} U = 0{,}18U = 635\ [Vrms]$$

For the 4[mm] intersecting square pattern, the dry-band discharge tends to follow the edges of the protuberance intersections. Therefore, the length of the discharge path is

$$Discharge\ path\ lenght = \frac{\Pi * protuberance\ diameter}{2\sqrt{2}} = 4{,}44\ [mm]$$

Therefore, the peak voltage gradient along a discharge would be

$$E_D = \frac{\sqrt{2}*630}{4{,}44} \cong 200\ [\frac{V}{mm}]$$

The peak voltage gradient along the 50mm of the pollution layer is

$$E_L = \frac{\sqrt{2}*3500}{50} \cong 100\ [\frac{V}{mm}]$$

The peak voltage gradient along the discharge is, therefore, significantly greater than the peak gradient along the leakage path of the pollution layer, thus causing the fall of current during dry-band discharging.

Comparison with the streamer-spark model

The measured fall of voltage of 630[V] is in good agreement with the predicted voltage for dry-band breakdown described by the streamer-spark model. According to this model, a discharge channel length (C+S) comprises a channel C (gradient 100[V/mm]) and the associated streamer S (gradient 500[V/mm]). For A.C. arc reignition, it is estimated that the length ratio C/S to be 5:1. Thus, for (C+S) =4.44[mm], the voltage drop across the discharge will be
C= 3.7[mm], S= 0.74[mm] and
UD = 0.74[mm] x 500[V/mm] + 3.7[mm] x 100[V/mm] =740[V]
which is of the same order given by the experimental value of 630[V].
The model also predicts that the current will be described by the relationship

$$i_D = 0{,}46(C + S)[A * m] \; or \; 2{,}05 \; [mA]$$

which is lower than the experimental values measured that were in the range of 15-30[mA]. However, the measured currents may be the sum of currents of parallel discharges. Overall, the experimental results support a model of a low current, small-scale spark development. [20]

CHAPTER 6

Full insulator manufacture

Two of the possible tests to achieve a better comprehension about the performances of the textured silicone rubber insulators under polluted conditions are the fog chamber and the rotating wheel experiments.
Both these tests need full insulator prototypes.
For this reason several insulators have been built. The scope was the same as the IPT: record and understand how the arc was developing on the textured surfaces.
Two types of conventional insulators of different profiles have been manufactured: Type 1 and Type 2.

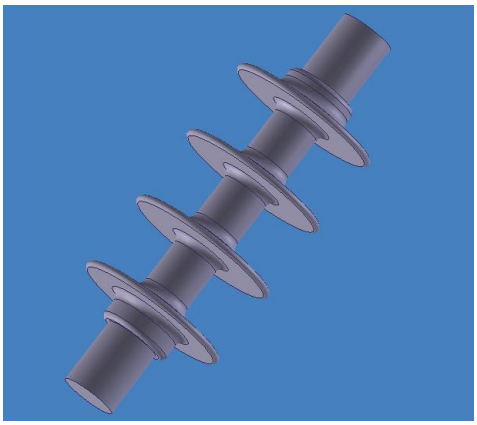

Figure 6.1: Type 1 conventional 11 [kV] silicone rubber insulator design

Both profile designs are based on commercially available insulators. Type 2 is characterised by a longer creepage distance and bigger sheds than Type 1. Also, Type 2 shank diameter does not remain the same for all sections, but the middle section has a smaller diameter.
It has been chosen to manufacture a Type 1 insulator with the metal mould available among the facilities.
The table shows both insulator dimensions.

Dimensions [mm]	**Type 1**	**Type 2**
Creepage distance (Lc)	375	530
End fitting separation (L)	175	134
Shank diameter (d)	28/42	28/42
Shed diameter (D)	90	142

Shed separation (s)	46	50
Core diameter	18	18
Form factor (F)	2,76	2,78

Table 6.1: test insulators Type 1 and Type 2 and their dimensions.

The test insulators have been cast in the high voltage laboratory. The housing was made of room temperature vulcanised, two component, silicone rubber (RTV-2).[11]
The housing was cast over a glass fibre core with metal terminals attached on each end (figure 6.2).

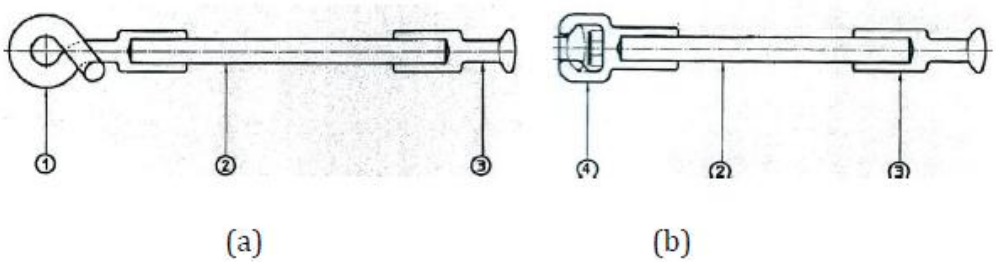

Figure 6.2. End fittings designs: pig and pin design (a) and socket and pin design (b). Pigtail (1), core (2), pin (3) and socket (4).

The metal end-fittings of the insulator cores came in two designs: pigtail and pin design (figure 6.2a) and socket and pin design (figure 6.2b). The glass fibre cores had attached fittings made of stainless steel while the PEEK cores fittings made of aluminium. Due to the poor adhering properties of silicone rubber to metal surfaces, a special adhering primer was used to precondition the metal fittings to achieve a firm bonding between the terminals and the polymeric housing.
The available silicone rubber from Wacker Chemie were used for all the castings. Cylindrical prototypes, without sheds, were also prepared. These simplified samples were made of the same housing material and cast over the same cores utilised for the full insulators. Testing of such samples aimed to benchmark the moulding procedures before moving to shedded insulator designs.

6.1 Casting of full insulators using metal moulds

The polymeric housing was cast using a metal tooling fabricated by the Manufacturing Centre at Cardiff University. The steel mould was machined using electrical discharge machining (EDM) techniques and the cavity was formed by separate metal inserts mounted on the mould metal plates. Two sets of metal inserts were manufactured, one for each insulator type, thus using the same mould plates to get both design variations. A hollow channel connecting the mould exterior with the cavity, called the injection gate, is used to inject the silicone rubber during casting.

[11] *The same material used for the rectangular specimens.*

Smaller channels are constructed to ensure the venting of the cavity, thus inhibiting the formation of voids in the material caused by entrapped air (figure 6.3b). The insulator core is carefully placed in position and both mould plates are combined and secured with the help of threaded rods and bolts.

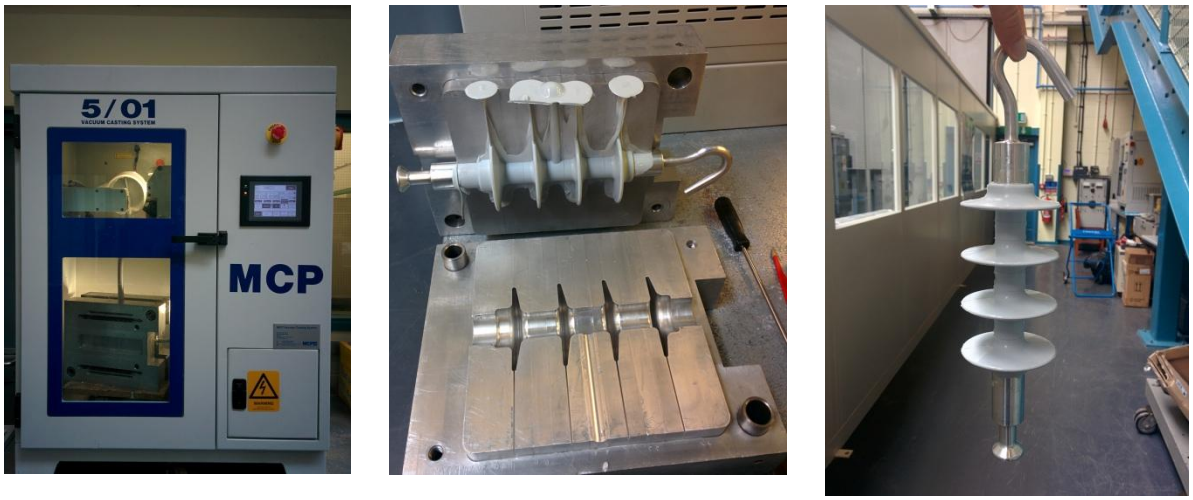

Figure 6.3: a) vacuum casting injection, b) full conventional insulator metal mould, c) full insulator manufactured

When the material fills up the cavity, it starts to emerge from the venting channels and the casting machine was then switched off and the mould placed for curing in an oven at 50^{O} Celsius for 8 hours. After the mould had been left to cool down for an hour, the mould plates were gently separated to reveal the cast. The insulator was then removed and inspected for any obvious imperfections or voids. If there was no problem, it was left for another 24 hours in room temperature or 2 hours in 50^{O} Celsius to make sure that the cross-linking of the polymer had been completed.
Any extra rubber material that was attached to the cast, due to the material filling the injection gate and the venting channels, has been removed with a sharp scalpel. The insulator was gently cleaned with warm water and allowed to rest for another 1-2 days and then it was ready to be tested.
In figure 6.3a the casting operation can be seen, while in 6.3c the shedded conventional insulator has just been fabricated. It was the first attempt and the result was good.[12]
For this fabrication 332 [g] of 600A housing material and 37 [g] of curative 600B have been used and the waste was very little, ensuring the correctness of the employed quantities.

[12] *No particular difficulties have been evident with the metal moulds during this project.*

6.2 Casting of textured insulators using silicone moulds

The silicone rubber preparation and the vacuum casting procedure, described in section 2.3 for a steel mould, was followed for the case of silicone rubber moulds.
This mould kind has been manufactured in [20] by the stereolithograhy technique.
Several stereolithograhy models made of a particular resin served as the positive samples for the manufacturing of the silicone rubber moulds. These models have been built using a SLA 5000 3D material printer within the Manufacturing Engineering Centre (MEC) at Cardiff School of Engineering.
Even the silicone moulds have been manufactured in [20] thanks to the same vacuum casting machine.
The second casting was a conventional cylinder type manufacture.
The respective silicone mould has been used.
It was cleaned thoroughly to remove any material left from previous castings or other contaminants. It is important to verify that the ventilation and injection channels are not blocked. Silicone rubber from previous casts tends to get trapped in these channels, not allowing the air bubbles escaping from the mould cavity during casting.

Figure 6.4: casting in the silicone mould

Silicone rubber for the casting of insulators, unlike the case of metal moulds, tends to adhere to the silicone rubber mould. A thorough lubrication of the silicone mould is crucial for the cast quality and the lifetime of the mould.
If the mould is not lubricated or regions remain without a lubricant, the silicone rubber injected in the silicone mould will eventually bind with the mould during curing. The retrieval of the cast becomes impossible or the cast is severely damaged and the mould incapacitated.
A spray wax release agent, ALCHEMIE R5, was sprayed on the mould cavity to form a very thin layer. The release agent was sprayed from a minimum distance of 50 – 60[cm] to ensure a uniform thin layer. For this reason, it is difficult to lubricate the deep shed regions that are more susceptible to entrap the cast. A thin layer of Vaseline, using a small brush, was used to grease the cylinder and eventually the sheds if necessary.

After the mould was lubricated, the core was placed in position and the mould sealed with adhesive tape, leaving the ventilation and injection channels unblocked (figure 6.4). After the preparation the mould was positioned inside the lower chamber of the casting machine in the correct position, regulating the height of the installation. This to guarantee that the pipe was perfectly inserted into the injection channel but not too inserted causing a contact with the internal part of the mould.
The procedure followed was the same as for the preparation of the rectangular sample. After casting, the mould was put in the oven at 50^{O} Celsius for 8 hours, and a day rest has been left to ensure the cross-linking of the polymer had been completed.
After this time, the adhesive tape was removed and the mould was opened gently to avoid damaging the cast. The insulator was removed from the mould and both were thoroughly cleaned with hot water and a clean wipe cloth to remove any grease.
For this first cylinder insulator 100 [g] of 600A and 11 [g] of 600B were employed. The result was an acceptable insulator with some small deformations where the two mould parts were in contact to close the cavity (figure 6.5a). This is addressed to the relative long age of the silicone mould, it will be replaced soon with a metal mould which will be fabricated in the Mechanical Workshop at Cardiff University.

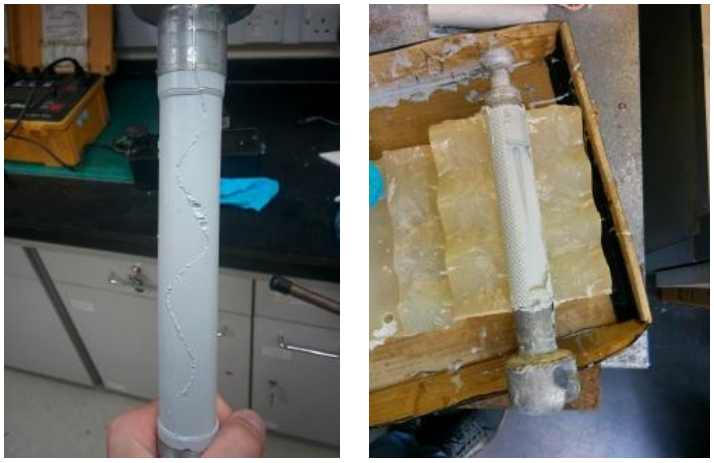

Figure 6.5: a) cylinder conventional insulator, b) bad result on a cylinder textured prototype

The third attempt was the manufacture of the 4[mm] square arrangement cylinder (with no sheds). Since the tests on the IPT machine revealed a good behavior of this kind of texture, it has been chosen to adopt is as pattern for the full textured insulator.
100 [g] of 600A and 11 [g] of 600B have been used. The procedure was the same but the mould was different. The result was not acceptable because a material drop from the bigger hole has verified. The hole is necessary for the core insertion, but it wasn't well closed and the material flowed through the split.
In figure 6.5b the cylinder not completely fulfilled from the SiR can be seen.
Another attempt with the same mould has been done. 150 [g] of 600A and 16,67 [g] of 600B materials have been adopted. This time the mould was closed and strongly pressed to guarantee a good fixing and prevent a material flow from the splits which would be eliminated (figure 6.6).

Figure 6.6: fixing of the silicone mould

The material flow from the bigger hole where the core was inserted was not totally eliminated, but the amount of silicone rubber flowed out was limited. The silicone mould was put in the oven at 50^{O} Celsius for 8 hours and which was left another day to rest. After this time it was opened and the cylinder was gently removed from the housing with the help of the scalpel. The result was a good textured cylinder insulator (figure 6.7) ready to be tested in the fog chamber and analysed with the infrared and the high speed cameras.

Figure 6.7: good realization of the cylinder textured insulator

The insulator manufacture was the previous step to the tests in fog chamber and rotating wheel. These tests were not developed in this project research because the attention has been focalized to analyse the data extracted from the inclined plane test to achieve some results, which could be extended to the full insulator prototypes. However, these have already done in the previous literature, here the next step will be perform one of the two mentioned tests, focusing the attention on the high speed camera recordings.

CHAPTER 7

Conclusions

The aim of this thesis is to increase the comprehension of the physical phenomena correlated with the performance of the insulators for outdoor applications. Several experiments were possible and the decision has been begun with the inclined plane test. Rectangular specimens and their behaviours, when an AC voltage was applied, have been investigated.

The inclined-plane tests revealed an outstanding improvement in terms of resistance against tracking and erosion introduced by textured patterns. Based on the discharge activity pattern and the loss of material due to thermal damage, the 4[mm] and 6[mm] intersecting square patterns stood out as the most promising configurations for the development of a full insulator prototype. This has been achieved comparing the results with the conventional samples, in which dissipate power and accumulated energy were bigger. The current rms values was also bigger and the waveform was different: in the textured samples the current peaks are limited by the surface shape.

This result verified the outcomes reached from the previous researchers, which reported that the test was successfully passed from the 100[%] of the textured samples but from 0[%] of the conventional.

This performance improvement is attributed to a modified surface discharge behaviour, where dry-bands formed near the HV electrode, span the width of the sample and migrate towards the ground electrode by means of short parallel dynamic streamer discharge lines aligned at 45^{o} to the electric field in the square arrangement texture (which goes from the higher to the lower electrodes). The associated reduction in surface current density and a high mobility of discharges across the ground electrode, in turn, minimise the material damage due to discharge activity.

The power dissipation cut down is reached by reducing both the electric field and current density ($P=E\cdot J$). This may be achieved by increasing both the surface area and the creepage distance of the insulator without increasing the overall longitudinal length of the insulator [34].

Moreover, textured patterns reduce damage to polymeric insulators due to surface discharges, compared with non-textured insulators of the same material, by introducing multiple paths for current conduction: as soon as one current path starts to dry as a result of Joule heating, its resistance will increase.

At this point, the current flow will switch to an alternative path of lower resistance before severe thermal damage occurs [34].

The infrared records confirmed the current measurements as they revealed a more uniform distribution of current for the textured samples whereas non-textured samples are characterised by a higher current density at the narrow region of the pollution stream, resulting in severe damage.

Current measurements also showed that the inception of the parallel discharges across the moving dry-band for textured samples was associated with a fall rather than an increase of leakage current and that the conductance of the pollution layer when the discharges are present is lower than the conductance of the layer with no discharges. The limitation inhibited the instability observed for non-textured samples where intense arcing caused severe damage. This different behaviour has been confirmed from the high speed camera recordings, even if the data have to be deeply analysed and a different camera setup has to be adopted in future.
A LabVIEW data acquisition system was developed to monitor and store the test voltage and leakage current waveforms.
A post-processing analysis with DIAdem has been done and thanks to the electric parameters calculated the report tables were carried out.
The results on the textured 4 and 6[mm] surfaces brought to a full insulator manufacture with these textures. This will be test in future in the fog chamber and with the rotating wheel to show if the results achieved with the IPT can be extended to the full insulator and other consideration about the resistance to tracking and erosion can be carried out.
A note on the silicone rubber hydrophobicity has to be mentioned.
Silicone rubber materials exhibit good water repellency, which helps to suppress the surface leakage current. The development of leakage current is associated with a temporary loss of hydrophobicity, by both physical and chemical changes of the surface properties when subjected to different electrical and environmental conditions. The ability of the materials to resist tracking and erosion will be significantly improved because of the migration of the silicone fluid from the bulk to the surface which help in maintaining the surface hydrophobicity and reducing the heat generated from the current discharges.

7.1 Future work

Regarding the work which has been done in this project research, the data acquired from the high speed camera need to be analysed in a different way to extract useful information about the movement of the electric streamers on the textured surfaces, in correlation with the FLIR and the electrical data.
Furthermore, long-term performance of textured insulators will be investigated.
1. The tracking wheel facilities in Cardiff University will be used to assess the ability of textured insulators to resist tracking and erosion. The fog chamber can also be used to facilitate the 1000[h] salt-fog test. Such tests will investigate whether the outstanding anti-tracking and anti-erosion performance of textured designs brought up during inclined-plane tests, will be observed for full textured insulators.
2. For all artificial testing of outdoor insulators, their ability to fully replicate service conditions is limited. The research programme could be extended to investigate the performance of textured insulators in field tests where the test objects will be subjected

to service stresses. The information and results acquired from both the laboratory exploration and the field tests will be the basis of shaping a proposal for the commercial development and release of textured insulators for adverse environmental conditions. In the field, there are more complex conditions and factors which may affect the performance of the silicone rubber insulators. It is recommended that further laboratory tests be performed to simulate outdoor conditions such as the accumulation of dust, snow and/or ice. It is proposed that textured insulators be used in areas subject to extreme temperature variations, and thus a better evaluation of performance under extremely high and low temperatures would be beneficial.

3. Since the electric field is considered the drive of the electric current on the surface of the insulators which in turn responsible for surface damage, a further study investigating the distribution of the electric field on the surface of the insulators needs to be done.

4. Since HVDC transmission systems are used in service, and due to its unidirectional electric field on the surface, insulators can accumulate contaminants more than those accumulated when working under AC systems. The performance of the insulators under pollution conditions, the flashover voltage, the surface erosion under DC electric stress are possibly different compared to insulators working under AC energisation.

5. Study of degradation and ageing of outdoor insulators resulting from UV exposure is a potential research area which could help to assess long-term material performance under normal weather conditions. The time of exposure to UV radiation in these experiments is not considered, while it is always present in outdoor operating condition. More tests need to be performed in correlation with field service conditions as the insulators are exposed for long time periods to direct sunlight.

Bibliograhy

[1] IEC 60587:2007, 'Electrical insulating materials used under severe ambient conditions. Test methods for evaluating resistance to tracking and erosion', 2007

[2] http://www.parliament.uk/documents/post/pn163.pdf

[3] IEC 60815:2008, 'Selection and dimensioning of high-voltage insulators intended for use in polluted conditions_Part 1: Definitions, information and general principles', 2008

[4] IEC 60507:1991, 'Artificial pollution tests on high-voltage insulators to be used on a.c. systems', 1991

[5] Williams, D.L., Haddad, A., Rowlands, A.R., Young, H.M., and Waters, R.T., 'Formation and characterization of dry bands in clean fog on polluted insulators', IEEE Trans. Dielectr. Electr. Insul., Vol. 6, (5): pp. 724-731, 1999

[6] Haddad, A. and Waters, R.T., Insulating Structures, UK Patent 2406225, 2003

[7] Haddad, A., Waters, R., Griffiths, H., Chrzan, K., Harid, N., Sarkar, P., and Charalampidis, P., 'A new approach to anti-fog design for polymeric insulators', IEEE Trans. Dielectr. Electr. Insul., Vol. 17, (2): pp. 343-350, 2010

[8] Crespo-Sandoval, J., "Condition Monitoring of Outdoor Insulation using Artificial Intelligence Techniques," PhD Thesis, University of Wales Cardiff, 2005.

[9] Adamson, A., "Physical chemistry of surfaces," 5th edition, New York, Wiley, 1990.

[10] Garbass, F., Morra, M., and Occhiello, E., "Surface energetic and contact angle," Jone Wiley Sons, England, pp. 161-199, 1994.

[11] STRI GUIDE: "Hydrophobicity Classification Guide," Guide 1, 92/1, 1992.

[12] Nekeb, A,. "Effect of some climatic conditions in the performance of outdoor HV silicone rubber insulators", PhD thesis, High Voltage Energy Systems Group, Cardiff University, 2014.

[13] CIGRE Task Force 33.04.01, 'Polluted Insulators: A review of current knowledge', 2000

[14] Gorur, R., Cherney, E., and Hackam, R., "The AC and DC performance of polymeric insulating materials under accelerated aging in a fog chamber," Power Delivery, IEEE Transactions on.3, 1892-1902, 1988.

[15] Wilkins, R., and Billiings, M., "Effect of discharges between electrodes on the surface of organic insulation," Trans. IEE, vol.116, pp. 1777-1784, 1969.

[16] Billiings, M., Warren, L., and Wilkins, R., "Thermal erosion of electrical insulation materials," Trans. IEEE, vol. EI-6, pp. 82-90, 1971.

[17] Waters, R., Haddad, A., Griffiths, H., Harid, N., Charalampidis, P., Sarkar, P., “Dry-band discharges on polluted silicone rubber insulation: control and characterization,” IEEE Transactions on Dielectrics and Electrical Insulation, vol.18, no.6, pp.1995-2003, December 2011.

[18] Ahmed, A., Singer, H., Mukherjee, P., “A numerical model using surface charges for the calculation of electric fields and leakage currents on polluted insulator surfaces,” Conference on Electrical Insulation and Dielectric Phenomena, vol.1, pp.25-28, Oct1998.

[19] Waters, R., Haddad, A., Griffiths, H., Harid, N., and Sarkar, P., “Partial-arc and spark models of the flashover of lightly polluted insulators,” IEEE Trans. Dielectr. Electr. Insul., vol. 17, no. 2, pp. 417-424, 2010.

[20] Charalampidis, P,. “Characterisation of textured insulators for overhead lines and substations”, PhD thesis, High Voltage Energy Systems Group, Cardiff University, 2012.

[21] Karady, G.G., Shah, M., and Brown, R.L., 'Flashover mechanism of silicone rubber insulators used for outdoor insulation-I', IEEE Trans. Power Del., Vol. 10, (4): pp. 1965-1971, 1995

[22] Karady, G., Shah, M., and Brown, R., “Flashover mechanism of silicone rubber insulators used for outdoor insulation –I,” IEEE Transaction on power Delivery, vol. 10, no. 4, pp.1965-1971, 1995.

[23] IEC 62730: “HV polymeric insulators for indoor and outdoor use tracking and erosion testing by wheel test and 5 000h test”, 2012.

[24] Lightning and Insulator Subcommitte, "Application of Insulators in a Contaminated Environment," IEEE Transactions on Power Apparatus and Systems, vol. PAS-98, no. 5, pp. 1676-1695, Sept. 1979.

[25] H. Ahmad, “Investigation of electrical properties of field grading materials based ZNO microvaristors”, pag. 67 ; School of Engineering, Cardiff University, United Kingdom, 2017.

[26] https://en.wikipedia.org/wiki/Peristaltic_pump

[27] High-Speed M Series Multifunction Data Acquisition - 16-Bit, up to 1.25 MS/s, up to 80 Analog Inputs

[28] DAQ SCB-68 68-Pin Shielded Connector Block User Manual

[29] DAQ Accessories Selection Guide

[30] Charalampidis, P,. “Characterisation of textured insulators for overhead lines and substations”, PhD thesis, High Voltage Energy Systems Group, Cardiff University, 2012.

[31] http://www.flirmedia.com/MMC/THG/Brochures/RND_017/RND_017_US.pdf

[32] “Correlation of Damage, Dry Band Arcing Energy, and Temperature in Inclined Plane Testing of Silicone Rubber for Outdoor Insulation”. Luiz H. Meyer, Shesha H. Jayaram and Edward A. Cherney University of Waterloo, Electrical and Computer Engineering Department, Waterloo, ON N2L 3G1, Canada

[33] http://photron.com/wp-content/uploads/2014/07/FASTCAM_SA5.pdf

[34] Haddad, A., Waters, R., Griffiths, H., Chrzan, K., Harid, N., Sarkar, P., and Charalampidis, P., "A new approach to anti-fog design for polymeric insulators," IEEE Trans. Dielectr. Electr. Insul., vol. 17, no. 2, pp. 343-350, 2010.

[35] Swift, D., Haddad, A., , and Warne, D., "Insulators for outdoor applications," Advances in high voltage engineering, ISBN 0852961588, 2004.